AD_____

AWARD NUMBER: W81XWH-05-1-0572

TITLE: Hypoxia and Prx1 in Malignant Progression of Prostate Cancer

PRINCIPAL INVESTIGATOR: Young-Mee Park, Ph.D.

CONTRACTING ORGANIZATION: Health Research, Incorporated
Buffalo, New York 14263

REPORT DATE: September 2006

TYPE OF REPORT: Annual

PREPARED FOR: U.S. Army Medical Research and Materiel Command
Fort Detrick, Maryland 21702-5012

REPORT DOCUMENTATION PAGE

Form Approved
OMB No. 0704-0188

1. REPORT DATE *(DD-MM-YYYY)*	**2. REPORT TYPE**	**3. DATES COVERED** *(From - To)*
01-09-2006	Annual	1 Sep 2005 – 31 Aug 2006

4. TITLE AND SUBTITLE

Hypoxia and Prx1 in Malignant Progression of Prostate Cancer

5a. CONTRACT NUMBER

5b. GRANT NUMBER
W81XWH-05-1-0572

5c. PROGRAM ELEMENT NUMBER

6. AUTHOR(S)

Young-Mee Park, Ph.D.

E-Mail: young-mee.park@roswellpark.org

5d. PROJECT NUMBER

5e. TASK NUMBER

5f. WORK UNIT NUMBER

7. PERFORMING ORGANIZATION NAME(S) AND ADDRESS(ES)

Health Research, Incorporated
Buffalo, New York 14263

8. PERFORMING ORGANIZATION REPORT NUMBER

9. SPONSORING / MONITORING AGENCY NAME(S) AND ADDRESS(ES)
U.S. Army Medical Research and Materiel Command
Fort Detrick, Maryland 21702-5012

10. SPONSOR/MONITOR'S ACRONYM(S)

11. SPONSOR/MONITOR'S REPORT NUMBER(S)

12. DISTRIBUTION / AVAILABILITY STATEMENT
Approved for Public Release; Distribution Unlimited

13. SUPPLEMENTARY NOTES

14. ABSTRACT

Hypoxia has been proposed to function as a micro-environmental pressure to select for a subset of cancer cells with an increased ability to survive and proliferate. The activation of Nrf2 and the up-regulation of prx1 expression by changes of oxygenation are likely to contribute to the malignant progression of cancer and to modify the treatment response of cancer cells. The information provided in the current study suggests that the Nrf2-Prx1 axis may serve as a fruitful target for cancer prognosis and therapy. Identifying the key regulatory components and understanding the molecular basis of prx1 gene regulation by Nrf2 are critical to the development of intervention strategies. Future research will be aimed at finding out whether Nrf2-Prx1 activation can be suppressed by genetic and/or pharmacological approaches, and whether suppressing the Nrf2-Prx1 axis will inhibit the malignant progression or reverse treatment resistance in pre-clinical models. We provide the first evidence that suggests hypoxia increases AR function in human prostate cancer cells, and Prx1 enhances the hypoxia-mediated AR activation. Delineating the molecular mechanisms by which hypoxia affects AR function will provide insight into the treatment resistance and malignant progression of prostate cancer cells. Novel therapeutic approaches should be developed to prevent hypoxia and/or its consequences to enhance the efficacy of androgen deprivation therapy, a treatment that has not been Improved significantly since its introduction over 50 years ago.

15. SUBJECT TERMS
Prx1, Hypoxic tumor microenvironment, Unstable oxygenation condition, Malignant progression

16. SECURITY CLASSIFICATION OF:			**17. LIMITATION OF ABSTRACT**	**18. NUMBER OF PAGES**	**19a. NAME OF RESPONSIBLE PERSON**
a. REPORT	**b. ABSTRACT**	**c. THIS PAGE**			USAMRMC
U	U	U	UU	78	**19b. TELEPHONE NUMBER** *(include area code)*

Table of Contents

Cover……1

SF 298…… 2

Table of Contents…… 3

Introduction…….... 4

Body…… 4-14

Key Research Accomplishments…… 14-15

Reportable Outcomes…… 15

Conclusions…….. 15-16

References…… 16

Appendices……16-78

Introduction

The objective of this research is to define the role of Prx1 in hypoxia-response of prostate cancer cells and the underlying regulatory mechanisms involved. This study will provide a sound scientific basis upon which the roles of Prx1 can be elucidated in prostate cancer, enabling the development of new therapeutic approaches to inhibit its malignant progression.

Body

Task 1. To establish the molecular basis for Prx1 regulation by hypoxia and its constitutive elevation in highly metastatic human prostate cancer cells (Months 1-36)

Despite numerous recent reports on increased Prx1 expression under various conditions, little information is available on the mechanism responsible for the abnormal elevation of Prx1 level in prostate cancer. We hypothesized that the hypoxic and unstable oxygenation microenvironment of a tumor might be crucial for *prx1* up-regulation. We cloned the human *prx1* promoter and identified NF-E2-related factor 2 (Nrf2) as a key transcription factor. Hypoxia/reoxygenation, an *in vitro* condition suited to mimic changes of oxygenation, increased Nrf2 nuclear localization and its binding to the electrophile responsive elements (EpRE) located at the proximal (-536 to -528) and distal (-1429 to -1421) regions of the *prx1* promoter. A significant reduction of both steady-state and hypoxia/reoxygenation-mediated *prx1* gene expression was demonstrated in Nrf2 knockout cells. A detailed research accomplishment associated with Task 1 is described below.

Up-regulation of prx1 expression by hypoxia/reoxygenation and multiple sequence alignment analysis of the prx1 upstream sequences. To test whether a hypoxic and unstable oxygenation condition activates *prx1* gene expression, human prostate cancer LNCaP cells were exposed to 4 h of hypoxia, followed by reoxygenation in a CO_2 incubator. RT-PCR analysis demonstrated a significant up-regulation of *prx1* expression during reoxygenation (Figure 1A). The amount of Prx1 protein accumulation by hypoxia/reoxygenation closely correlated with the mRNA level (Figure 1B). Hypoxia treatment alone, however, did not up-regulate *prx1* gene expression even when the cells were treated with longer periods of hypoxia (Figure 1C). Increased *prx1* mRNA level was consistently observed in reoxygenated cells regardless of the prior duration of hypoxia. These results are consistent with the hypothesis that dynamic changes of oxygenation of a tumor may trigger the transcriptional activation of *prx1* expression. The human *prx1* gene may not be a target of HIF-1α, because HIF-1α binding to the hypoxia-responsive element (HRE) is known to increase during continuous exposure to hypoxia, and to decline immediately by oxygen replenishment (1)

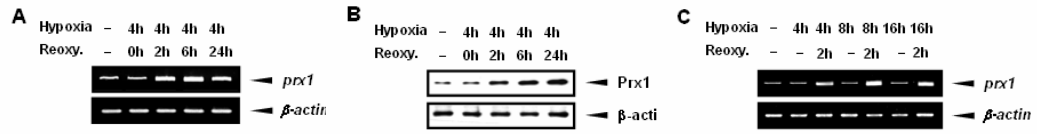

Figure 1. Up-regulation of *prx1* expression by hypoxia/reoxygenation. Panel A, Human prostate cancer LNCaP cells were exposed to hypoxia for 4 h, followed by reoxygenation for 0, 2, 6, or 24 h. Total RNA was isolated and RT-PCR analysis was carried out using primer pairs specific for human *prx1* gene. *β-actin* gene was used as a control. Panel B, Protein extracted from cells treated as above was subjected to Western blot analysis. Equal amounts of protein (10 μg) were separated by SDS-PAGE and probed with an antibody specific to Prx1. β-actin was used as a loading control. Panel C, Cells were exposed to 4, 8, or 16 h of hypoxia, followed by 2 h of reoxygenation. Total RNA was isolated, and RT-PCR was carried out using human *prx1* primer pairs. *β-actin* gene was used as a control.

Since no information is available on the transcriptional regulation of the human *prx1* gene, we carried out a computer-based sequence analysis of the mouse, rat, and human *prx1* upstream

sequences. About 5 kb genomic sequences upstream of *prx1* were retrieved in Fasta format from the UCSC genome browser (http://genome.ucsc.edu). Multiple sequence alignment analysis was performed with a locally installed Clustal X (2) program in combination with MEME (Multiple Em for Motif Elicitation) (3), and CONREAL (CONserved Regulatory Elements anchored ALignment) (4) programs. The computer-based sequence analysis revealed that the 5' 2.1 kb segment upstream of the human *prx1* contains most of the sequence conservation across the three mammalian species. No obvious HIF-1α responsive element was found in these *prx1* upstream regions.

Cloning of the human prx1 promoter and identification of two EpRE sites as critical cis-elements for prx1 up-regulation in response to hypoxia. The 5' 2.1 kb region upstream of the human *prx1* gene was PCR-cloned, and the luciferase reporter vector, pGL3-2100, was generated. Genomic DNA from the Wi-26 human embryonic epithelial cells was used in order to avoid possible mutations of the promoter region in cancer cells. A series of deletion vectors were constructed as described in Materials and Methods for the purpose of examining the transcriptional activation of *prx1*. The pGL3-2100 reporter vector was transfected into LNCaP cells, and luciferase activities were analyzed at 0, 0.5, 2, 6, or 24 h during reoxygenation after 4 h of hypoxia treatment. The luciferase activity was highest at 6 h of reoxygenation (data not shown). This time point was chosen to study the promoter activities of the deletion constructs. The importance of the 5'-1500 to -1000 and -700 to -500 regions to hypoxia/reoxygenation-mediated *prx1* activation became evident from the analysis. As shown in Figure 2A, a significant reduction of the promoter activity was observed in cells transfected with pGL3-1000 and pGL3-500 when compared to the pGL3-2100 transfected cells. An examination of these two regions with the use of various promoter analysis programs, including TransFac, indicated that both regions contain potential electrophile responsive element (EpRE), also known as antioxidant response element (ARE). The consensus sequence of EpRE, 5'-TGAC*NNN*GC-3', is a DNA binding element of the transcription factor, NF-E2-related factor 2, or Nrf2 (5). The proximal EpRE site is at -536 to -528 (EpRE1), and the distal site at -1429 to -1421 (EpRE2) (Figure 2B). The conventional EpRE displays sequence similarity to the AP-1-response element (5'-TGAC/GTCA-3'). One of the critical features of EpRE is the 'GC' at the 3' end of the EpRE core; this feature is met by *prx1*-EpRE1 and -EpRE2. Suffice it to note that EpRE1 and EpRE2 possess one sequence mismatch in the forth or third nucleotide, respectively. Previous studies have also reported a correlation between *prx1* mRNA accumulation and activation of

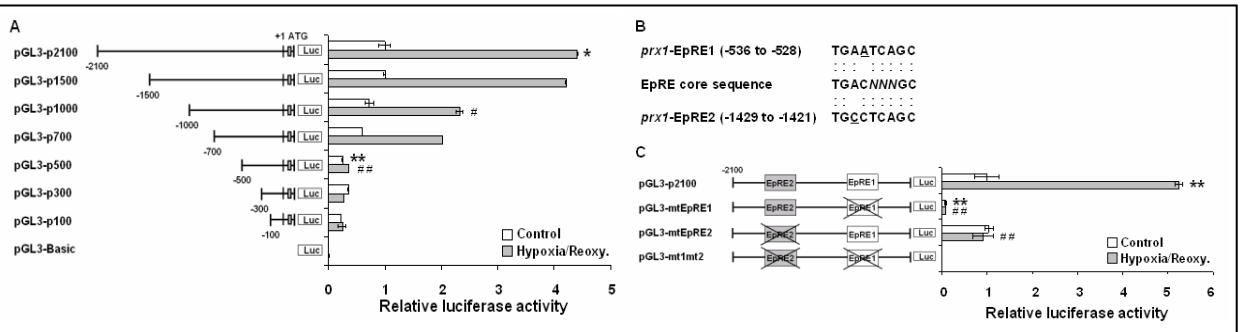

Figure 2. Analysis of hypoxia/reoxygenation-responsive *prx1* promoter activities. Panel A. LNCaP cells were transfected with a series of *prx1* promoter reporter vectors. The pRLTK vector containing the *Renilla* luciferase gene was co-transfected to normalize the transfection efficiency. Twenty-four hours after transfection, cells were exposed to hypoxia for 4 h, followed by reoxygenation for 6 h. The data are presented as the ratio of the normalized luciferase activities. The numbers on the promoter vectors represent the positions starting from the transcription initiation site of the human *prx1* gene (+1). $P^{*} < 0.05$ or $P^{**} < 0.01$, compared to control pGL3-2100 value. $P^{\#} < 0.05$ or $P^{\#\#} < 0.01$, compared to pGL3-2100 reporter activity after hypoxia/reoxygenation. Panel B. EpRE1 and EpRE2 sequences present in the human *prx1* promoter were compared with the conventional EpRE core sequences. The nucleotide sequence of EpRE1 or EpRE2 that differs from the core sequence is underlined. Panel C. The pGL3-mtEpRE1, -mtEpRE2, and the double mutant, -mt1mt2, were transfected into LNCaP cells together with the pRLTK normalizing vector. Relative luciferase activities were analyzed as described in Panel A. $P^{**} < 0.01$, compared to control pGL3-2100 value. $P^{\#\#} < 0.01$, compared to pGL3-2100 reporter activity after hypoxia/reoxygenation.

Nrf2 (6). To verify the significance of EpRE1 and EpRE2, EpRE1 mutant (pGL3-mtEpRE1), EpRE2 mutant (pGL3-mtEpRE2), and the double mutant (pGL3-mt1mt2) reporter vectors were constructed from pGL3-p2100 (Figure 2C). The mutations were designed to disrupt the Nrf2 recognition sequences of EpRE1 and EpRE2. When pGL3-mtEpRE1 was transfected, both steady-state and hypoxia/reoxygenation-responsive reporter activities were completely lost. When pGL3-mtEpRE2 was transfected, hypoxia/reoxygenation-responsive promoter activity was significantly reduced even though EpRE1 was intact, indicating that the presence of both EpRE1 and EpRE2 are required for hypoxia/reoxygenation-mediated activation of *prx1*. The fact that the steady-state promoter activity of pGL3-mtEpRE2 was comparable to that of pGL3-2100 suggests that EpRE1, but not EpRE2, may be critical for baseline *prx1* expression.

EpRE binding activity of Nrf2 is increased by hypoxia/reoxygenation. The EpRE binding activities were examined during reoxygenation after 4 h of hypoxia treatment in LNCaP cells. As shown in Figure 3A, increases of EpRE1- and EpRE2-binding activities were observed as early as 0.5 h during reoxygenation upon withdrawal from hypoxia. The EpRE-binding activities were specific since the DNA-binding complexes became undetectable when molar excess of the unlabeled competitor of the EpRE1- or EpRE2-containing probe was added. The addition of heat shock element (HSE), a classical stress-response element, did not inhibit EpRE-binding activities. The binding activity of EpRE1 declined with time, in contrast to the sustained activity of EpRE2. The reason for this difference is unclear, although a possible role of the adjacent sequences of the EpRE1 and EpRE2-containing probes, and the profile of Nrf2 interaction with other nuclear factors, may be responsible. When nuclear extracts of LNCaP cells were incubated with the Nrf2 antibody, the disappearance of the EpRE-binding complexes was clearly evident (Figure 3B).

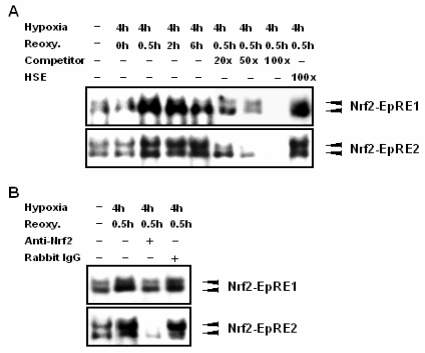

Figure 3. Binding of Nrf2 to EpRE1 and EpRE2 in response to hypoxia/reoxygenation. Panel A. Nuclear extracts were prepared from LNCaP cells immediately after 4 h of hypoxia (0 h) or 0.5, 2, or 6 h during reoxygenation. EMSA was performed using radio-labeled EpRE1 or EpRE2-containing oligonucleotides. Unlabeled EpRE1 or EpRE2 was used as a specific competitor. Unlabeled heat shock responsive element (HSE) was used as a non-specific competitor. Representative results from three independent experiments are shown. Panel B. Nuclear extracts from cells treated with 4 h hypoxia/0.5 h reoxygenation were incubated with an anti-Nrf2 antibody. The specificity of Nrf2 binding to EpRE1 or EpRE2 was confirmed by using an anti-rabbit IgG as a negative control. Representative results from three independent experiments are shown.

Increased nuclear localization and trans-activation of Nrf2 by hypoxia/reoxygenation. To test whether the *prx1* promoter is functional for other Nrf2 inducers, pGL3-2100 promoter activities were examined in LNCaP cells treated with *tert*-butylhydroquinone (tBHQ). The latter is one of the classical activators of Nrf2 (7). As shown in Figure 4A, treatment with 20 uM tBHQ also increased the *prx1* promoter activity. Immunofluorescence studies confirmed the increased nuclear localization of Nrf2 in cells subjected to hypoxia/reoxygenation or treated with tBHQ (Figure 4B). Nrf2 localization was examined by incubation with an anti-Nrf2 antibody; the location and integrity of the nucleus was probed by DAPI staining of the same cells. Overlaying the Nrf2 and DAPI images (cyan color) confirms the nuclear localization of Nrf2. In control cells, low levels of Nrf2 expression were observed in the cytoplasm and the nucleus. The Nrf2/F-actin overlay (orange color) images display the cytoplasmic localization of Nrf2. Nuclear fractions were then prepared, and as shown in Figure 4C, there was significantly increased Nrf2 accumulation in the nucleus as demonstrated by Western blot analysis. An important role of Nrf2 in *prx1* trans-activation was also demonstrated in Nrf2 knockout cells. The accumulation of *prx1* mRNA was significantly diminished in Nrf2 -/- cells when compared to Nrf2 +/+ MEF cells

(Figure 4D). However, neither baseline nor hypoxia/reoxygenation-responsive expression of *prx1* mRNA was completely abolished in cells lacking Nrf2. It is conceivable that in addition to Nrf2, various regulatory factors might be involved in coordinating and relaying different cellular signals to the transcriptional machinery of the *prx1* gene, as is true for other genes involved in cell growth and survival regulation.

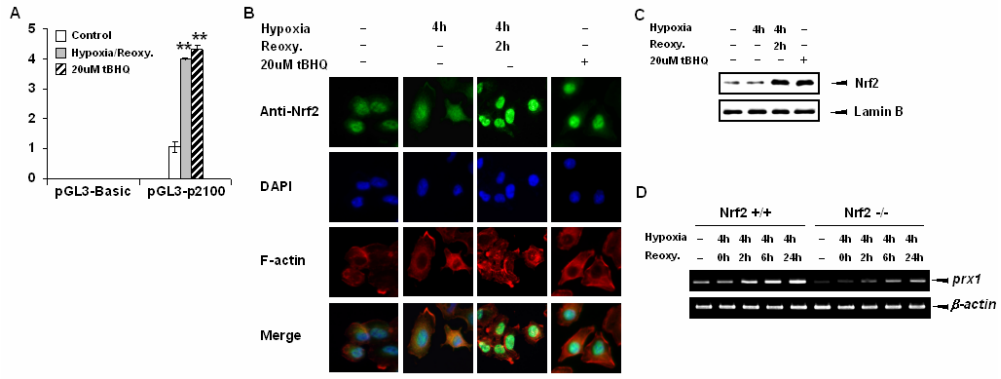

Figure 4. Stabilization of Nrf2 in the nucleus by hypoxia/reoxygenation. Panel A. pGL3-p2100 was transfected into LNCaP cells together with pRLTK. Twenty-four hours after transfection, cells were treated with 4 h hypoxia/6 h reoxygenation or 20 μM tBHQ for 3 h. Luciferase activities were analyzed in cell extracts. *P*** < 0.01, compared to control pGL3-2100 value. Panel B. LNCaP cells were treated with 4 h hypoxia/2 h reoxygenation or 20 μM tBHQ for 3 h. Immunocytochemistry was performed using an anti-Nrf2 antibody and FITC-conjugated secondary antibody. The location of the nuclei was visualized by using DAPI (blue) counter-staining. F-actin was stained with rhodamine-conjugated phalloidin for cytoplasmic counter-staining. The DAPI and F-actin images of the same field are shown separately or merged with the Nrf2 immunofluorescence images. Panel C. Equal amounts of nuclear protein (10 μg) from cells treated as described in Panel B were subjected to Western blot analysis using an anti-Nrf2 antibody. Analysis of lamin B expression was performed as a loading control for nuclear fraction. Representative results from three independent experiments are shown. Panel D. Nrf2 +/+ and Nrf2-/- MEF cells were exposed to 4 h of hypoxia, followed by 0, 2, 6, or 24 h of reoxygenation. Total RNA was isolated, and RT-PCR analysis was performed by using primer pairs specific for the mouse *prx1* gene. *β-actin* gene was analyzed as a control. Representative results from three independent experiments are shown.

Plans

Continuing research include the chromatin immunoprecipitation experiments to further validate the role of Nrf2 in dysregulated elevation of Prx1 in prostate cancer cells, and validating the key findings in other prostate cancer cell lines. Since our most recent results indicate a possible involvement of Kelch-like ECH-associated protein, Keap1, we will investigate the role of Keap1 in regulating Nrf2 mediated Prx1 trans-activation. We anticipate that we will be in a position to report these findings within a few months.

Task 2. To investigate the molecular mechanisms by which Prx1 regulates hypoxia-mediated PSA expression and AR activation in prostate cancer cells (Months 1-36)

Recent studies demonstrate that prostate cancer cells grow in a hypoxic microenvironment and that the extent of tumor hypoxia correlates with poor clinical outcome. More recently, androgen deprivation, the most common form of prostate cancer therapy, was itself suggested to generate a state of transient hypoxia. Since the androgen receptor (AR) plays a critical role in prostate cancer, we investigated the potential role of hypoxia in regulating AR function. We found that hypoxia increased AR activation in LNCaP prostate cancer cells. Our results demonstrated that Prx1 over-expression increased AR binding to the androgen responsive element (ARE), increased PSA accumulation, and increased ARE-reporter gene activities. Our research accomplishment associated with Task 2 is detailed below.

Hypoxia increases ARE-binding activity of AR and PSA expression. The LNCaP cells are known to have a mutated but functional AR, and secrete prostate specific antigen (PSA) *in vitro* and *in vivo*. As a first step to examine whether hypoxia influences the AR activity, electrophoretic mobility shift assay (EMSA) was performed with radiolabeled oligonucleotides containing the androgen responsive element (ARE) as a probe. In order to mimic a hypoxic microenvironment *in vitro*, two hypoxia treatment protocols were tested. In the first protocol, cells were exposed to hypoxia for up to 24 h and the ARE-binding activity of AR was analyzed at different times during this period. Alternatively, cells were exposed to hypoxia for 4 h, returned to normoxic CO_2 incubator, and the ARE-binding activity of AR was analyzed under normoxic conditions. When EMSA was performed in cells treated with either hypoxia protocol, significant increases of ARE-binding activities were observed. Our results showed that the ARE-binding activity reached a maximum level at 4 h when cells were exposed continuously to hypoxia (Figure 5A). The ARE-binding activity increased further when cells were analyzed under normoxic conditions after the 4 h of hypoxia treatment. This additional increase of ARE-binding activity reached a maximum level at 2 h at normoxic condition (Figure 5B). The ARE-binding activity was specific since the DNA-binding complexes became undetectable when molar excess of unlabeled competitor ARE probe was added. Supershift assays using antibody specific to AR also demonstrated the binding of AR to the ARE-containing probe (Figure 5C). Since the ARE-binding activities of AR were most pronounced after exposure to 4 h of hypoxia, all subsequent experiments were performed using this condition.

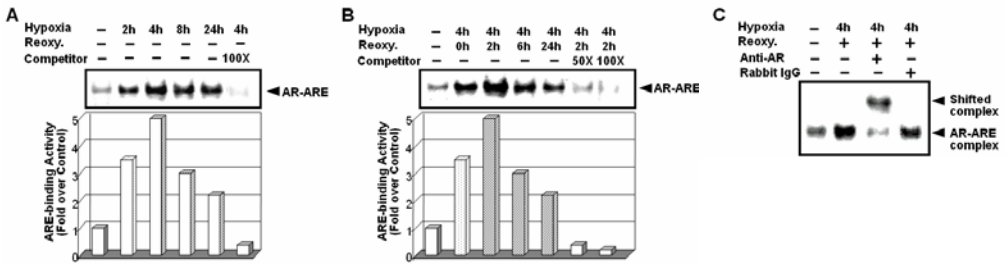

Figure 5. Hypoxia increases ARE-binding activity of AR. Panel A, LNCaP cells were exposed to hypoxia and harvested after various hours of hypoxia treatment. EMSA was performed using ARE-containing oligonucleotides (Santa Cruz Biotechnology, Santa Cruz, CA) radiolabled with γ-^{32}P ATP (MP biomedicals, Irvine, CA) as a probe. The location of ARE-binding complexes is indicated by arrow. ARE-binding activity was quantitated using the Molecular Imager FX System (Bio-Rad, Hercules, CA). Panel B, LNCaP cells were treated with 4 h of hypoxia. Cells were then incubated at normoxic conditions for up to 24 h. EMSA was performed at the indicated times under normoxic conditions. ARE-binding activity was quantitated as above. *C,* Nuclear extracts obtained from LNCaP cells 2 h after 4 h hypoxia treatment were subjected to supershift assay using anti-AR antibody. Specificity was confirmed using rabbit IgG (Santa Cruz Biotechnology, Santa Cruz, CA). Arrows indicate positions of AR-ARE and supershifted complexes.

We wanted to validate the functional significance of the increased AR-ARE complex by hypoxia. PSA is one of the best-characterized genes regulated by AR. Since LNCaP cells express and secrete PSA, we examined the changes of PSA regulation after hypoxia treatment. Our results demonstrated an increased accumulation of *PSA* mRNA during a 24 h period after hypoxia treatment (Figure 6A). Consistent with the increased PSA mRNA level, increased accumulation of cellular PSA protein and increased secretory PSA into the culture medium were confirmed by Western blot analysis (Figure 6B) and ELISA assay (Figure 6C), respectively.

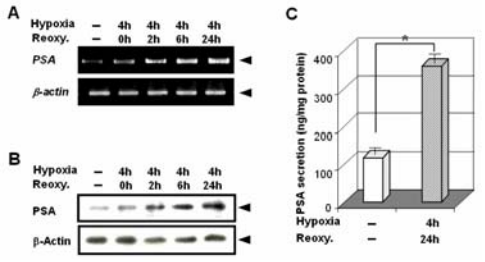

Figure 6. Up-regulation of PSA expression and secretion by hypoxia. Panel A, RT-PCR analysis was carried out at the indicated times after 4 h of hypoxia treatment with PCR primer pairs specific for the PSA gene. *β-Actin* gene was amplified as a control. Panel B, Equal amounts of proteins obtained from cells treated as above were subjected to Western blot analysis using anti-PSA antibody (Lab Vision, Fremont, CA). *β*-Actin antibody (Sigma, St. Louis, MO) was used as a loading control. Panel C, The amounts of the secreted PSA in the medium were determined using ELISA 24 h after 4 h hypoxia treatment. Values are expressed as means ± standard deviations of triplicate samples. **P* < 0.05 compared with control.

Hypoxia increases AR trans-activation. Activated AR exerts its trans-activation function by binding to the DNA containing an androgen responsive element, ARE. To examine whether the effect of hypoxia is specific to PSA only, we transfected LNCaP cells with an ARE-luciferase reporter construct. Our result demonstrated a significant increase of luciferase activity after hypoxia treatment (Figure 7A), confirming that increased trans-activation of AR by hypoxia is not limited to the PSA gene. In order to rule out that the increased ARE-luciferase activity was due to increased AR protein level, we carried out Western blot analysis using anti-AR antibody. As shown in Figure 7B, we did not detect any change in AR protein level after 4 h of hypoxia treatment. That hypoxia increases AR trans-activation is new and suggests a novel role for hypoxia in regulating AR activity in prostate cancer cells. To further verify that the effect of hypoxia on AR trans-activation was not an artifact in LNCaP cells, we employed the DU145 human prostate cancer cells which are devoid of AR. We introduced the exogenous AR into the DU145 cells together with the ARE-luciferase, and exposed them to 4 h of hypoxia and analyzed the ARE-luciferase activity after hypoxia treatment. As shown in Figure 8, our result clearly demonstrated that hypoxia induced the trans-activation of exogenous AR to stimulate the ARE-luciferase activities. The magnitude of the increase in ARE-luciferase activity in DU145 cells was similar to that observed in LNCaP cells. Collectively, these data validate our conclusion that hypoxia increases the AR-ARE binding activity and AR target gene expression.

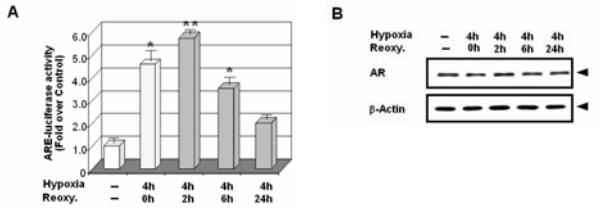

Figure 7. Hypoxia induces ARE-luciferase promoter activity. Panel A, LNCaP cells were transfected with the ARE-luciferase construct. At 24 h after transfection, cells were treated with 4 h of hypoxia and the luciferase activity was analyzed at the indicated time points following hypoxia treatment. Normalized mean luciferase activity measured in ARE-luciferase transfected cells without hypoxia treatment (control) was set to 1.0. *P* ** < 0.01, *P* * < 0.05 compared with control. Panel B, Aliquots of samples used in Panel A were subjected to Western blot analysis using AR-specific antibody (Santa Cruz Biotechnology, Santa Cruz, CA). The *β*-Actin antibody (Sigma, St. Louis, MO) was used as a loading control.

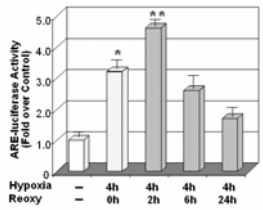

Figure 8. Effect of hypoxia on exogeneous addition of AR in DU145 cells. DU145 cells were co-transfected with pSG5hAR and ARE-luciferase reporter plasmid. At 24 h after transfection, cells were treated with 4 h hypoxia and luciferase activity was carried out at the indicated time points following hypoxia treatment. Normalized mean luciferase activity measured in cells transfected with pSG5hAR and ARE-luciferase without hypoxia treatment (control) was set to 1.0. *P* ** < 0.01, *P* * < 0.05 compared with control.

Hypoxia stimulates the nuclear translocation of AR and its promoter occupancy. Activated AR translocates from the cytosol to the nucleus to trans-activate its target genes. To examine the effect of hypoxia on the subcellular distribution of AR, we carried out Western blot analysis using nuclear and cytosolic extracts obtained from control and hypoxia-treated LNCaP cells. As shown in Figure 9A, hypoxia increased nuclear AR and decreased cytosolic AR. Total AR expression levels were not changed, which confirmed that hypoxia does not affect the level of AR protein expression. Increased nuclear localization of AR was further confirmed by immunofluorescence cell staining and confocal microscopy (Figure 9B). Propidium iodide staining of the same cells verified the location and integrity of the nuclei. Virtually identical results were obtained in DU145 cells after the exogenous introduction of AR (data not shown). Since hypoxia increases ARE-binding, PSA expression, ARE-lucifierase activity, and AR translocation to the nucleus, the next step was to examine whether hypoxia increased the recruitment of AR to the promoter of its target gene in the natural chromatin milieu. We carried out chromatin immunoprecipitation (ChIP) assays using the AR-specific antibody. To control for possible nonspecific interactions and DNA contaminations of the solutions, samples precipitated with rabbit IgG were included. As shown in Figure 10, our result demonstrated that hypoxia

increased the PSA promoter occupancy by AR. The increased PSA promoter occupancy was AR specific since no signal was detected from rabbit IgG control samples. The results obtained from DNA that was PCR amplified from chromatin extracts before immunoprecipitation (input) are shown for comparison.

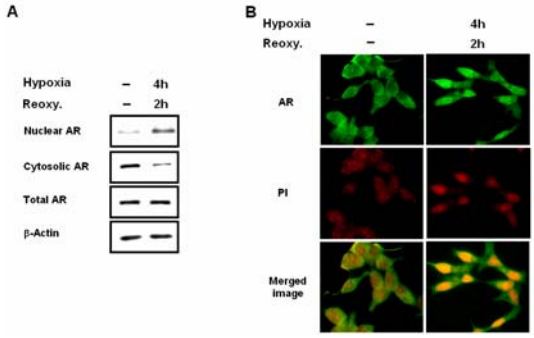

Figure 9. Effect of hypoxia on subcellular redistribution of AR. Panel A, LNCaP cells were treated with 4 h of hypoxia. Cells were then incubated for 2 h under normoxic condition. Nuclear and cytosolic extracts were isolated, and Western blot analysis was performed using anti-AR antibody. Total cell lyates prepared from parallel samples were also analyzed using anti-AR antibody. The *β*-Actin antibody (Sigma, St. Louis, MO) was used as a loading control. Panel B, LNCaP cells grown on coverslips were treated with 4 h hypoxia. Cells were then incubated for 2 h under normoxic conditions, fixed, and stained with anti-AR antibody or with normal rabbit IgG. PI staining shows the location and integrity of the nuclei. Green fluoresence represents AR and red fluorescence represents PI staining. Samples incubated with normal rabbit IgG showed diffuse background signals (data not shown).

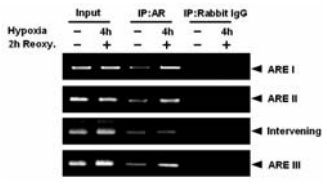

Figure 10. Hypoxia increases PSA promoter occupancy by AR. LNCaP cells were treated with 4 h hypoxia, incubated for 2 h under normoxic conditions, and processed for ChIP assays. The PCR primers derived from the proximal PSA promoter region that contained the ARE at 5' – 170 bp. Input shows results obtained from DNA that was PCR amplified from chromatin extracts before immunoprecipitation. Rabbit IgG lane shows PCR results obtained after immunoprecipitation with rabbit IgG. Gels are representative of three independent experiments.

Increased AR trans-activation by hypoxia is ligand-dependent. The effect of AR is mediated primarily through binding to androgen. However, numerous studies have suggested that the AR can also be activated by ligand-independent mechanisms. In order to test whether the increased AR activity induced by hypoxia is ligand-dependent or ligand-independent, experiments were carried out using androgen-depleted charcoal-stripped FBS (CS-FBS) medium. LNCaP cells were switched to the CS-FBS medium at 24 h prior to hypoxia treatment. The cells were then treated with 4 h of hypoxia, nuclear extracts were isolated, and EMSA was performed. Our results revealed that the increased ARE-binding activity induced by hypoxia was abrogated completely in cells cultured in androgen-depleted medium, which indicates that the binding of androgen to AR is necessary for the AR stimulatory effect exerted by hypoxia (Figure 11A). In addition, the steady state ARE-binding activity of AR observed in LNCaP cells grown in normal FBS medium was lost when cells were cultured in androgen-depleted medium. Subsequent AR chromatin immmunoprecipitation assays corroborated that increased AR trans-activation by hypoxia is ligand-dependent. The increased promoter occupancy induced by hypoxia was not observed in cells cultured in androgen-depleted CS-FBS medium (Figure 11B).

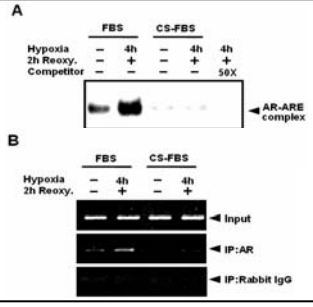

Figure 11. Hypoxia-mediated increase of AR activation and the PSA promoter occupancy of AR are androgen-dependent. Panel A, LNCaP cells grown in normal FBS medium or in charcoal-stripped FBS (CS-FBS)-containing medium were treated with hypoxia for 4 h. Cells were then incubated at normoxic conditions for 2 h, and processed for EMSA using radiolabeled ARE-containing oligonucleotide as a probe. Unlabelled oligonucleotides were used as a competitor. Panel B, ChIP assays were performed in LNCaP cells treated as above using anti-AR antibody. Input shows results obtained from DNA that was PCR amplified from chromatin extracts before immunoprecipitation. Rabbit IgG lane shows PCR results obtained from chromatin extracts immunoprecipitated with rabbit IgG.

When the synthetic androgen R1881 (10 nM) was supplemented to the CS-FBS medium during hypoxia treatment, the AR stimulatory effect of hypoxia was restored and the increased promoter occupancy was again observed (Figure 12A). In those cells grown in normal FBS medium, AR promoter occupancy was further increased when R1881 (10 nM) treatment was combined with hypoxia. Since the AR stimulatory effect of hypoxia was further enhanced when R1881 was added to normal FBS medium, we were curious to find out whether hypoxia might sensitize the AR to androgen. To answer this question, we treated cells in CS-FBS medium with increasing concentrations of R1881, either alone or in combination with hypoxia. As shown in Figure 12B, R1881 alone at concentrations below < 1 nM did not stimulate ARE-luciferase activity. However, hypoxia greatly enhanced the effectiveness of these lower concentrations of R1881. Hypoxia treatment increased ARE-luciferase activity by 14 fold in 0.01 nM R1881, and by 8 fold in 0.1 nM R1881 supplemented CS-FBS medium when compared with to cells treated with R1881 alone at the respective concentrations. The above results were were reported ***(Cancer Research, 2006, also see Appendix 1)***.

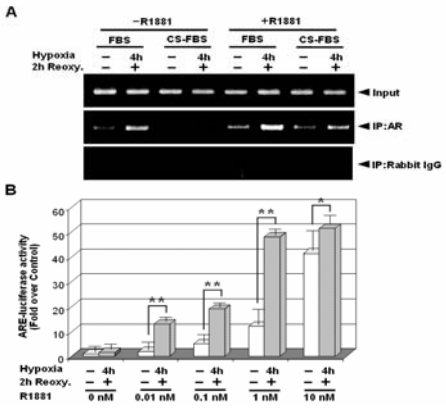

Figure 12. Hypoxia sensitizes the AR to androgen. Panel A, LNCaP cells grown in normal FBS medium or in charcoal-stripped FBS (CS-FBS)-containing medium were treated with 4 h hypoxia with or without R1881 (10 nM) supplementation. Cells were then incubated for 2 h at normoxic condition and processed for ChIP assays using anti-AR antibody. Panel B, LNCaP cells grown in charcoal-stripped FBS (CS-FBS) were transfected with an ARE-luciferase vector. At 24 h after transfection, cells were treated with indicated concentrations of R1881 for 4 h at normoxic condition or at hypoxic condition. Cells were then incubated for an additional 2 h at normoxic condition and processed for ARE-luciferase activity assays. Normalized mean luciferase activity measured in cells transfected with ARE-luciferase without R1881 or hypoxia treatment was set to 1.0. *P* ** < 0.01 compared with R1881 treatment alone. Values are expressed as the means ± SD of triplicate samples.

Effect of Prx1 level on PSA expression and AR activity by hypoxia. We determined whether Prx1 affects PSA levels, a marker used to monitor the progression of prostate cancer. As shown in Figure 13, we found increased PSA secretion after hypoxia treatment. Moreover, the amounts of secreted PSA were significantly increased by Prx1 over-expression. To investigate whether elevated PSA secretion by Prx1 resulted from increased PSA mRNA levels, we carried out RT-PCR analysis using PSA specific primers and found an up-regulation of PSA mRNA and protein by hypoxia (Figure 14A). We also found that Prx1 over-expression increased hypoxia-responsive PSA protein expression (Figure 14B). These results suggest an important role for Prx1 in regulating PSA expression in response to hypoxia. Since PSA is regulated by AR, we examined whether Prx1 affects the DNA-binding activity of AR to ARE that contains the AR consensus-binding motif. We found that hypoxia induces AR-ARE complex formation (Figure 15), indicating that AR is activated by hypoxia. We also found that Prx1 increases hypoxia-responsive AR-ARE formation.

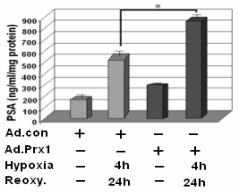

Figure 13. Effect of Prx1 over-expression on PSA secretion. PSA secretion by ELISA kit (Beckman Coulter). Samples were harvested at 24 h after hypoxia treatment. Values, means ± SD (n=3). **P* < 0.05 vs. Ad.con.

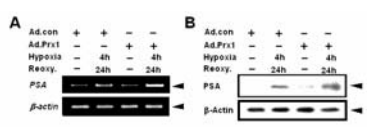

Figure 14. Effect of Prx1 over-expression on PSA regulation. Panel A. RT-PCR analysis of PSA. Panel B. Western blot with the PSA Ab (Labvision).

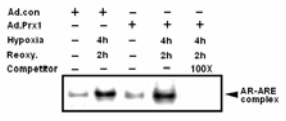

Figure 15. Effect of Prx1 over-expression on AR ARE-binding activity in response to hypoxia. Cells were harvested at 2 h after hypoxia treatment. Gel shift assay using radiolabeled ARE-oligonucleotide as a probe (Santa Cruz).

To examine if Prx1 also regulates ligand stimulated AR activity, we treated LNCaP cells with a physiological level (10 nM) of synthetic androgen R1881. Our data clearly demonstrated that Prx1 increases the ARE-binding activity and trans-activating activity of AR in androgen stimulated cells (Figure 16). We generated the shRNA to knock-down the expression of Prx1. A scrambled sequences from the selected target sequence were also designed to create a control shRNA. The U6-driven shRNA were generated by PCR using the pGEM U6 promoter template. The PCR primers were directed to the U6 cassette with the addition of the selected target sequence. The resulting PCR products were cloned into the TOPO vector by using the pENTR directional TOPO cloning kit (Invitrogen). The Prx1 shRNA constructs were tested for their ability to knock down Prx1 expression in LN3 cells. Out of the four constructs we tested, one construct containing the sequence 5'-CTTCAAAGCCACAGCTGTTCTCAAGAGAAACAG CTGTGGCTTTGAAGTT-3' was found to be most efficient. The control shRNA did not affect Prx1 expression (Figure 17). As shown in Figure 18, Prx1 knock-down reduced PSA mRNA accumulation in both LN3 sublines in response to hypoxia. The PSA mRNA levels correlated well with PSA protein expression by Western blot analysis.

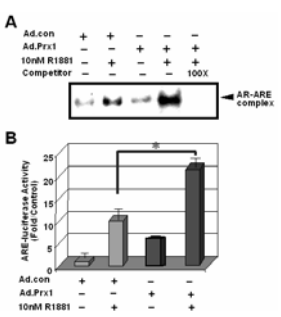

Figure 16. Effect of Prx1 over-expression on AR activity of androgen-treated cells. Panel A. Cells were exposed to R1881 and ARE-binding activity was analyzed by gel shift assay. Panel B. Cells were exposed to R1881 and ARE-luciferase assays were performed. *P < 0.05 *vs.* Ad.con.

Figure 17. Prx1 knock down in LN3 cells. Western blot with the Prx1 Ab. Scrambled: shRNA control. sh. Prx1: sh RNA Prx1. The *β*-Actin antibody was used as a loading control.

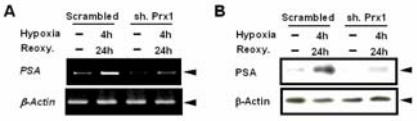

Figure 18. Effect of Prx1 knock-down on PSA regulation. Cells were harvested at 24 h after hypoxia treatment. Panel A. RT-PCR analysis of PSA. Panel B. Western blot with the PSA Ab (Labvision).

Evidences suggesting an interaction of Prx1 and androgen receptor. Since AR translocates to the nucleus upon activation, we examined a subcellular distribution of AR in Ad.con and Ad.Prx1 infected LNCaP cells. As shown in Figure 19, we found an increased AR nuclear translocation in Prx1 over-expressing cells in response to hypoxia. We next carried out confocal microscopy analysis and found a co-localization of Prx1 and AR in the nucleus after hypoxia treatment (Figure 20). We next examined a possible interaction of Prx1 and AR using immunoprecipitation (IP) assays. As shown in Figure 21, IP and reciprocal IP with Prx1 and AR Ab suggest a physical interaction of Prx1 and AR in response to hypoxia. These results are consistent with the nuclear staining of Prx1 in human prostate cancer tissues and suggest a physiological relevance of Prx1 nuclear staining in advanced prostate cancer. It is our working hypothesis that Prx1 physically interacts with AR to increase AR nuclear translocation and its trans-activating activity. The AR activity-enhancing function of Prx1 is very likely to contribute to the malignant progression and emergence of aggressive prostate cancer.

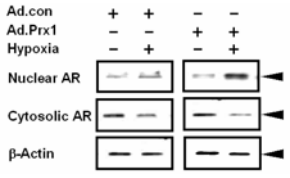

Figure 19. Effect of Prx1 over-expression on AR nuclear localization. Nuclear and cytosolic extracts obtained from LNCaP cells 2 h after hypoxia treatment was analyzed by Western blot using anti-AR Ab.

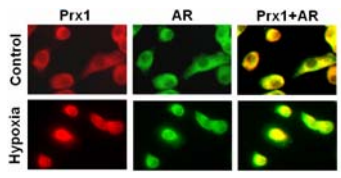

Figure 20. Nuclear co-localization of Prx1 and AR. Cells were treated with hypoxia, fixed and stained with anti-Prx1 or anti-AR Ab followed by anti-rabbit Alexa 488 (red, Prx1) or anti-mouse Alexa 594 (green, AR). Yellow, merged image. Cells incubated with rabbit- or mouse-IgG showed diffuse background signals (data not shown).

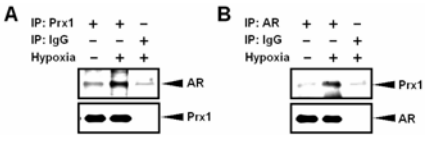

Figure 21. Prx1 and AR Immunoprecipitation analysis. Cells treated as in Fig. 21 were subjected to IP and reciprocal IP with anti-Prx1 (Panel A) or anti-AR Ab (Panel B). Rabbit- and mouse IgG, non specific control.

Analysis of protein redox modification by hypoxia. Accumulated experimental and clinical evidences suggest that hypoxia-response is one of the critical factors determining survival and progression of cancer cells. However, limited information is available on how cancer cells sense hypoxia and activate/integrate relevant biological pathways. We have attempted to identify molecules that are sensitive to redox-changes induced by hypoxia. The pK_a value of most protein thiol residues is about 8.5. Thus, most thiol containing molecules do not readily react with ROS at neutral pH. Only those proteins containing reactive thiols will readily react with and get oxidized by ROS due to their lower pK_a values. It is our working hypothesis that a subset of redox-sensitive molecules are oxidized by hypoxia and the effects of Prx1 are exerted *via* its ability to control the oxidation/function of a subset of redox-sensitive proteins. A first step to test this hypothesis is to identify these redox-sensitive proteins. We have established a modified proteomics approach to visualize the redox-sensitive proteins. We employed a thiol specific agent, N-(biotinyl)-N'-(iodoacetyl) ethylenediamine (BIAM, Molecular Probes) with some modifications of the previously described procedure (8). A schematic of the modified thiol proteomics approach is depicted in Figure 22.

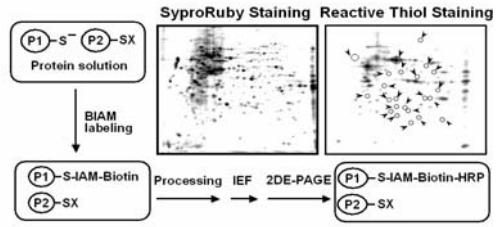

Figure 22. Schematics and display of BIAM labeling of reactive thiol-containing proteins. Protein extracts were labeled with BIAM at pH 6.5. One sample was processed for total protein staining by SyproRuby, and another processed for reactive thiol-containing proteins by HRP-conjugated streptavidin.

We carried out time course experiments in LNCaP cells to characterize the global redox change profiles of BIAM-labeled proteins following hypoxia treatment. Our data demonstrated that hypoxia treatment affects the redox status of a significant number of proteins. Results presented in Figure 23 demonstrate that the redox-sensitive molecules can be detected by the BIAM-labeling procedure and hypoxia-responsive changes of their redox status can be monitored by the modified proteomics approach we have developed. To gain further insight into the pattern of protein thiol redox changes induced by hypoxia, we analyzed the time course changes of BIAM-labeled proteome profiles by PDquest (BioRad version 7.2). High-level match set analysis algorithms were employed to obtain the normalized intensity values described in our recent work (9). Parallel time course experiments without hypoxia treatment were also carried out as controls. The values were transformed into $\log_2$ scale and the bioinformatics-based statistical analyses were carried out in collaboration with Dr. Haitao Zhang at our institute Scatter plot and Pearson's correlation analysis was first performed to probe significant changes of BIAM-labeled proteome profiles in response to hypoxia. Next, to obtain further insight, clustering analysis was performed using the Hierarchical Clustering Explorer software from the University of Maryland. The analysis was based on the average linkage method with the similarity matrix computed from the Euclidean Distance. The normalized intensity values were then used to calculate the treatment to control signal ratios for each spot and subjected to clustering analysis using the Self Organizing Maps (SOM) algorithm (10). This analysis was performed using custom PERL scripts and the GeneCluster 2.0 program from the Center for Genome Research, Whitehead Institute. Six distinct patterns of redox changes evolved from the SOM analysis (Figure 24). These and related findings were reported ***(Prep. Biochem and Biotech., 2006, also see Appendix 2).*** This study led to a productive collaboration with Dr. Clement Ip, a colleague at our Institute. We showed that an organic selenium compound, methylseleninic acid (MSA) causes global thiol/disulfide redox modification of numerous proteins that are distributed in various subcellular compartments ***(Prep. Biochem. and Biotech.,***

2006, also see Appendix 3). Since these changes are expected to lead to protein misfolding, we investigated whether the accumulation of misfolded proteins initiates the "unfolded protein response" or UPR. We found that endoplasmic reticulum stress signal mediators are targets of selenium action and identified Grp78 as one of the key players ***(Oncogene, 2006, also see Appendix 4).*** These studies demonstrate the broader applicability of the modified thiol proteomics approach in cancer research. It is noteworthy that thiol redox-modification patterns caused by selenium are clearly distinct from those obtained from the cells exposed to hypoxia.

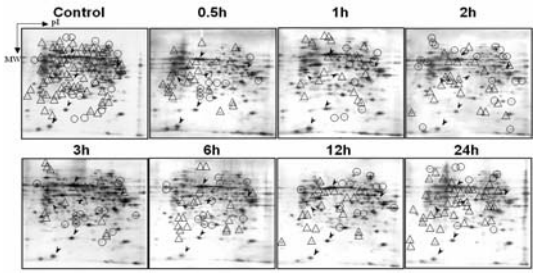

Figure 23. Changes of BIAM-labeled proteome profiles after hypoxia. Starting from the control panel and moving across the timeline, triangles and circles denote the protein spots of which BIAM labeling intensity was decreased or increased, respectively, after hypoxia treatment. The arrows denote representative internal control spots used for normalization.

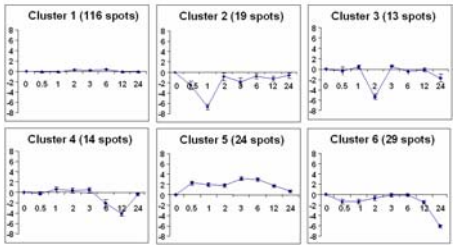

Figure 24. The SOM clustering analysis of hypoxia-responsive changes of BIAM labeled proteins. Data from Figure 27 were analyzed by SOM. The Y-axis represents the $\log_2$-transformed treatment/control ratio. Values, mean ± SEM.

Plans

We will continue to investigate the molecular mechanisms by which Prx1 regulates hypoxia-mediated PSA expression and AR activation, which include the effect of Prx1 levels on NC-dimerization and ligand binding activity of AR. Upon finishing these experiments, we plan on reporting our findings that Prx1 enhances hypoxia-induced AR activity. In addition, we found that the interaction of Prx1 with AR requires hypoxia-induced oxidation of the Prx1 active site Cys^{52}-SH to Cys^{52}-$SO_{2/3}H$. Hyper-oxidation of Cys^{52} is known to play a critical role in the structural and functional switching of Prx1 from an enzyme to a molecular chaperone. Our continuing research will also include the in-depth analyses of these new findings.

Task 3. To test the prognostic value of Prx1 in disease relapse and progression (Months 12-36)

The research accomplished this year strongly supports the role of Nrf2 in regulating Prx1 trans-activation. We will analyze the he prognostic value of Nrf2 activation (nuclear expression) as well as Prx1. We have optimized the Nrf2 immunohistochemistry conditions as well as Prx1. We will establish a detailed database of patient cohorts by medical chart review. We will also Identify the human CaP tissue specimens that match with the established database for subsequent statistical analyses.

Key Research Accomplishments

- Cloning and characterization of the human Prx1 promoter
- Identifying the critical regulatory components responsible for Prx1 up-regulation prostate cancer cells
- Establishing the role of hypoxia on AR trans-activation and PSA expression
- Delineating the molecular mechanisms of hypoxia-induced AR activation

- Identifying the effect of Prx1 in enhancing hypoxia-induced AR activation
- Developing the modified thiol proteomics approach to characterize proteins whose redox status is sensitively modulated by hypoxia

Reportable Outcomes

The following four manuscripts resulted from this research.

Soo-Yeon Park, Yun-Jeong Kim, Allen Gao, James Mohler, Sergio Onate, Hidalgo AA, Clement Ip, Park Eun-Mi, Sun-Young Yoon and Young-Mee Park
"Hypoxia increases androgen receptor activity in prostate cancer cells"
Cancer Research, 66 (10):5121-5129, 2006

Eun-Mi Park, Kyoung-Soo Choi, Soo-Yeon Park, Sun-Hee Baek, Rama Dey-Rao, Haitao Zhang, Yeul Hong Kim, Clement Ip, Park JH, and Young-Mee Park
Preparative Biochemistry and Biotechnology, 36:65-79, 2006

Jong-Sik Lee, Yong-Beom Ma, Kyoung-Soo Choi, Sun-Hee Baek, Ke Zu, Haitao Zhang, Clement Ip, Soo-Yeon Park, Yeul Hong Kim, Eun-Mi Park, and Young-Mee Park
"Neural network-based analysis of thiol proteomics data in identifying potential selenium targets"
Preparative Biochemistry and Biotechnology, 36:37-64, 2006

Ke Zu, T. Bihani, A. Lin, Young-Mee Park, K. Mori and Clement Ip
"Enhanced selenium effect on growth arrest by BiP/GRP78 knockdown in p53-null human prostate cancer cells"
Oncogene, 25:546-554, 2006

Conclusions

Hypoxia has been proposed to function as a microenvironmental pressure to select for a subset of cancer cells with an increased ability to survive and proliferate. The activation of Nrf2 and the up-regulation of *prx1* expression by changes of oxygenation are likely to contribute to the malignant progression of cancer and to modify the efficacy of chemo- and radiotherapies. The information provided in the current study suggests that the Nrf2-Prx1 axis may serve as a fruitful target for cancer prognosis and therapy. Identifying the key regulatory components and understanding the molecular basis of *prx1* gene regulation by Nrf2 are critical to the development of intervention strategies. Future research will be aimed at finding out whether Nrf2-Prx1 activation can be suppressed by genetic and/or pharmacological approaches, and whether suppressing the Nrf2-Prx1 axis will inhibit the malignant progression or reverse treatment resistance in pre-clinical models.

We provide the first evidence that suggests hypoxia increases AR function in human prostate cancer cells and Prx1 enhances the hypoxia-mediated AR activation Delineating the molecular mechanisms by which hypoxia affects AR function will provide insight into the treatment resistance and malignant progression of prostate cancer cells. Novel therapeutic approaches should be developed to prevent hypoxia and/or its consequences to enhance the efficacy of androgen deprivation therapy, a treatment that has not been Improved significantly since its introduction over 50 years ago.

We believe that this study will provide vital new information to delineate the molecular mechanisms by which Prx1 regulates the behavior of prostate cancer cells and promote its

malignant progression. The information generated and the approaches we have taken in this study will serve as a fundamental basis upon which the role of Prx1 can be elucidated in prostate cancer and in other human malignancies, ultimately leading to the development of new prognostic/therapeutic approaches.

References

1. Greco, O., Marples, B., Joiner, M. C., and Scott, S. D. How to overcome (and exploit) tumor hypoxia for targeted gene therapy. J Cell Physiol, *197:* 312-325, 2003.
2. Jeanmougin, F., Thompson, J. D., Gouy, M., Higgins, D. G., and Gibson, T. J. Multiple sequence alignment with Clustal X. Trends Biochem Sci, *23:* 403-405, 1998.
3. Bailey, T. L. and Elkan, C. Fitting a mixture model by expectation maximization to discover motifs in biopolymers. Proc Int Conf Intell Syst Mol Biol, *2:* 28-36, 1994.
4. Berezikov, E., Guryev, V., Plasterk, R. H., and Cuppen, E. CONREAL: conserved regulatory elements anchored alignment algorithm for identification of transcription factor binding sites by phylogenetic footprinting. Genome Res, *14:* 170-178, 2004.
5. Nguyen, T., Sherratt, P. J., and Pickett, C. B. Regulatory mechanisms controlling gene expression mediated by the antioxidant response element. Annu Rev Pharmacol Toxicol, *43:* 233-260, 2003.
6. Ishii, T., Itoh, K., Takahashi, S., Sato, H., Yanagawa, T., Katoh, Y., Bannai, S., and Yamamoto, M. Transcription factor Nrf2 coordinately regulates a group of oxidative stress-inducible genes in macrophages. J Biol Chem, *275:* 16023-16029, 2000.
7. Xu, C., Li, C. Y., and Kong, A. N. Induction of phase I, II and III drug metabolism/transport by xenobiotics. Arch Pharm Res, *28:* 249-268, 2005.
8. Kim, J. R., Yoon, H. W., Kwon, K. S., Lee, S. R., and Rhee, S. G. Identification of proteins containing cysteine residues that are sensitive to oxidation by hydrogen peroxide at neutral pH. Anal Biochem, *283:* 214-221, 2000.
9. Park, E. M., Choi, K.S., Park, S.Y., Kong, E.S., Zhang, H., Ip, C., Park Y.M. A display thiol-proteomics approach to characterize global redox modification of proteins by selenium: Implication for the anticancer action of selenium. Cancer Genomics and Proteomics, *2:* 25-36, 2005.
10. Tamayo, P., Slonim, D., Mesirov, J., Zhu, Q., Kitareewan, S., Dmitrovsky, E., Lander, E. S., and Golub, T. R. Interpreting patterns of gene expression with self-organizing maps: methods and application to hematopoietic differentiation. Proc Natl Acad Sci U S A, *96:* 2907-2912, 1999.

Appendices

Appendix 1. Soo-Yeon Park, Yun-Jeong Kim, Allen Gao, James Mohler, Sergio Onate, Hidalgo AA, Clement Ip, Park Eun-Mi, Sun-Young Yoon and Young-Mee Park
"Hypoxia increases androgen receptor activity in prostate cancer cells"
Cancer Research, 66 (10):5121-5129, 2006

Appendix 2. Eun-Mi Park, Kyoung-Soo Choi, Soo-Yeon Park, Sun-Hee Baek, Rama Dey-Rao, Haitao Zhang, Yeul Hong Kim, Clement Ip, Park JH, and Young-Mee Park
"Analysis of Protein Redox Modification by Hypoxia"
Preparative Biochemistry and Biotechnology, 36:65-79, 2006

Appendix 3. Jong-Sik Lee, Yong-Beom Ma, Kyoung-Soo Choi, Sun-Hee Baek, Ke Zu, Haitao Zhang, Clement Ip, Soo-Yeon Park, Yeul Hong Kim, Eun-Mi Park, and Young-Mee Park
"Neural network-based analysis of thiol proteomics data in identifying potential selenium targets"

Preparative Biochemistry and Biotechnology, 36:37-64, 2006

Appendix 4. Ke Zu, T. Bihani, A. Lin, Young-Mee Park, K. Mori and Clement Ip
“Enhanced selenium effect on growth arrest by BiP/GRP78 knockdown in p53-null human prostate cancer cells”
Oncogene, 25:546-554, 2006

Hypoxia Increases Androgen Receptor Activity in Prostate Cancer Cells

Soo-Yeon Park,[1] Yun-Jeong Kim,[1] Allen C. Gao,[2] James L. Mohler,[3] Sergio A. Onate,[3] Alejandro A. Hidalgo,[3] Clement Ip,[4] Eun-Mi Park,[1] Sun Young Yoon,[1] and Young-Mee Park[1]

Departments of [1]Cell Stress Biology, [2]Medicine, [3]Urologic Oncology, and [4]Cancer Chemoprevention, Roswell Park Cancer Institute, Buffalo, New York

Abstract

Recent studies show that prostate cancer cells are able to survive in a hypoxic tumor environment, and the extent of tumor hypoxia correlates with poor clinical outcome. Androgen deprivation, the most common form of prostate cancer therapy, was itself shown to induce a state of transient hypoxia at the microenvironmental level. Because androgen receptor (AR) signaling plays a critical role in prostate cancer, we investigated the effect of hypoxia in regulating AR function. We found that in LNCaP prostate cancer cells, AR binding to the androgen-responsive element (ARE), prostate-specific antigen accumulation, and ARE-reporter gene activity were increased after hypoxia treatment. Hypoxia-enhanced AR function was also observed when AR was exogenously introduced into AR-null DU145 cells. Confocal microscopy and chromatin immunoprecipitation assays showed that AR translocation to the nucleus and AR recruitment to the prostate-specific antigen promoter were facilitated after hypoxia treatment. The AR stimulatory effect seemed to be ligand-dependent because it was abrogated when cells were cultured in an androgen-depleted medium, but was restored with the addition of R1881, a synthetic androgen. The sensitivity of AR activation to R1881 was also increased after hypoxia treatment. Although concentrations of <1 nmol/L R1881 did not induce ARE reporter activity under normoxic conditions, exposure to hypoxia greatly potentiated the AR response to low levels of R1881. Collectively, our results provide compelling evidence that changes in hypoxia/reoxygenation stimulate AR trans-activation and sensitization. The AR-stimulatory effect of an unstable tissue oxygenation milieu of a tumor is likely to contribute to treatment resistance and the emergence of recurrent prostate cancer. (Cancer Res 2006; 66(10): 5121-9)

Introduction

Every year, an estimated 230,000 new cases of prostate cancer are diagnosed, and approximately 30,000 men will die from prostate cancer in the U.S. (1). Eppendorf pO_2 microelectrode studies of human prostate carcinoma showed that cancer cells can survive and grow in a hypoxic microenvironment (2, 3). Studies suggest that hypoxia in prostate cancer is one of the key factors in determining tumor progression and may also predict clinical outcome (4–7). Hypoxia is a reduction in the normal level of tissue oxygen tension, usually defined as an overall reduced oxygen availability or partial pressure below critical levels (8). Tissue oxygenation within a tumor, however, is highly unstable and heterogeneous as a consequence of the architectural and functional abnormalities of the vascular network (9, 10). Fluctuations in blood flow in the tumor microvasculature can lead to perfusion-limited hypoxia in the tumor parenchyma (11, 12). In terms of the ultrastructure, tumor vasculature has numerous "holes" or "openings," widened interendothelial junctions, and a discontinuous or absent basement membrane (9, 13–15). Aberrant blood vessels can be shut down locally at any time, but the same defects also allow closed vessels to be reopened, resulting in the localized and often acute reoxygenation within a tumor. In addition to the reopening of the temporarily closed/blocked vessels (9, 13–15), dynamic changes of hypoxia/reoxygenation may also occur as a result of regional angiogenesis. A heterogeneous and unstable tissue oxygenation/blood flow milieu of a tumor has been proposed to serve as a selection pressure for a subpopulation of cells with an increased survival advantage to preferentially proliferate (16).

Androgen receptor (AR) plays a critical role in the development, progression, and treatment response of prostate cancer (17, 18). Ligand binding to AR activates the receptor and induces the transcription of AR-regulated genes (17, 19). Because prostate cancer arises as an androgen-dependent cancer, androgen deprivation is the most common form of therapy. Although effective in blocking tumor growth at the beginning, the treatment eventually fails and most men will relapse due to adaptive progression of the surviving prostate cancer cells. The recurrent cancer is commonly referred to as "androgen-independent." However, it usually continues to express AR and AR-regulated genes (20), suggesting a functional role of AR in the survival and growth of recurrent prostate cancer cells. Recently, Mohler et al. (21) showed that androgens are still present in the recurrent prostate cancer tissue at levels that are sufficient to activate AR. These studies suggest that the state of "androgen-independence" may be a misnomer. Prostate cancer that recurs during androgen deprivation therapy may not be "androgen-independent" but continue to depend on AR/androgen for survival and growth. Several other mechanisms have been proposed to explain the abnormal activation of AR in recurrent prostate cancer. These include mutation of AR, AR gene amplification (22–24), or the activation of AR by non-androgen ligands (25–28). Although alterations of the AR gene have been correlated with response to androgen deprivation therapy, the majority of patients do not have AR mutations or amplification, and retain active AR signaling (29, 30).

Studies with castrated rat, transgenic mouse, and xenograft models all suggest that androgen deprivation generates a state of

Requests for reprints: Young-Mee Park, Department of Cell Stress Biology, Roswell Park Cancer Institute, Buffalo, NY 14263. Phone: 716-845-3190; Fax: 716-845-8899; E-mail: young-mee.park@roswellpark.org.

doi:10.1158/0008-5472.CAN-05-1341

transient hypoxia in the prostate tissue (31–33). Androgen deprivation causes rapid endothelial cell death, degeneration of capillaries, and vasoconstriction in the prostate. These studies imply that recurrent prostate cancer cells must survive an acute transient hypoxia in order to survive and undergo clonal expansion. Considering the critical role of the AR in disease progression and treatment response, we hypothesize that unstable, dynamic changes of tissue oxygenation milieu of a tumor influence AR function in some prostate cancer cells, and in doing so, contribute to their survival and malignant progression.

Materials and Methods

Cell culture. LNCaP and DU145 human prostate cancer cells were obtained from the American Type Culture Collection (Manassas, VA). Cells were cultured in RPMI 1640 supplemented with 10% fetal bovine serum (FBS), 2 mmol/L glutamine, 100 units/mL penicillin, and 100 μg/mL streptomycin. In some experiments, cells were switched to a medium containing 2% charcoal-stripped FBS (CS-FBS; Hyclone, Logan, UT) 24 hours prior to hypoxia treatment.

Hypoxia treatment. The culture medium was replaced with deoxygenated RPMI 1640 before hypoxia treatment as reported previously (34). Deoxygenated medium was prepared prior to each experiment by equilibrating the medium with a hypoxic gas mixture containing 5% CO_2, 85% N_2, and 10% H_2 at 37°C. The oxygen concentration in the hypoxic chamber and the exposure medium was maintained at <0.05%, and was monitored by using an oxygen indicator (Forma Scientific, Marietta, OH). All experiments were done at 70% to 80% confluency at a pH between 7.2 and 7.4 for the duration of the experiment.

Western blot analysis. Equal amounts of protein were analyzed in duplicate by SDS-PAGE. Protein concentrations were measured by the method of Lowry et al. (35). One gel was stained with Coomassie blue, destained and dried for recordkeeping. A second gel was transferred to a nitrocellulose membrane in a Trans-Blot apparatus (Bio-Rad, Hercules, CA) for Western blot analysis. The following monoclonal antibodies were used: anti-AR (Santa Cruz Biotechnology, Santa Cruz, CA), anti–prostate-specific antigen (PSA; Lab Vision, Fremont, CA), anti-HIF-1α (BD Biosciences, San Jose, CA), and anti-β-actin (Sigma, St. Louis, MO). Immunoreactive proteins were detected with secondary antibody and visualized using an enhanced chemiluminescence detection system (Amersham Pharmacia Biotech, Piscataway, NJ).

Transfection and luciferase assay. An aliquot of 3×10^5 cells was placed in a six-well plate and transfected with DNA using LipofectAMINE PLUS reagent (Invitrogen, Carlsbad, CA) according to the manufacturer's instruction. The pSG5hAR expression vector (36) was used to express AR. The androgen-responsive element (ARE)–luciferase reporter plasmid was used to assess AR trans-activation. This construct contains three repeats of the ARE ligated in tandem with the luciferase reporter (37). The total amount of plasmid DNA was normalized to 1 μg/well by the addition of empty plasmid. Luciferase activity was determined by using the Luciferase assay system (Promega, Madison, WI). Luciferase activities were normalized by protein concentration and transfection efficiency. To monitor the transfection efficiency, pCMVβ (Clontech, Palo Alto, CA) was transfected and β-Gal assay was done with the β-Gal enzyme assay system (Promega). All transfection experiments were done in triplicate wells and repeated at least thrice.

Nuclear and cytosol lysate preparation. Nuclear and cytosol lysates were prepared as described previously (38). Briefly, cells were harvested, washed twice with PBS, resuspended in a hypotonic buffer [10 mmol/L HEPES-KOH (pH 7.9), 1.5 mmol/L $MgCl_2$, 10 mmol/L KCl, and 0.1% NP40] and incubated on ice for 10 minutes. Nuclei were precipitated with 3,000 × *g* centrifugation for 10 minutes at 4°C. After washing once with the hypotonic buffer, nuclei were lysed in a lysis buffer [50 mmol/L Tris-HCl (pH 8.0), 150 mmol/L NaCl, and 1% Triton X-100], incubated on ice for 30 minutes and precleared with 20,000 × *g* centrifugation for 15 minutes at 4°C. To prepare the cytosol lysate, cells were collected and resuspended in 50 mmol/L Tris-HCl (pH 7.4) containing 0.25 mol/L sucrose, 0.1 mmol/L EDTA, 0.7 mmol/L 2-mercaptoethanol, and 2 mmol/L disopropyl fluorophosphate. The cell suspensions were sonicated and centrifuged at 105,000 × *g* for 1 hour at 4°C.

Electromobility gel shift assay. Twenty micrograms of nuclear protein extract was incubated in 20 μL of a solution containing 10 mmol/L HEPES (pH 7.9), 80 mmol/L NaCl, 10% glycerol, 1 mmol/L DTT, 1 mmol/L EDTA, 100 μg/mL poly(deoxyinosinic-deoxycytidylic acid), and radiolabeled double-stranded oligonucleotide containing the AR consensus binding motif 5′-CTAGAAGTCTGGTACAGGGTGTTCTTTTTGCA-3′ (Santa Cruz Biotechnology). ARE-binding complexes were resolved on a 4.5% nondenaturing polyacrylamide gel containing 2.5% glycerol in 0.25× Tris-borate/EDTA at room temperature, and the results were autoradiographed. ARE-binding activity was quantitated by using the Molecular Imager FX System (Bio-Rad). For AR supershift experiments, 20 μg of nuclear protein extract was incubated with the monoclonal AR antibody (Santa Cruz Biotechnology) for 1 hour at 4°C before incubation with the γ-^{32}P ATP radiolabeled probe. The DNA binding activity of HIF-1α was determined by electromobility gel shift assay (EMSA) by using radiolabeled double-stranded oligonucleotide containing the HIF-1α binding motif 5′-TCTGTACGTGAC-CACACTCACCTC-3′ (Santa Cruz Biotechnology).

RNA isolation and RT-PCR analysis. Total RNA was isolated as described previously (34). The RNA was dissolved in DNase I buffer and incubated for 15 minutes with RNase-free DNase I (20 units/mL) in the presence of RNasin. The RNA concentration was determined by measuring UV absorption and samples with comparable A_{260}/A_{280} ratios were used for RT-PCR analysis. Sequences of the PCR primer pairs used for the amplification of *PSA* were: forward 5′-GGCAGGTGCTTGTAGCCTTCTC-3′, and reverse 5′-CACCCGAGCAGGTGCTTTTGC-3′; *VEGF*, forward 5′-GAAG-TGGTGAAGTTCATGGATGTC-3′, and reverse 5′-CGATCGTTCTGTATCAG-TCTTTCC-3′; and *β-actin*, forward 5′-GATCGTCTAGATTCCTATGTGGG-CGACGA-3′, and reverse 5′-GATCGGAATTCCAGCGAACCGCTCATTG-3′. PCR was carried out using a thermal cycler (Perkin-Elmer 9600, Boston, MA). The amplified products were separated by electrophoresis on a 1.5% agarose gel, stained with ethidium bromide, and photographed under UV illumination.

PSA ELISA analysis. PSA secretion was quantitated by ELISA following the manufacturer's protocol (Beckman Coulter, Fullerton, CA). The experiments were repeated thrice.

Immunofluorescence and confocal microscopy. Cells were grown on six-well Teflon-coated microscope slides (Erie Scientific, Erie, PA), underwent hypoxia for 4 hours and returned to normoxic CO_2 incubator. After 2 hours of incubation in a CO_2 incubator, cells were fixed in 3.7% formaldehyde for 20 minutes and permeabilized in methanol for 15 minutes on ice. AR-specific polyclonal antibody (Santa Cruz Biotechnology) was diluted (1:500) in antibody dilution buffer [5% BSA, 0.005% saponin in PBS (pH 7.2)] and incubated with fixed cells for 1 hour at room temperature. Slides were immersed in washing buffer [0.005% saponin in PBS (pH 7.2)] for 1 hour. Samples were then incubated for 1 hour at room temperature with Alexa 488 anti–rabbit secondary antibody (Molecular Probes, Eugene, OR) and propidium iodide (50 μg/mL) for nuclear staining. Slides were washed and mounted with coverslips in Vectashield solution (Vector Laboratories, Burlingame, CA). Normal rabbit IgG (Santa Cruz Biotechnology) at 1:100 dilution was used as a negative control. Confocal microscopy was done by using a Bio-Rad MRC 1024 confocal laser scanning microscope. Control cells were processed identically except for the hypoxia treatment.

Chromatin immunoprecipitation assay. Chromatin immunoprecipitation (ChIP) assays were carried out following a previously described procedure (39). Briefly, formaldehyde was added directly to control and hypoxia-treated LNCaP cells. The cross-linking process was limited to <30 minutes because longer incubation with formaldehyde caused cells to aggregate, and prevented efficient sonication of the chromatin. After cross-linking, cells were lysed in lysis buffer containing protease inhibitors. Nuclei were isolated and chromatin was sheared to an average length of 250 to 500 bp using sonication. The sheared chromatin was precleared with salmon sperm DNA/protein A-sepharose and precipitated with an antibody specific to AR (2 μg/mL, Santa Cruz Biotechnology). Rabbit IgG control

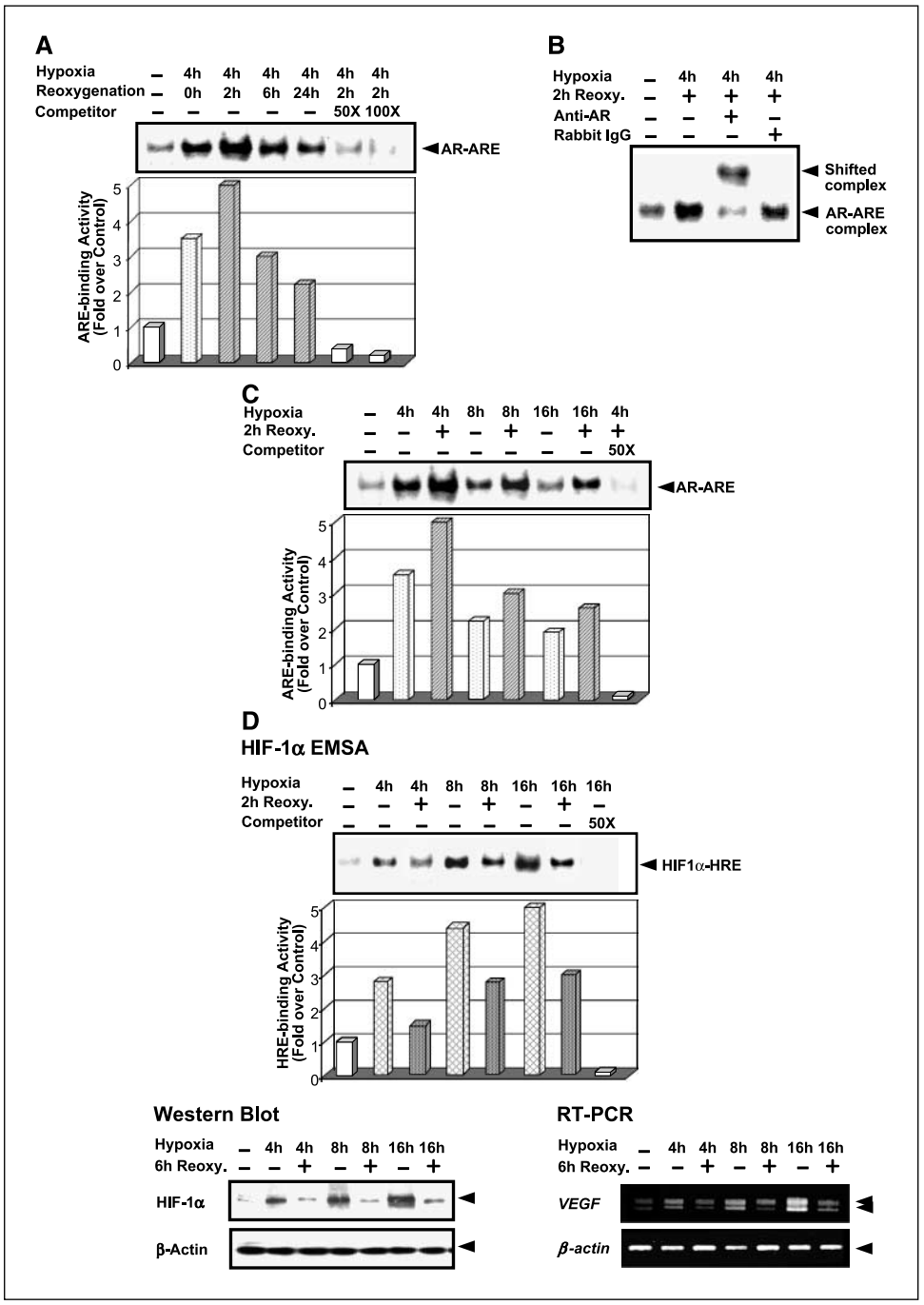

Figure 1. Hypoxia increases AR-ARE binding activity. *A,* LNCaP cells were exposed to 4 hours of hypoxia. Cells were then reoxygenated for up to 24 hours. EMSA was performed at the indicated times after hypoxia treatment. The ARE-containing oligonucleotides (Santa Cruz Biotechnology) radiolabeled with γ-^{32}P ATP (MP Biomedicals, Irvine, CA) were used as a probe. Unlabelled oligonucleotides were used as a competitor. *Arrow,* location of ARE-binding complexes. ARE-binding activity was quantitated using the Molecular Imager FX System (Bio-Rad). *B,* nuclear extracts obtained from LNCaP after 2 hours following 4 hours of hypoxia treatment were subjected to supershift assay using an anti-AR antibody. Specificity was confirmed by using rabbit IgG (Santa Cruz Biotechnology). *Arrows,* positions of AR-ARE and supershifted complexes. *C,* cells were exposed to 4, 8, or 16 hours of hypoxia followed by 2 hours of reoxygenation. AR-ARE binding activities were analyzed by EMSA. *D,* cells underwent 4, 8, or 16 hours of hypoxia followed by 2 hours of reoxygenation. HIF-1α binding activities were analyzed by EMSA using the HIF-1α-responsive element (HRE) containing oligonucleotides (Santa Cruz Biotechnology) as a probe. Unlabelled oligonucleotides were used as a competitor. *Arrow,* location of the HIF1α-HRE binding complexes. Western blot analysis of HIF-1α was carried out after 4, 8, or 16 hours of hypoxia treatment, followed by 6 hours of reoxygenation. The blots were probed with an anti-HIF-1α antibody (BD Biosciences). β-Actin antibody (Sigma) was used as a loading control. RT-PCR analysis of *VEGF* mRNA was carried out after 4, 8, or 16 hours of hypoxia treatment followed by 6 hours of reoxygenation. Two alternatively spliced *VEGF* mRNA, VEGF-121 (*lower band*) and VEGF-165 (*upper band*), were detected in LNCaP cells. *β-Actin* gene was amplified as a control.

was used to monitor nonspecific interactions. Immune complexes were adsorbed onto salmon sperm DNA/protein A-sepharose beads. After an extensive wash to reduce background, Ab/AR/DNA complexes were eluted. After precipitation, DNA was resuspended in water and PCR was carried out to amplify the proximal and upstream ARE regions identified in the *PSA* gene (40, 41). The following primer sequences were used to amplify the proximal (ARE I/II) and upstream ARE regions: ARE I, forward 5′-TCTGCCTTTGTCCCCTAGAT-3′, reverse 5′-AACCTTCATTCCCCAG-GACT-3′; ARE II, forward 5′-GTTGGGAGTGCAAGGAAAAG-3′, reverse 5′-CGCCCAGGATGAAACAGAAA-3′; and ARE III, forward 5′-CCTC-CCAGGTTCAAGTGATT-3′, reverse 5′-GCCTGTAATCCCAGCACTTT-3′. The intervening region between ARE I/II and ARE III regions of the *PSA* gene that does not contain ARE was amplified as a negative control by using forward 5′-CTGTGCTTGGAGTTTACCTGA-3′ and reverse 5′-GCA-GAGGTTGCAGTGAGCC-3′ primer pair. Triplicate PCR reactions were conducted for each sample and the experiments were repeated at least thrice.

Statistical analysis. Statistical significance was examined using Student's *t* tests. The two-sample *t* test was used for two-group comparisons. Values were reported as mean $\pm$ SD. $P < 0.05$ was considered significant and indicated by asterisks in the figures.

Results

ARE-binding activity of AR is increased after hypoxia treatment. LNCaP is a widely used cell model for human prostate cancer studies because it is one of the limited androgen-responsive prostate cancer cell lines. LNCaP cells express a functional AR, and

secrete PSA *in vitro* and *in vivo*. In order to examine whether dynamic changes of hypoxic conditions are capable of influencing AR activity, cells were exposed to hypoxia for 4 hours and returned to a normoxic CO_2 incubator. The ARE-binding activity of AR was analyzed at 0, 2, 6, or 24 hours during reoxygenation after hypoxia treatment. As shown in Fig. 1*A*, significant increases of ARE-binding activities were observed after 4 hours of hypoxia treatment. The increase was evident as soon as the cells were withdrawn from hypoxia, reached a maximum at 2 hours during reoxygenation, and gradually declined with time. The ARE-binding activity was specific because the DNA-binding complexes became undetectable when molar excess of the unlabeled competitor of the ARE probe was added. Supershift assays with an antibody specific to AR confirmed the binding of AR to the ARE-containing probe (Fig. 1*B*). When cells were exposed to a longer period of hypoxia (i.e., 8 or 16 hours) followed by 2 hours of oxygenation, the AR stimulatory effect was also consistently observed, although the maximal AR stimulatory effect was seen after 4 hours of hypoxia treatment (Fig. 1*C*). No appreciable changes of AR protein levels were detected at 2 hours of reoxygenation after 4, 8, or 16 hours of hypoxia treatment (data not shown).

We questioned whether the ability of hypoxia to induce HIF-1α signaling might be a contributing factor to AR activation. As shown in Fig. 1*D*, HIF-1α activities were decreased during reoxygenation after hypoxia treatment. Unlike AR, HIF-1α activities were increased progressively as a function of time of exposure to hypoxia. Consistent with these changes of HIF-1α activities, the levels of HIF-1α protein and *VEGF* mRNA accumulation were increased by longer duration of hypoxia, and decreased during reoxygenation. The decrease of HIF-1α protein and *VEGF* mRNA levels were pronounced at 6 hours of reoxygenation. These results suggest that the mechanisms of AR stimulation by hypoxia/reoxygenation are unique and unlikely to involve HIF-1α signaling. However, a possible cross-talk between the AR and HIF-1α pathways during continuous hypoxia cannot be excluded.

Hypoxia increases AR trans-activation. We wanted to validate the functional significance of the AR-ARE complex formation after transient hypoxia treatment. PSA is one of the best-characterized genes regulated by AR. Because LNCaP cells express and secrete PSA, we examined the changes of PSA regulation after 4 hours of hypoxia treatment. Our results showed an increased accumulation of *PSA* mRNA during reoxygenation following hypoxia treatment (Fig. 2*A*). Consistent with the increased *PSA* mRNA level, increased accumulation of cellular PSA protein and increased secretory PSA in the culture medium were confirmed by Western blot analysis (Fig. 2*B*) and ELISA assay (Fig. 2*C*), respectively.

Activated AR exerts its trans-activation function by binding to the DNA containing an ARE. We next examined the effect of hypoxia on AR trans-activation by transfecting LNCaP cells with an ARE-luciferase reporter construct. As shown in Fig. 2*D*, a significant increase of luciferase activity was observed after hypoxia treatment, confirming that increased trans-activation of AR after hypoxia treatment is not limited to the *PSA* gene. In order to rule out that the increased ARE-luciferase activity was due to increased AR protein level, we carried out Western blot analysis with an anti-AR antibody (*bottom*). We did not detect any change in AR protein levels up to 24 hours after reoxygenation.

To further verify that the effect of transient hypoxia on AR trans-activation was not unique to LNCaP cells, we turned to the DU145 human prostate cancer cells which are devoid of AR. We introduced exogenous wild-type AR together with the ARE-luciferase into the DU145 cells, exposed them to 4 hours of hypoxia, and analyzed the ARE-luciferase activity. As shown in Fig. 3*A*, transient exposure to hypoxia induced the trans-activation of exogenous AR and stimulated ARE-luciferase activity. The pattern of AR activity changes in the DU145 cells was similar to that observed in LNCaP

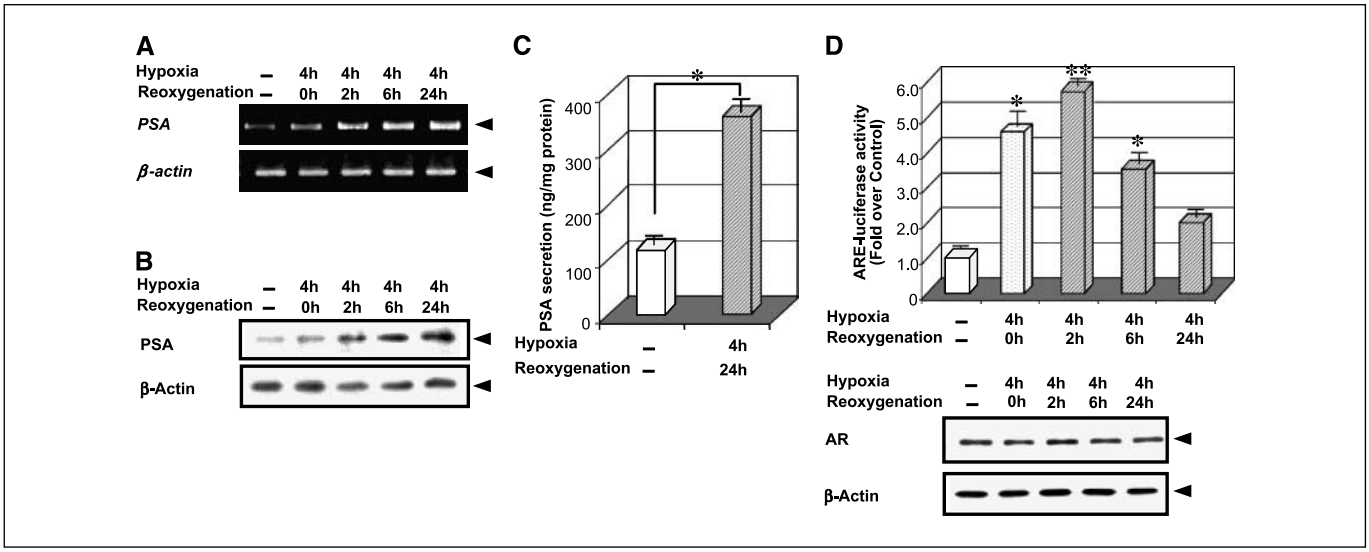

Figure 2. Hypoxia increases PSA expression and induces ARE-luciferase promoter activity. *A,* RT-PCR analysis was carried out at the indicated times after 4 hours of hypoxia treatment with PCR primer pairs specific for the *PSA* gene. *β-Actin* gene was amplified as a control. *B,* equal amounts of proteins obtained from cells treated as in (*A*) were subjected to Western blot analysis using anti-PSA antibody (Lab Vision). β-Actin antibody (Sigma) was used as a loading control. *C,* the amounts of the secreted PSA in the medium were determined using ELISA after 4 hours of exposure to hypoxia followed by 24 hours of reoxygenation. *Columns,* mean of triplicate samples; *bars,* ±SD. *, $P < 0.05$ compared with control. *D,* cells were transfected with the ARE-luciferase construct. At 24 hours after transfection, cells were exposed to 4 hours of hypoxia and the luciferase activity was analyzed at the indicated time points after hypoxia treatment. Normalized mean luciferase activity measured in ARE-luciferase transfected cells without hypoxia treatment (control) was set to 1.0. **, $P < 0.01$; *, $P < 0.05$ compared with controls. Aliquots of cells used in luciferase assays were processed for Western blot analysis and probed with AR-specific antibody (Santa Cruz Biotechnology). The β-actin antibody (Sigma) was used as a loading control.

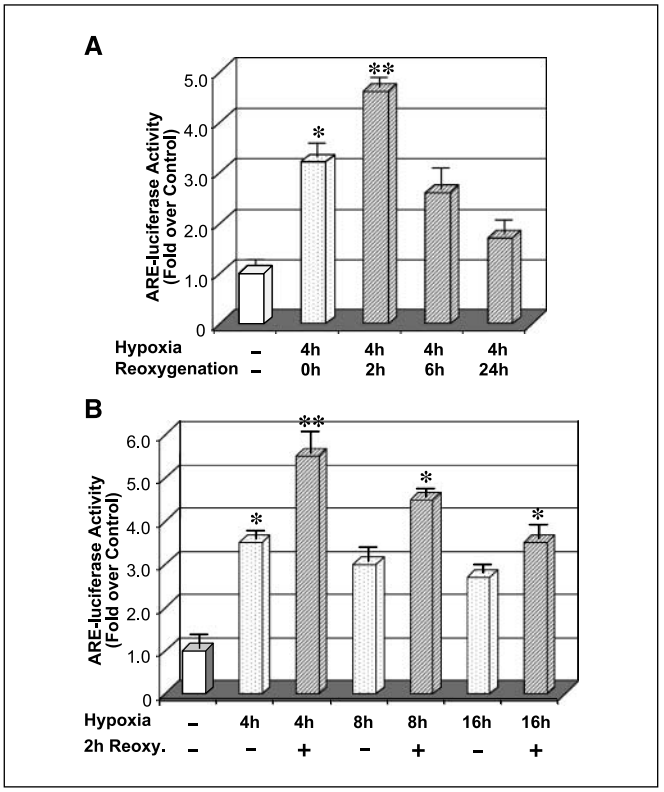

Figure 3. Effect of hypoxia on exogenous addition of AR in DU145 cells. *A,* DU145 cells were cotransfected with wild-type AR containing pSG5hAR and ARE-luciferase reporter plasmids. At 24 hours after transfection, cells were exposed to 4 hours of hypoxia and luciferase activities were measured at the indicated time points after hypoxia treatment. Normalized mean luciferase activity measured in cells transfected with pSG5hAR and ARE-luciferase without hypoxia treatment was set to 1.0. **, $P < 0.01$; *, $P < 0.05$ compared with controls. *B,* cells transfected with pSG5hAR and ARE-luciferase vectors underwent 4, 8, or 16 hours of hypoxia followed by 2 hours of reoxygenation. Luciferase activities were measured, and analyzed as described above.

cells. When the DU145 cells were exposed to longer periods of hypoxia, the maximal AR stimulatory effect of hypoxia was also seen after 4 hours of hypoxia treatment. Collectively, these data validate our conclusion that dynamic changes of hypoxia/reoxygenation enhance AR-ARE binding activity and AR target gene expression.

Hypoxia stimulates the nuclear translocation of AR and its promoter occupancy. Activated AR translocates from the cytosol to the nucleus to trans-activate its target genes. To examine the effect of hypoxia/reoxygenation on the subcellular distribution of AR, LNCaP cells were treated with 4 hours of hypoxia followed by 2 hours of reoxygenation. Nuclear and cytosolic extracts obtained from control and hypoxia-treated cells were subjected to Western blot analysis. As shown in Fig. 4*A*, transient hypoxia increased nuclear AR and decreased cytosolic AR, but did not affect total AR levels. Increased nuclear localization of AR was further confirmed by immunofluorescent cell staining and confocal microscopy (Fig. 4*B*). Propidium iodide staining of the same cells verified the location and integrity of the nuclei. Virtually identical results were obtained in DU145 cells after the exogenous introduction of AR (data not shown).

The next step was to examine whether hypoxia increased the recruitment of AR to the promoter of its target gene in the natural chromatin milieu. ARE I/II are in the proximal promoter region at ~163 and ~390 bp, respectively, whereas ARE III resides at ~4 kb upstream of the *PSA* transcription site (40). We carried out ChIP assays on these AREs with the AR-specific antibody. A schematic diagram of these three ARE regions is shown in Fig. 5*A*. To control for possible nonspecific interactions and DNA contaminations of the solutions, samples precipitated with rabbit IgG were included. As shown in Fig. 5*B*, our results showed that transient hypoxia clearly increased the AR occupancy of ARE regions in the *PSA* gene. The recruitment of AR to ARE I/II and ARE III was specific as no signal was detected in the rabbit IgG control samples. We did not find an increase of AR recruitment to the nonspecific intervening region located between the proximal and upstream AREs. The results obtained from the DNA that was PCR-amplified from chromatin extracts before immunoprecipitation (input) are shown for comparison.

Increased AR trans-activation by hypoxia is ligand-dependent. Although the effect of AR is known to be mediated through ligand binding, numerous studies have suggested that AR can also be activated by ligand-independent mechanisms. In order to determine whether hypoxia-enhanced AR activity is ligand-dependent or ligand-independent, we carried out the following experiment in a CS-FBS medium. LNCaP cells were switched to the CS-FBS medium 24 hours prior to hypoxia treatment. Cells were then exposed to 4 hours of hypoxia followed by 2 hours of reoxygenation. Nuclear extracts were isolated, and EMSA was done.

Our results showed that hypoxia induction of ARE-binding activity was abrogated completely in cells cultured in an androgen-depleted medium, suggesting that the binding of androgen to AR is necessary for the AR stimulatory effect (Fig. 6*A*). Not surprisingly, the steady state ARE-binding activity of AR was also lost under androgen deprivation. Subsequent AR ChIP assays corroborated that increased AR trans-activation by transient hypoxia is ligand-dependent because increased promoter occupancy was not observed in cells cultured in an androgen-depleted CS-FBS medium. Figure 6*B* shows the data from the ARE I region, although similar results were obtained from the other ARE regions.

When the synthetic androgen, R1881 (10 nmol/L), was supplemented to the CS-FBS medium, the AR stimulatory effect of hypoxia was restored and the increased promoter occupancy of AR was again observed (Fig. 6*C*). In those cells grown in a normal FBS medium, AR promoter occupancy was further increased when R1881 was combined with hypoxia. We were curious to find out whether hypoxia might sensitize the AR to androgen. To answer this question, we treated cells in a CS-FBS medium with increasing concentrations of R1881, either alone or in combination with hypoxia. As shown in Fig. 6*D*, R1881 alone at concentrations <1 nmol/L did not stimulate ARE-luciferase activity. However, hypoxia greatly enhanced the effectiveness of lower concentrations of R1881. The AR-sensitizing effect of hypoxia was most dramatic at subphysiologic R1881 concentrations (<1 nmol/L). The magnitude of AR sensitization by hypoxia was less pronounced at physiologic levels of R1881 (10 nmol/L) when AR might be saturated with the ligand. Our results showed that hypoxia enhances AR sensitivity without noticeably affecting AR levels at a given concentration of R1881 (*bottom*). Treatment with R1881 alone slightly increased the AR levels. Similar results were obtained when the exogenous AR was introduced into DU145 cells. The magnitude of AR sensitization was comparable to that observed in LNCaP cells (data not shown). These results suggest that hypoxia sensitizes AR trans-activating activity to subphysiologic levels of androgen.

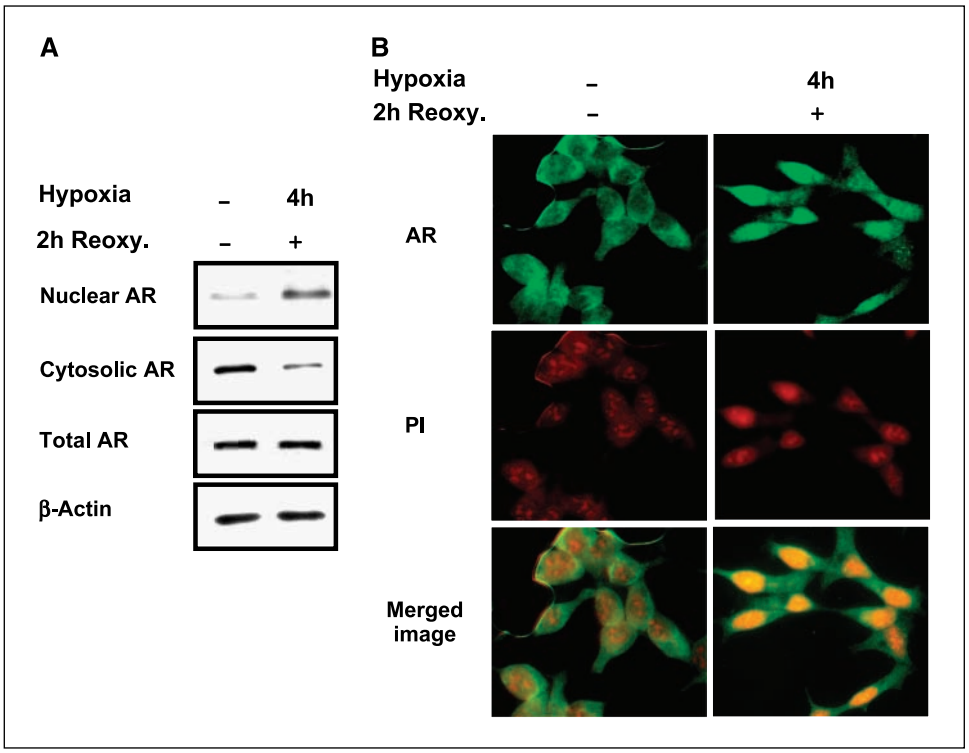

Figure 4. Effect of hypoxia on subcellular redistribution of AR. *A,* LNCaP cells underwent 4 hours of hypoxia followed by 2 hours of reoxygenation. Nuclear and cytosolic extracts were isolated, and Western blot analysis was performed by using anti-AR antibody. Total cell lysates prepared from parallel samples were also analyzed with anti-AR antibody. The β-actin antibody (Sigma) was used as a loading control. *B,* LNCaP cells grown on coverslips were exposed to 4 hours of hypoxia. Cells were then reoxygenated for 2 hours under normoxic conditions, fixed, and stained with anti-AR antibody or with normal rabbit IgG. Propidium iodide staining shows the location and integrity of the nuclei. AR (*green*) and propidium iodide (*red*) staining. Samples incubated with normal rabbit IgG showed diffuse background signals (data not shown).

Discussion

AR signaling plays an important role in prostate cancer. Despite our awareness of the effects of tumor hypoxia on the behavior of prostate cancer cells, the effect of hypoxia on AR activity has not been well characterized. In this study, we provide new insights into the action of AR in the context of unstable, dynamic, and often acute changes of tissue oxygenation of a tumor at the microenvironmental level. We showed that transient hypoxia clearly increases AR function in human prostate cancer cells. Our results show that the AR-ARE binding and AR-regulated gene expression are increased after hypoxia treatment. Confocal microscopy and ChIP assays confirmed that the AR translocation to the nucleus and the recruitment of AR to the PSA promoter are increased after hypoxia treatment. Hypoxia also sensitizes AR trans-activation to very low concentrations of androgen. The importance of our research finding is underlined by the realization that, in addition to the inherently abnormal and unstable vascular network of a tumor, changes of hypoxia/reoxygenation also emerge in a variety of clinical situations in prostate cancer. These situations include a localized and acute hypoxic microenvironment induced by

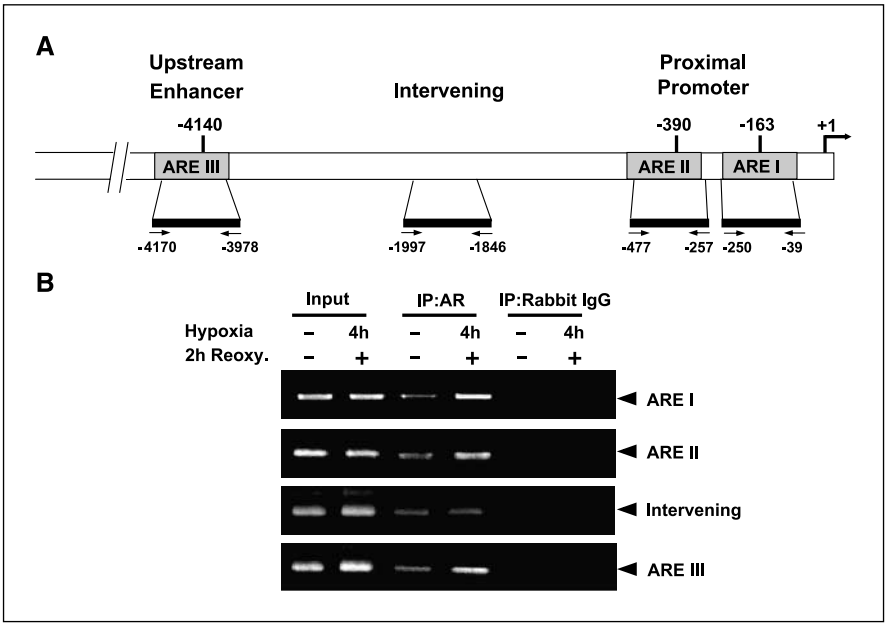

Figure 5. Hypoxia increases PSA promoter occupancy by AR. *A,* a schematic diagram of three ARE regions of the *PSA* gene. Locations of the primer pairs used to amplify ARE regions and nonspecific intervening regions are indicated. The numbers are the positions upstream to the *PSA* gene transcription start site. *B,* LNCaP cells underwent 4 hours of hypoxia, reoxygenated for 2 hours, and processed for ChIP assays using primer pairs in (*A*). *Input,* results obtained from DNA that was PCR-amplified from chromatin extracts before immunoprecipitation. *Rabbit IgG lane,* PCR results obtained after immunoprecipitation with rabbit IgG. Gels are representative of three independent experiments.

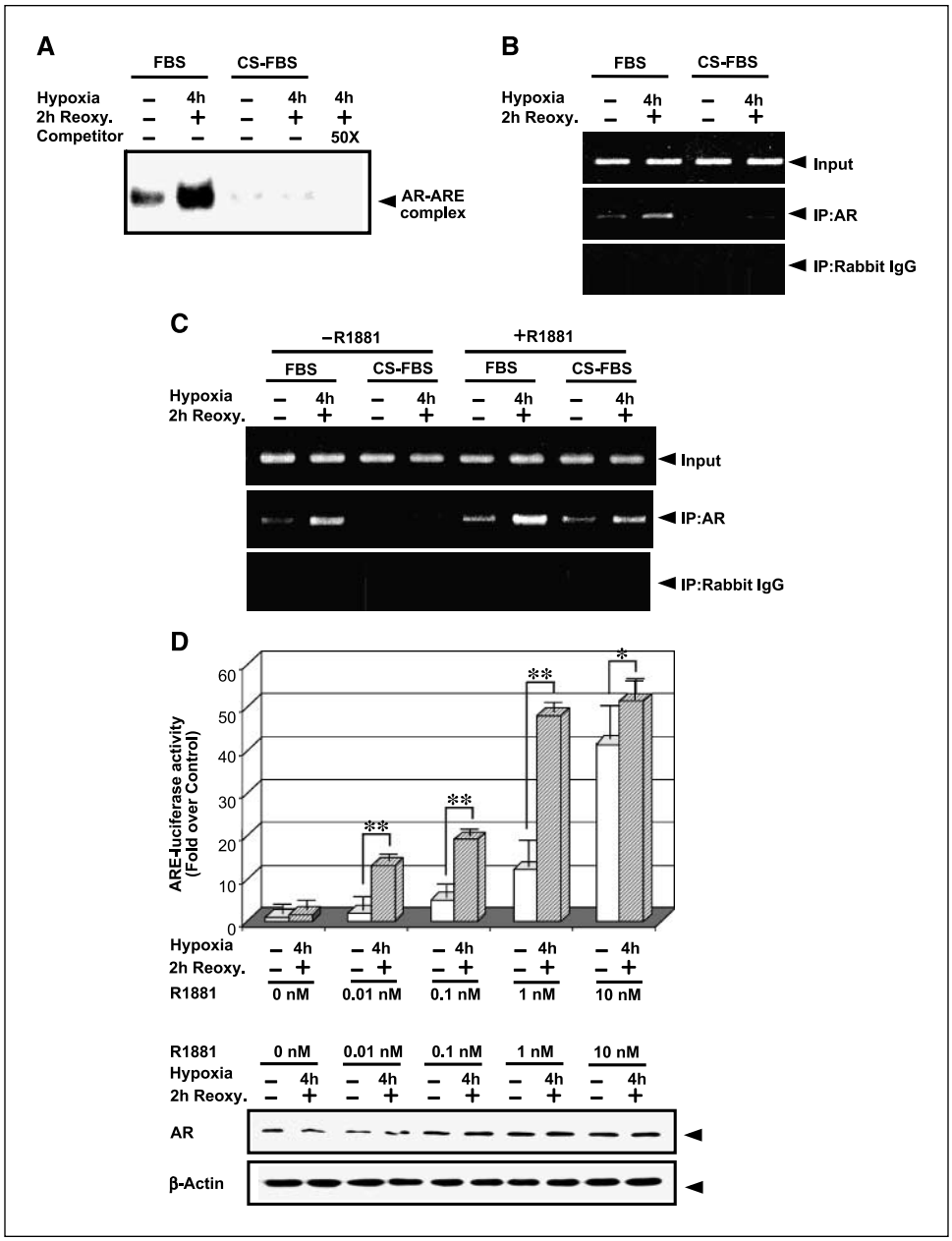

Figure 6. Increased AR trans-activation and sensitization by hypoxia is ligand-dependent. *A,* LNCaP cells grown in a normal FBS medium or in CS-FBS-containing medium underwent hypoxia for 4 hours. Cells were then reoxygenated for 2 hours, and processed for EMSA using radiolabeled ARE-containing oligonucleotide as a probe. Unlabelled oligonucleotides were used as a competitor. *B,* ChIP assays were performed in LNCaP cells treated as above using anti-AR antibody. Primer pairs amplifying the ARE I region were used for ChIP assay. *Input,* results obtained from DNA that was PCR-amplified from chromatin extracts before immunoprecipitation. *Rabbit IgG lane,* PCR results obtained from chromatin extracts immunoprecipitated with rabbit IgG. Gels are representative of three independent experiments. *C,* LNCaP cells grown in a normal FBS medium or in CS-FBS-containing medium underwent 4 hours of hypoxia with or without R1881 (10 nmol/L) supplementation. Cells were then incubated for 2 hours under normoxic conditions and processed for ChIP assays using anti-AR antibody. Primer pairs amplifying the ARE I-region were employed for ChIP assay. *D,* LNCaP cells grown in CS-FBS medium were transfected with an ARE-luciferase vector. At 24 hours after transfection, cells were treated with the indicated concentrations of R1881 for 4 hours under hypoxia or normoxic conditions. Cells were then reoxygenated for 2 hours at normoxic condition, and processed for ARE-luciferase activity assays. Normalized mean luciferase activity measured in cells transfected with ARE-luciferase without R1881 or hypoxia treatment was set to 1.0. **, $P < 0.01$ compared with R1881 treatment alone. *Columns,* mean of triplicate samples; *bars,* ±SD. Aliquots of samples used in luciferase assay were subjected to Western blot analysis using AR-antibody (*bottom*). The β-actin antibody was used as a loading control.

vasculature destruction after castration, or during neoadjuvant androgen deprivation therapy prior to radiation therapy, or in recurrent tumors during androgen deprivation therapy.

A recent study by Mohler et al. (21) suggests that prostate cancer which recurs during androgen deprivation therapy is not necessarily androgen-independent but continues to depend on androgen for growth. The measurement of androgens revealed that there are significant amounts of dihydrotestosterone, in the order of ~1.45 nmol/L. The presence of AR-regulated gene products in these tissues suggests that AR is active in recurrent prostate cancers. For comparison, benign prostate contains ~8.13 nmol/L of dihydrotestosterone (21). Our finding that transient hypoxia stimulates AR activity at very low levels of R1881 (<1 nmol/L) suggests an intriguing possibility that hypoxia permits AR to function at subphysiologic levels of androgens, and may facilitate the survival and growth of some prostate cancer cells during androgen deprivation therapy.

Prostate cancer cells are known to be heterogeneous in their molecular makeup. Using autopsy samples from men who died of recurrent prostate cancer, Shah et al. (30) elegantly showed the evidence of molecular heterogeneity within the same patient as well as among patients. Our use of LNCaP and DU145 cells for the present study is meant to simulate the backdrop of heterogeneity. For example, LNCaP cells possess functional p53 and wild-type retinoblastoma protein (RB; ref. 42), whereas DU145 cells possess p53 mutation and are RB null (42, 43). The increased AR activation by hypoxia occurs not only in LNCaP cells, but also in DU145 cells when wild-type AR is exogenously introduced. We believe that the AR stimulatory effect of hypoxia may be generalizable to different subsets of prostate cancer cells.

During the course of our study, we noted an article by Ghafar et al. (44) that examined hypoxia-responsive gene expression in LNCaP cells. These authors reported a decrease in PSA and AR

protein levels during continuous exposure to hypoxia for 24 hours, as well as during reoxygenation after 24 hours of hypoxia treatment. We did not find any change in AR protein up to 24 hours of reoxygenation after 4 hours of hypoxia treatment. In our study, a treatment condition of 24 hours of hypoxia followed by >16 hours of reoxygenation was too severe for LNCaP cells; we were unable to perform the 24-hour time point experiment after >16 hours of hypoxia treatment because most cells did not survive. Both LNCaP and DU145 cells were ~30% growth-inhibited after 4 hours of hypoxia treatment based on the clonogenic survival assay (data not shown).

How does hypoxia increase AR function and what is the underlying molecular mechanism? Cumulative evidence seems to point to reactive oxygen species (ROS) as a second messenger. The role of ROS in stimulating the PI3K/PTEN and mitogen-activated protein kinase pathways via protein tyrosine kinase was shown in cells treated with platelet-derived growth factor (PDGF) or epidermal growth factor (EGF) (45–47). Considering that mitogen-activated protein kinase signaling by EGF receptor HER-2/neu tyrosine kinase and other growth factors was shown to increase the activation of AR (27, 48), it is plausible that ROS may play a role in mediating the cross-talk between the peptide growth factors and the AR activation signaling pathways. Future studies are needed to clarify whether ROS acts as a second messenger, and if so, what specific ROS-mediated molecular pathways are linked to AR activation.

Oxidation-reduction (redox) based regulation of transcription factors is fundamental to the control of cell function. Disulfide bond formation between distant cysteines has been suggested as a mechanism to induce conformational changes of proteins (49). An alternative possibility is that ROS generated by hypoxia might directly modify redox-sensitive residues contained in AR. Redox-dependent activation of recombinant AR prepared in insect cells has been reported (50). Lastly, changes in the balance between steroid receptor coactivators and corepressors may affect AR activation (51, 52). Although the prevalence of these events and their relationship to clinical androgen-independence remains unclear, it is tempting to speculate on the possible role of hypoxia in altering the equilibrium of coregulators. All of these are important biological and clinical issues that warrant more intensive future investigation. Delineating the molecular mechanisms by which dynamic changes of hypoxia/reoxygenation affect AR function will provide valuable insights into treatment resistance and malignant progression of prostate cancer cells. Novel therapeutic approaches should be developed to prevent hypoxia and/or its consequences to enhance the efficacy of androgen deprivation therapy, a treatment that has not been improved significantly since its introduction >50 years ago (53).

Acknowledgments

Received 4/15/2005; revised 3/6/2006; accepted 3/16/2006.

Grant support: NIH grants CA111846 (Y-M. Park), CA09796 (C. Ip), DOD grant PC050127 (Y-M. Park), and Cancer Center Support grant CA16056.

The costs of publication of this article were defrayed in part by the payment of page charges. This article must therefore be hereby marked *advertisement* in accordance with 18 U.S.C. Section 1734 solely to indicate this fact.

We thank Dr. Chawnshang Chang (University of Rochester) for the AR expression vector.

References

1. Jemal A, Murray T, Ward E, et al. Cancer statistics, 2005. CA Cancer J Clin 2005;55:10–30.

2. Movsas B, Chapman JD, Horwitz EM, et al. Hypoxic regions exist in human prostate carcinoma. Urology 1999;53:11–8.

3. Movsas B, Chapman JD, Hanlon AL, et al. Hypoxia in human prostate carcinoma: an Eppendorf pO_2 study. Am J Clin Oncol 2001;24:458–61.

4. Movsas B, Chapman JD, Greenberg RE, et al. Increasing levels of hypoxia in prostate carcinoma correlate significantly with increasing clinical stage and patient age: an Eppendorf pO(2) study. Cancer 2000;89:2018–24.

5. Movsas B, Chapman JD, Hanlon AL, et al. Hypoxic prostate/muscle pO_2 ratio predicts for biochemical failure in patients with prostate cancer: preliminary findings. Urology 2002;60:634–9.

6. Hochachka PW, Rupert JL, Goldenberg L, Gleave M, Kozlowski P. Going malignant: the hypoxia-cancer connection in the prostate. Bioessays 2002;24:749–57.

7. Nahum AE, Movsas B, Horwitz EM, Stobbe CC, Chapman JD. Incorporating clinical measurements of hypoxia into tumor local control modeling of prostate cancer: implications for the α/β ratio. Int J Radiat Oncol Biol Phys 2003;57:391–401.

8. Zander R, Vaupel P. Proposal for using a standardized terminology on oxygen transport to tissue. Adv Exp Med Biol 1985;191:965–70.

9. Moulder JE, Rockwell S. Tumor hypoxia: its impact on cancer therapy. Cancer Metastasis Rev 1987;5:313–41.

10. Vaupel P, Kallinowski F, Okunieff P. Blood flow, oxygen and nutrient supply, and metabolic microenvironment of human tumors: a review. Cancer Res 1989; 49:6449–65.

11. Kimura H, Braun RD, Ong ET, et al. Fluctuations in red cell flux in tumor microvessels can lead to transient hypoxia and reoxygenation in tumor parenchyma. Cancer Res 1996;56:5522–8.

12. Brown JM. Evidence for acutely hypoxic cells in mouse tumours, and a possible mechanism of reoxygenation. Br J Radiol 1979;52:650–6.

13. Brown JM, Giaccia AJ. The unique physiology of solid tumors: opportunities (and problems) for cancer therapy. Cancer Res 1998;58:1408–16.

14. Dewhirst MW. Concepts of oxygen transport at the microcirculatory level. Semin Radiat Oncol 1998;8: 143–50.

15. Kallman RF. The phenomenon of reoxygenation and its implications for fractionated radiotherapy. Radiology 1972;105:135–42.

16. Harris AL. Hypoxia—a key regulatory factor in tumour growth. Nat Rev Cancer 2002;2:38–47.

17. Isaacs JT. Role of androgens in prostatic cancer. Vitam Horm 1994;49:433–502.

18. Isaacs JT. The biology of hormone refractory prostate cancer. Why does it develop? Urol Clin North Am 1999; 26:263–73.

19. Trapman J, Cleutjens KB. Androgen-regulated gene expression in prostate cancer. Semin Cancer Biol 1997;8: 29–36.

20. van der Kwast TH, Schalken J, Ruizeveld de Winter JA, et al. Androgen receptors in endocrine-therapy-resistant human prostate cancer. Int J Cancer 1991;48: 189–93.

21. Mohler JL, Gregory CW, Ford OH III, et al. The androgen axis in recurrent prostate cancer. Clin Cancer Res 2004;10:440–8.

22. Taplin ME, Bubley GJ, Shuster TD, et al. Mutation of the androgen-receptor gene in metastatic androgen-independent prostate cancer. N Engl J Med 1995;332: 1393–8.

23. Visakorpi T, Hyytinen E, Koivisto P, et al. *In vivo* amplification of the androgen receptor gene and progression of human prostate cancer. Nat Genet 1995;9:401–6.

24. Taplin ME, Rajeshkumar B, Halabi S, et al. Androgen receptor mutations in androgen-independent prostate cancer: Cancer and Leukemia Group B Study 9663. J Clin Oncol 2003;21:2673–8.

25. Culig Z, Hobisch A, Cronauer MV, et al. Androgen receptor activation in prostatic tumor cell lines by insulin-like growth factor-I, keratinocyte growth factor, and epidermal growth factor. Cancer Res 1994;54:5474–8.

26. Hobisch A, Eder IE, Putz T, et al. Interleukin-6 regulates prostate-specific protein expression in prostate carcinoma cells by activation of the androgen receptor. Cancer Res 1998;58:4640–5.

27. Craft N, Shostak Y, Carey M, Sawyers CL. A mechanism for hormone-independent prostate cancer through modulation of androgen receptor signaling by the HER-2/neu tyrosine kinase. Nat Med 1999;5:280–5.

28. Lee SO, Lou W, Hou M, Onate SA, Gao AC. Interleukin-4 enhances prostate-specific antigen expression by activation of the androgen receptor and Akt pathway. Oncogene 2003;22:7981–8.

29. Chen CD, Welsbie DS, Tran C, et al. Molecular determinants of resistance to antiandrogen therapy. Nat Med 2004;10:33–9.

30. Shah RB, Mehra R, Chinnaiyan AM, et al. Androgen-independent prostate cancer is a heterogeneous group of diseases: lessons from a rapid autopsy program. Cancer Res 2004;64:9209–16.

31. Shabsigh A, Chang DT, Heitjan DF, et al. Rapid reduction in blood flow to the rat ventral prostate gland after castration: preliminary evidence that androgens influence prostate size by regulating blood flow to the prostate gland and prostatic endothelial cell survival. Prostate 1998;36:201–6.

32. Jain RK, Safabakhsh N, Sckell A, et al. Endothelial cell death, angiogenesis, and microvascular function after castration in an androgen-dependent tumor: role of vascular endothelial growth factor. Proc Natl Acad Sci U S A 1998;95:10820–5.

33. Hayek OR, Shabsigh A, Kaplan SA, et al. Castration induces acute vasoconstriction of blood vessels in the rat prostate concomitant with a reduction of prostatic nitric oxide synthase activity. J Urol 1999;162:1527–31.

34. Baek SH, Lee UY, Park EM, et al. Role of protein kinase Cδ in transmitting hypoxia signal to HSF and HIF-1. J Cell Physiol 2001;188:223–35.

35. Lowry OH, Rosebrough NJ, Farr AL, Randall RJ. Protein measurement with the folin phenol reagent. J Biol Chem 1951;193:265–75.

36. Yeh S, Chang C. Cloning and characterization of a specific coactivator, ARA70, for the androgen receptor in human prostate cells. Proc Natl Acad Sci U S A 1996;93:5517–21.

37. Onate SA, Boonyaratanakornkit V, Spencer TE, et al. The steroid receptor coactivator-1 contains multiple receptor interacting and activation domains that cooperatively enhance the activation function 1 (AF1) and AF2 domains of steroid receptors. J Biol Chem 1998;273:12101–8.

38. Lee SS, Kwon SH, Sung JS, Han MY, Park YM. Cloning and characterization of the rat Hsf2 promoter: a critical role of proximal E-box element and USF protein in Hsf2 regulation in different compartments of the brain. Biochim Biophys Acta 2003;1625:52–63.

39. Eberhardy SR, D'Cunha CA, Farnham PJ. Direct examination of histone acetylation on Myc target genes using chromatin immunoprecipitation. J Biol Chem 2000;275:33798–805.

40. Cleutjens KB, van der Korput HA, Ehren-van Eekelen CC, et al. A 6-kb promoter fragment mimics in transgenic mice the prostate-specific and androgen-regulated expression of the endogenous prostate-specific antigen gene in humans. Mol Endocrinol 1997;11:1256–65.

41. Shang Y, Myers M, Brown M. Formation of the androgen receptor transcription complex. Mol Cell 2002;9:601–10.

42. Carroll AG, Voeller HJ, Sugars L, Gelmann EP. p53 oncogene mutations in three human prostate cancer cell lines. Prostate 1993;23:123–34.

43. Bookstein R, Shew JY, Chen PL, Scully P, Lee WH. Suppression of tumorigenicity of human prostate carcinoma cells by replacing a mutated RB gene. Science 1990;247:712–5.

44. Ghafar MA, Anastasiadis AG, Chen MW, et al. Acute hypoxia increases the aggressive characteristics and survival properties of prostate cancer cells. Prostate 2003;54:58–67.

45. Bae YS, Kang SW, Seo MS, et al. Epidermal growth factor (EGF)-induced generation of hydrogen peroxide. Role in EGF receptor-mediated tyrosine phosphorylation. J Biol Chem 1997;272:217–21.

46. Rhee SG. Redox signaling: hydrogen peroxide as intracellular messenger. Exp Mol Med 1999;31:53–9.

47. Kwon J, Lee SR, Yang KS, et al. Reversible oxidation and inactivation of the tumor suppressor PTEN in cells stimulated with peptide growth factors. Proc Natl Acad Sci U S A 2004;101:16419–24.

48. Gioeli D, Ficarro SB, Kwiek JJ, et al. Androgen receptor phosphorylation. Regulation and identification of the phosphorylation sites. J Biol Chem 2002;277:29304–14.

49. Lee C, Lee SM, Mukhopadhyay P, et al. Redox regulation of OxyR requires specific disulfide bond formation involving a rapid kinetic reaction path. Nat Struct Mol Biol 2004;11:1179–85.

50. Liao M, Zhou Z, Wilson EM. Redox-dependent DNA binding of the purified androgen receptor: evidence for disulfide-linked androgen receptor dimers. Biochemistry 1999;38:9718–27.

51. Gregory CW, He B, Johnson RT, et al. A mechanism for androgen receptor-mediated prostate cancer recurrence after androgen deprivation therapy. Cancer Res 2001;61:4315–9.

52. Li P, Yu X, Ge K, et al. Heterogeneous expression and functions of androgen receptor co-factors in primary prostate cancer. Am J Pathol 2002;161:1467–74.

53. Huggins C, Hodges CV. Studies on prostatic cancer: I. The effect of castration, of estrogen and of androgen injection on serum phosphatases in metastatic carcinoma of the prostate. 1941. J Urol 2002;168:9–12.

Preparative Biochemistry & Biotechnology, 36: 65–79, 2006

ISSN 1082-6068 print/1532-2297 online
DOI: 10.1080/10826060500388520

Analysis of Protein Redox Modification by Hypoxia

Kyoung-Soo Choi, Soo-Yeon Park, Sun-Hee Baek, Rama Dey-Rao, and Young-Mee Park
Department of Cellular Stress Biology, Roswell Park Cancer Institute, Buffalo, NY, USA

Haitao Zhang, and Clement Ip
Department of Cancer Chemoprevention, Roswell Park Cancer Institute, Buffalo, NY, USA

Eun-Mi Park
Department of Chemistry, University of Incheon, Incheon, Korea

Yeul Hong Kim
Genomic Research Center for Lung and Breast/Ovarian Cancer, Korea University Medical School, Korea

Jong Hoon Park
Department of Biological Science, Sookmyung Women's University, Seoul, Korea

Abstract: We examined hypoxia-induced changes in global thiol proteome profile in human prostate cancer cells using a BIAM-based display method. We analyzed the kinetics of protein thiol modification by using a pattern recognition algorithm, self-organizing maps (SOM) clustering, and identified the BIAM-labeled proteins by MALDI-TOF and ESI-tandem mass spectrometry. We found 99 out of 215 of total BIAM-labeled proteins were affected by hypoxia treatment and, yet, with diverse

Address correspondence to Young-Mee Park, Department of Cellular Stress Biology, Roswell Park Cancer Institute, Elm & Carlton Streets, Buffalo, NY 14263, USA. E-mail: young-mee.park@roswellpark.org

patterns and kinetics of redox modification. Our study proved that proteomics analysis employing the BIAM-labeling method can provide valuable information pertaining to global changes in the redox status of proteins in response to hypoxia.

Keywords: Hypoxia, Oxidative stress, Redox modification, Proteomics

INTRODUCTION

In 2005, an estimated 232,090 new prostate cancers will be diagnosed and 30,350 men will die from prostate cancer.[1] Eppendorf pO_2 microelectrode studies of human prostate cancer demonstrated that prostate cancer cells can grow in a hypoxic microenvironment.[2,3] A series of studies suggests that local hypoxia in prostate cancer is a key factor in tumor growth and may predict clinical outcome.[4–7]

Hypoxia is a state of reduced O_2 availability or O_2 partial pressure below critical values.[8,9] The inadequate vascular geometry relative to the volume of oxygen consuming tumor cells creates diffusion-limited O_2 delivery (chronic hypoxia).[10] Moreover, dynamic changes in microregional blood flow in tumors due to a chaotic blood flow cause a transient hypoxia, which is followed by reperfusion.[11–13] Both chronic and transient hypoxia have been detected in animal tumor models, and clinical data confirm that they occur in human cancers as well.[14–17] In metastases of carcinomas, lower median pO_2 levels and higher hypoxic fractions were recorded, compared not only with the normal surrounding tissue, but also the primary tumors.[17,18] The characteristic hypoxic tumor microenvironment is shown to have a profound influence on malignant progression and therapeutic outcome.[19–24] Considering the well-known impact of hypoxia on malignant progression of cancers, it is not surprising that various genes that are consistent with tumor progression and metastasis are induced by hypoxia. Correspondingly, it is proposed that hypoxia functions as an environmental pressure to select for a subset of aggressive cells that have increased capability to progress and metastasize.[22,25–28]

Most research on hypoxia-response has concentrated on HIF-α pathways and hypoxia-inducible gene regulation. However, scanty information is available on "how cancer cells sense hypoxia." To delineate the novel molecular mechanisms of hypoxia in regulating the malignant progression of prostate cancer, it will be as important, if not more, as gene expression to identify the proximal target/effector molecules that immediately sense hypoxia and activate/integrate hypoxia response pathways.

Redox sensitive proteins are the most promising candidates for the "hypoxia-sensing molecule." Both chronic and transient hypoxia are accompanied by the generation of reactive oxygen species (ROS) causing oxidative stress to the cells. Transient hypoxia, periods of hypoxia followed by reperfusion, leads to a burst of ROS generation during the first minutes

after reoxygenation.[29,30] Although the specific mechanisms whereby ROS are generated are still under study, ROS generation during hypoxia has been demonstrated.[31–33]

Redox-mediated modification of cellular proteins confers a response to ROS and eventually changes in a variety of cellular processes. Structural and biochemical data now indicate that cysteine residues play a ubiquitous role in allowing proteins to respond to ROS.[34] Not all the cysteine residues on proteins are reactive. Only the ones with lower pK_a values due to the influence of neighboring nucleophilic groups and other stabilizing groups can exist as thiolate anion at neutral pH and, as a result, are sensitive to redox regulation. Therefore, proteins with these 'reactive thiols' are excellent and most likely candidates for the "hypoxia-sensing molecules."

In this study, we examined hypoxia-induced changes in global thiol proteome profile in human prostate cancer cells using a N-(biotinyl)-N′-(iodoacetyl) ethylenediamine (BIAM)-based display method. We also examined the kinetics of protein thiol modification by hypoxia treatment to find characteristic patterns of the modification using a self-organizing maps (SOM) clustering and identified hypoxia-sensitive thiol-containing proteins by MALDI-TOF and ESI-tandem mass spectrometry.

EXPERIMENTAL

Cell Culture

LNCaP human prostate cancer cells were obtained from the American Type Culture Collection (ATCC, Manassas, VA) and maintained in RPMI 1640 supplemented with 10% fetal bovine serum (FBS). The cells were cultured in the same medium containing 2 mM glutamine, 100 units/mL penicillin, and 100 μg/mL streptomycin.[35]

Hypoxia Treatment

Hypoxia treatment was performed as reported previously.[36] Briefly, culture medium was replaced with deoxygenated RPMI 1640 medium (GIBCO-BRL, Gaithersburg, MD) before hypoxia treatment at 37°C in a hypoxic chamber (Forma Scientific, Marietta, OH). Deoxygenated medium was prepared prior to each experiment by equilibrating the medium with a hypoxic gas mixture containing 5% CO_2, 85% N_2, and 10% H_2 at 37°C. The oxygen concentration in the hypoxic chamber and the exposure medium was maintained at less than 0.05% and monitored using an oxygen indicator (Forma Scientific, Marietta, OH). All experiments were performed at 70–80% confluency and medium pH was maintained between 7.2 and 7.4 for the duration of the experiment. In this study, cells were treated with

hypoxia for 4 h and returned to a normoxic CO_2 incubator. Four hours of hypoxic exposure was chosen because, in our preliminary experiments, reactive oxygen species (ROS) generation and the protein modification reached a maximum level at 4 h, when cells were exposed to continuous hypoxia, and longer exposure interfered with cell survival. At the indicated time after 4-h hypoxic treatment, the change in global thiol proteome profile was investigated. In a parallel experiment, control cultures without treatment were processed similarly.

Measurement of Reactive Oxygen Species (ROS) Formation

The rate of ROS formation was determined by flow cytometry analysis using the probe 2′,7′-dichlorofluorescin diacetate (DCFH-DA). DCFH is oxidized to fluorescent dichlorofluorescein (DCF) by reaction with ROS after deacylation in the cell.[37] Briefly, the cells loaded with DCFH-DA were subjected to 4-h hypoxia treatment. After the indicated time, fluorescent cells were analyzed by flow cytometry.

Western Blot Analysis

Equal amounts of proteins were analyzed, in duplicate, by SDS-polyacrylamide gel electrophoresis. One gel was stained with Coomassie blue, destained, and dried as a record. A second gel was transferred to a nitrocellulose membrane in a Trans-Blot apparatus (BioRad, Hercules, CA) for Western blot analysis. The following monoclonal antibodies were used: anti-caspase 3 (Cell signaling Technology, Beverly, MA), anti-PARP (Santa Cruz Biotechnology, Santa Cruz, CA), and anti-pJNK and anti-JNK 1 (Santa Cruz Biotechnology). Immunoreactive proteins were detected with a secondary antibody and visualized using an enhanced chemiluminescence detection system (Amersham Pharmacia Biotech, Piscataway, NJ). Protein concentrations were measured by the method of Lowry et al.[38] throughout the experiments.

N-(Biotinyl)-N′-(Iodoacetyl) Ethylenediamine (BIAM) Labeling of Reactive Thiols

Proteins with reactive thiols in LNCaP cells were labeled with a thiol-specific reagent, BIAM, as described previously.[39] Figure 1 shows schematics of the procedure. Briefly, cells were treated with 20 μM BIAM (Molecular Probes, Eugene, OR) in oxygen-free lysis buffer (50 mM 2-(N-morpholino) ethanesulfonic acid (pH 6.5), 100 mM NaCl, 0.5% (v/v) Triton X-100, 1 μg/mL leupeptin, and 10 μM phenylmethylsulfonyl fluoride) in a hypoxic chamber. Cells were homogenized in an anoxic condition, and the

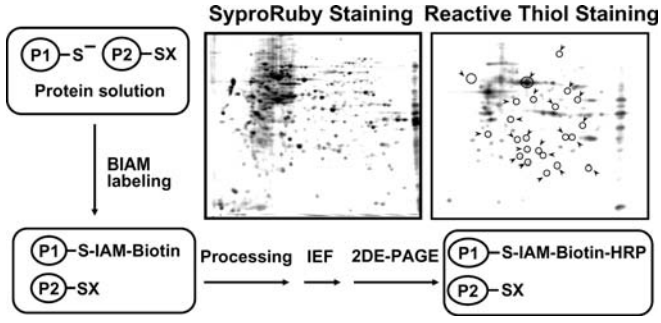

Figure 1. Schematics and display of BIAM labeling of reactive thiol-containing proteins. Protein extract from LNCaP cells was labeled with BIAM. After 2D gel electrophoresis, one sample was processed for total protein staining by SyproRuby, and another processed for reactive thiol-containing proteins by HRP-conjugated streptavidin.

labeling reaction was terminated by adding 20 mM β-mercaptoethanol. After centrifugation (10,000 g, 10 min, 4°C), the supernatant was subjected to 2D gel electrophoresis.

2D Gel Electrophoresis and Image Analysis

The BIAM-labeled protein extracts were subjected to 2D gel electrophoresis as described previously.[39] First-dimensional electrofocusing was performed on a pH 3–10 NL DryStryps (Amersham Biosciences, Piscataway, NJ) and the Second-dimensional SDS-PAGE was on a 12% polyacrylamide gel. Proteins were transferred to a PVDF membrane and detected with HRP-conjugated streptavidin (Amersham) and enhanced chemiluminescence. The image of the thiol specific-stained blots was analyzed by PDQuest (version 7.1, Bio-Rad) by using the total quantity of internal control spots for normalization. A second portion of the identical protein extract was subjected to 2D gel electrophoresis, stained with SyproRuby (Bio-Rad), and processed for the subsequent identification of labeled proteins. Only about 35% of total protein spots were consistently labeled by BIAM, as shown in Figure 1.

Data Analysis by Scatter Plot and Self-Organizing Maps (SOM) Clustering

The image data were analyzed by a scatter plot and self-organizing maps (SOM) clustering, as previously described.[39] The normalized intensity values were transformed to $\log_2$ scale and subjected, first, to scatter plot

analysis. For both the control and hypoxia-treatment data, the scatter plots were constructed by plotting the intensity value of each spot at the zero hour time point (x-axis) against the intensity value of the same spot at a different time point (y-axis). The Pearson's correlation coefficient was calculated using the formula:

$$r = \frac{\sum_{i=1}^{n}(x_i - \bar{x})(y_i - \bar{y})}{\sqrt{\left[\sum_{i=1}^{n}(x_i - \bar{x})^2\right]\left[\sum_{i=1}^{n}(y_i - \bar{y})^2\right]}}$$

Additionally, the normalized intensity values were used to calculate the treatment-to-control signal ratio for each spot. The $\log_2$-transformed ratios were subjected to unsupervised clustering analysis using the SOM algorithm.[40,41] The unsupervised method was used because we had no *a priori* expectation of what kind of clustering pattern would emerge, nor did we make any assumption. This analysis was performed using custom PERL scripts and the GeneCluster 2.0 program from the Center for Genome Research, Whitehead Institute, Massachusetts Institute of Technology.

Protein Identification by Mass Spectrometry

Protein spots were analyzed by MALDI-TOF mass spectrometry using M@LDI^{TM}-LR (Micromass, Beverly, MA) after tryptic in-gel digestion. The raw mass spectra were analyzed to obtain a list of monoisotopic peaks using ProteinLynx Global SERVER 2.0 program from Waters (http://www.waters.com). The protein candidates were identified using the National Center for Biotechnology Information (NCBI) database as the search engine. When the search results were ambiguous, the remaining tryptic mixture was subjected to ESI-tandem mass spectrometry using Q-TOF API US (Micromass). The peptide mass error was limited to 50 ppm.

RESULTS

We first evaluated oxidative stress caused by hypoxia treatment to the prostate cancer cells. Cells were loaded with 2′,7′-dichlorofluorescin diacetate (DCFH-DA), treated with hypoxia for 4 h and returned to a normoxic CO_2 incubator. The rate of reactive oxygen species (ROS) generation was measured by flow cytometry at 0.5, 1, 2, 3, 6, 12, or 24 h after hypoxia treatment. The rate of ROS generation increased immediately after the 4-h hypoxia treatment, peaked after 2 h, and began to decrease afterwards (Figure 2), which indicates that hypoxia treatment caused significant oxidative stress to LNCaP cells.

We next evaluated the effect of hypoxia on apoptotic cell death. One of the key events in initiation of apoptosis is the activation of caspases. A cascade of activation of caspases culminates in the cleavage of poly (ADP-ribose)

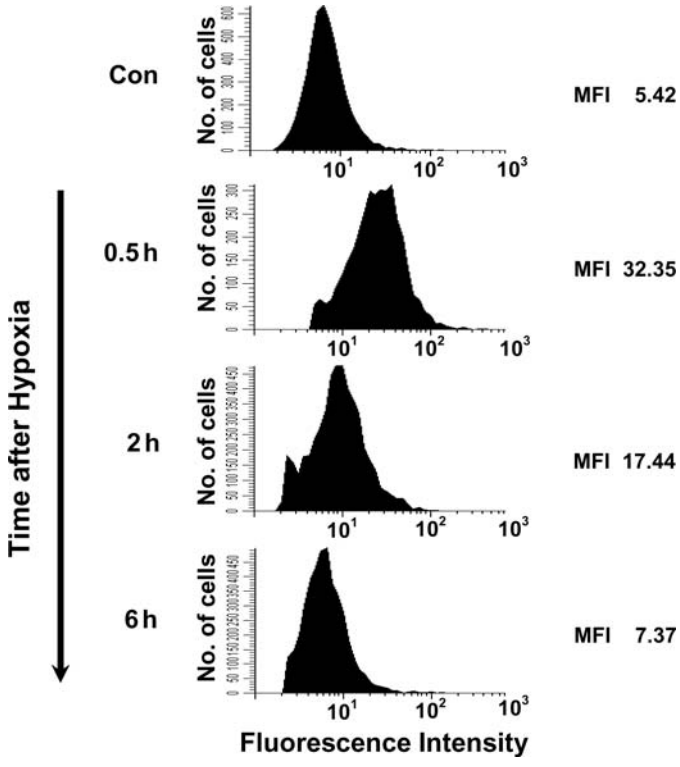

Figure 2. Effect of hypoxia on the rate of reactive oxygen species (ROS) generation. The LNCaP cells were analyzed for ROS formation at the indicated time after 4-h hypoxia treatment by flow cytometry. MFI, mean fluorescence intensity.

polymerase (PARP), a hallmark of apoptosis indicative of activation of the effector caspase 3. Figure 3 shows caspase 3 activation and PARP cleavage following hypoxia treatment. Although it is not completely understood how hypoxia leads to the activation of caspase pathways, the activation of JNK has been implicated in oxidative stress-mediated apoptosis. In order to probe whether JNK activation is involved in hypoxia-mediated apoptosis, we examined JNK phosphorylation. As shown in Figure 3, hypoxia induced activation of JNK.

Having confirmed that hypoxia induced oxidative stress and oxidative stress-mediated apoptosis, we investigated hypoxia-induced global protein redox modification in human prostate cancer cells. To probe into the protein redox changes, we used a thiol-specific reagent, BIAM-based display method. Since BIAM preferentially reacts with cysteine thiolates ($Cys\text{-}S^{-}$) and not with sulfhydryl groups (Cys-SH), only proteins with 'reactive thiols' are visualized. The thiol-specific-stained blots were analyzed by

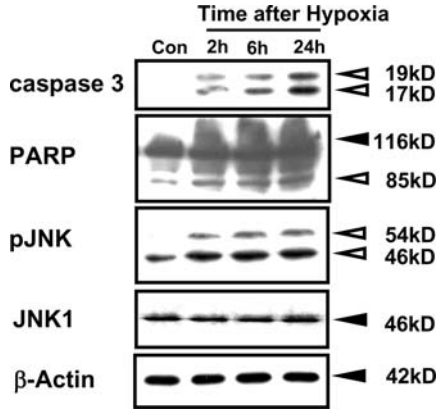

Figure 3. Effect of hypoxia on the caspase activation, PARP cleavage and JNK activation. Protein extracts from LNCaP cells were probed with activated caspase 3 Ab (Cell signaling) and PARP Ab (Santa Cruz) that recognizes full and cleaved forms of PARP. Activated JNK was probed with pJNK Ab (Santa Cruz). The membranes were stripped, and reprobed with JNK1 Ab (Santa Cruz).

PDQuest (version 7.1, Bio-Rad) to quantitate the subset of proteins sensitive to redox modification by hypoxia treatment.

A total of 215 protein spots were detected as labeled with BIAM in LNCaP cells. We found 99 spots out of a total of 215 spots were affected by hypoxia treatment. There are subsets of proteins with either increased or decreased BIAM labeling intensity. In Figure 4, triangles and circles denote the spots of which the BIAM labeling intensity was either decreased or increased, respectively. Not every sensitive spot is marked by a symbol, so as not to make the figure too cluttered, to show what we want to convey. A parallel time-course experiment without hypoxia treatment showed minimal changes in redox modification of protein thiols during this period (data not shown).

To characterize the subsets of proteins demonstrated hypoxia-induced redox changes further, we analyzed the time-course changes of the 215 BIAM-labeled spots by the Self Organizing Maps (SOM) algorithm. The analysis was done based on $\log_2$ transformation of the treatment to control signal ratios at each time point. The analysis revealed six different patterns of time-course changes, as shown in Figure 5. Cluster 1, which consists of 116 protein spots, exhibited very little change in the labeling intensity throughout the 24 h following hypoxia treatment. Clusters 2, 3, and 4, consisting of 46 proteins, that is, 21% of the total, exhibited reversible oxidation by hypoxia treatment. Cluster 2, with 19 proteins, showed an immediate and transient loss of reactive thiols, and reached a nadir at 1 h, followed by a rapid return to normal in 2 h. Cluster 3, with 13 proteins, also showed a transient loss and rapid recovery, but with about an hour-delayed time-course response,

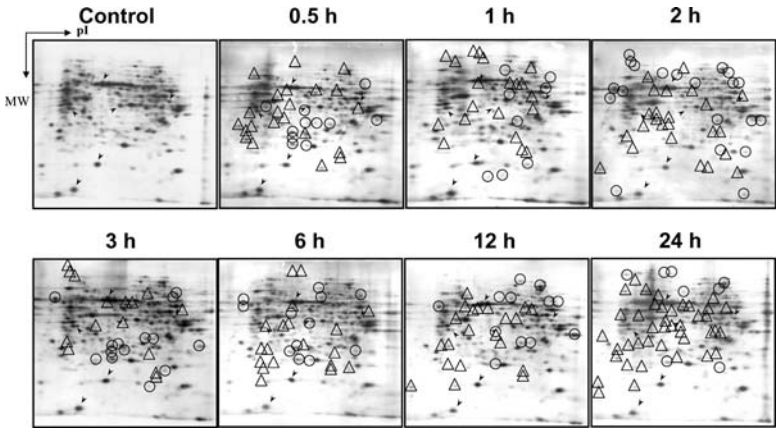

Figure 4. Changes in BIAM-labeled proteome profile after hypoxia treatment. Starting from the 0.5-h panel and moving across the timeline, the triangles and circles denote the same protein spots of which BIAM labeling intensity was decreased or increased, respectively, subsequent to hypoxia treatment. The arrows denote representative internal control spots used for normalization.

compared to Cluster 2. Cluster 4, with 14 proteins, showed a much more delayed response to the hypoxia treatment; their intensity loss peaked at 12 h and recovered to control at 24 h following hypoxia treatment. Cluster 5, which consists of 29 proteins, 13% of the total, exhibited irreversible loss of reactive thiols. Cluster 6, which consists of 24 proteins, 11% of the total, is the protein cluster that showed gain of the labeling intensity.

Table 1 lists examples of proteins that showed thiol modification following hypoxia. Although we did not pursue to generate a full scope of identification, the partial list provides a hint of a diverse metabolic pathway affected by hypoxia treatment.

DISCUSSION

In an effort to delineate molecular mechanisms of hypoxia in regulating the malignant progression of prostate cancer, we probed the hypoxia-induced redox modification of proteins in LNCaP cells. Hypoxia has been proposed to function as an environmental pressure to select for a subset of aggressive cells that have increased capability to progress and metastasize. There has been a large volume of reports on the effect of hypoxia on the expression and post-translational modification of specific and functionally related proteins, but not so many on the effect on the global proteome modification. Thus far, studies examining the influence of hypoxia on protein have been restricted to those proteins that show enhanced expression.

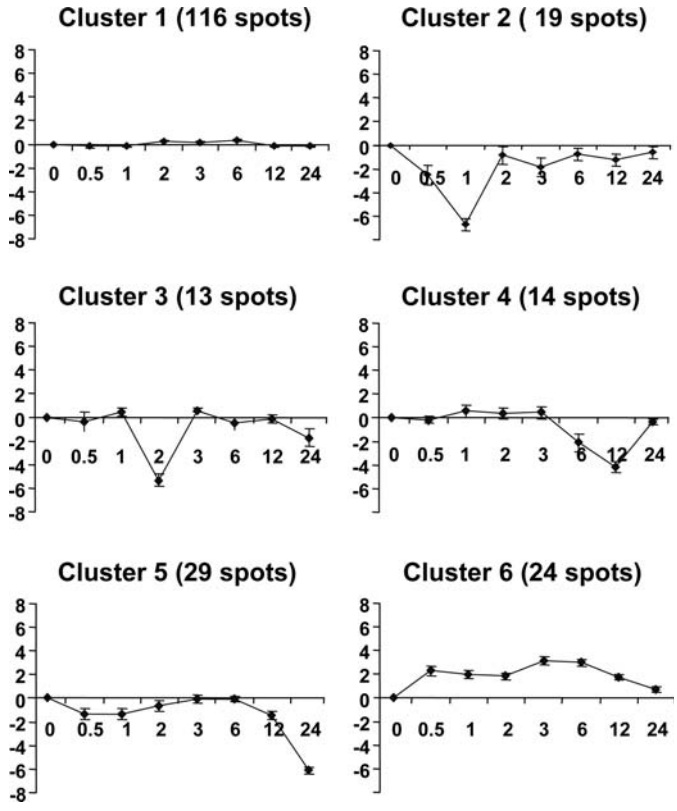

Figure 5. The SOM clustering analysis of hypoxia-responsive changes in BIAM-labeled proteins. Image analysis data extracted from Figure 4 were analyzed by SOM. The Y-axis represents the $\log_2$-transformed treatment to control ratio. The error bar represents mean $\pm$ SEM of this value.

We investigated the effect of hypoxia on a global protein redox modification. To our knowledge, this is the first report on the hypoxia-induced global redox protein modification. However, since the method employed in our study is based on the 2DE separation and subsequent specific staining, it has limitation of detecting only relatively high abundance proteins. Proteins with extreme molecular size or pI, and proteins with poor solubility also tend to escape the detection by methods based on the 2DE separation.

We specifically looked into the thiol proteome. It is based on two important facts; first, hypoxia is an oxidative stress agent, and second, thiol groups on proteins are very sensitive to the oxidation, which is often reversible. The results from Figures 1 and 2 confirmed that both hypoxia itself and hypoxia/reoxygenation could induce oxidative stress and oxidative stress-mediated apoptosis to cells, respectively. Protein cysteine residues play ubiquitous roles to mediate cellular responses to redox status through

Table 1. Identification of proteins redox-modified by hypoxia treatment

Cluster	Proteins
2	Aldolase A (E.C. 4.1.2.13) Death-associated protein kinase 1 (DAP kinase 1) Replication protein A2, 32 kD
3	Chaperonin containing TCP1 subunit 2 (beta) Neuropolypeptide h3 Bromodomain and PHD finger containing, 3 Eukaryotic translation initiation factor 3, subunit 2 beta, 36 kD Enolase 1 Glyceraldehyde 3-phosphate dehydrogenase
4	HP1Hs-gamma Nucleoside diphosphate kinase A (NDP kinase A, Tumor metastatic process-associated protein, matastasis inhibition factor nm23)
5	Neuronal apoptosis inhibitory protein Inorganic pyrophosphatase ATP synthase alpha chain, mitochondrial precursor
6	Mitocondrial ATP synthase, beta subunit Catechol-O-methyltransferase isoform S-COMT 3-oxoacid CoA transferase FLJ21963 protein Tubulin alpha 2 Prohibitin

their ability to both detect changes in redox status and transduce a change in protein structure and function. Not all thiol-containing proteins are modified. The sensitivity of the thiolate species to oxidation endows their redox sensitivity and, hence, ability to monitor redox status. The reactivity of redox-sensitive cysteine, that is, cysteine thiolate anion, is modulated by their molecular environment. For example, the thiolate anion is stabilized by proximity to hydrogen bond donors, basic residues, and metal ions. The protein thiols that can easily form thiolate anions are, therefore, called 'reactive thiols.' Importantly, modulating the reactivity of cysteine residues toward ROS determines the sensitivity of the response. These properties of protein thiols make them excellent and the most likely candidates for the "hypoxia-sensing molecule." The oxidation of thiol groups can be either reversible or irreversible. Oxidation of thiol groups to sulfoxides is irreversible, in general. In contrast, oxidation of thiol groups into disulfide forms is reversible because the disulfide can be reduced by thiol-disulfide oxidoreductases at the expense of reducing power such as NADPH or glutathione.[42,43] S-thiolation (a mixed-disulfide formation of protein thiols with low molecular weight thiols such as glutathione) is the most well known form of reversible protein thiol modification because glutathione is the most abundant

thiol-containing redox couple present in cells. S-thiolation of various proteins has been reported in cells experiencing hypoxia.[44,45]

In the present study, 46% of the total BIAM-labeled proteins, that is, 99 out of 215, were affected by hypoxia treatment. Among the affected proteins, 76% and 24% of proteins showed decrease and increase in the BIAM label intensity, respectively. The clusters 2, 3, and 4 showed transient decreases. The reversible nature suggests that they were oxidized in the form of disulfide. Cluster 5, which showed a marked decrease in BIAM label intensity after 12 h, is likely to include not only the irreversibly oxidized proteins but also the ones that were degraded. Cluster 6 represents thiol proteins increased following hypoxia. They are likely to be the proteins with increased expression rather than with redox-regulation. Unlike proteins in clusters 1 to 4, the proteins that belong to cluster 5 and 6, indeed, showed decreased and increased density, respectively, in SyproRuby stained gels (data not shown).

The proteins of which thiols are reversibly modified, that is, proteins in clusters 2 to 4, are thought to be involved in hypoxia-induced metabolic regulation. The early responders are the most likely candidates to function as hypoxia-sensing molecules, and the relatively late responders may be involved in the compensatory mechanisms associated with cellular remodeling following hypoxia. The global, and yet diverse nature of the response to hypoxia shown in our results suggests that complex metabolic adjustments are made to cope with the hypoxia-induced changes. This is supported by the fact that redox modification of many individual thiol proteins, including enzymes and signaling proteins, has been shown to have a profound effect on their functions/activities.[46,47] However, it is worth noting that not every thiol modification results in the activity change; for example, activity of glyceraldehydes 3-phosphate dehydrogenase is inhibited by thiol modification but that of aldolase is not.

In summary, we have shown that hypoxia treatment induces a global, and yet diverse, pattern of protein redox modification. Our study proved that proteomics analysis employing BIAM labeling can provide valuable information pertaining to global changes occurring at the level of the redox status of proteins in response to hypoxia.

ACKNOWLEDGMENTS

This work was supported by NIH CA109480, CA111846, CA09796, U.S. Army PC050127, and Korea Health 21 R & D project 01-PJ3-PG6-01GN07, Korea Ministry of Science and Technology KOSEF R11-2005-017.

REFERENCES

1. Jemal, A.; Murray, T.; Ward, E.; Samuels, A.; Tiwari, R.C.; Ghafoor, A.; Feuer, E.J.; Thun, M.J. Cancer Statistics 2005. CA Cancer J. Clin. **2005**, *55*, 10–30.

2. Movsas, B.; Chapman, J.D.; Horwitz, E.M.; Pinover, W.H.; Greenberg, R.E.; Hanlon, A.L.; Iyer, R.; Hanks, G.E. Hypoxic regions exist in human prostate carcinoma. Urology **1999**, *53*, 11–18.
3. Movsas, B.; Chapman, J.D.; Hanlon, A.L.; Horwitz, E.M.; Pinover, W.H.; Greenberg, R.E.; Stobbe, C.; Hanks, G.E. Hypoxia in human prostate carcinoma: an Eppendorf PO_2 study. Am. J. Clin. Oncol. **2001**, *24*, 458–461.
4. Movsas, B.; Chapman, J.D.; Greenberg, R.E.; Hanlon, A.L.; Horwitz, E.M.; Pinover, W.H.; Stobbe, C.; Hanks, G.E. Increasing levels of hypoxia in prostate carcinoma correlate significantly with increasing clinical stage and patient age: an Eppendorf pO_2 study. Cancer **2000**, *89*, 2018–2024.
5. Movsas, B.; Chapman, J.D.; Hanlon, A.L.; Horwitz, E.M.; Greenberg, R.E.; Stobbe, C.; Hanks, G.E.; Pollack, A. Hypoxic prostate/muscle pO_2 ratio predicts for biochemical failure in patients with prostate cancer: preliminary findings. Urology **2002**, *60*, 634–639.
6. Hochachka, P.W.; Rupert, J.L.; Goldenberg, L.; Gleave, M.; Kozlowski, P. Going malignant: the hypoxia-cancer connection in the prostate. Bioessays **2002**, *24*, 749–757.
7. Nahum, A.E.; Movsas, B.; Horwitz, E.M.; Stobbe, C.C.; Chapman, J.D. Incorporating clinical measurements of hypoxia into tumor local control modeling of prostate cancer: implications for the alpha/beta ratio. Int. J. Radiat. Oncol. Biol. Phys. **2003**, *57*, 391–401.
8. Boyer, P.; Chance, B.; Ernester, L.; Mitchell, P.; Racker, E.; Slater, E.C. Oxidative phosphorylation and photo phosphorylation. Ann. Rev. Biochem. **1977**, *46*, 955–1026.
9. Zander, R.; Vaupel, P. Proposal for using a standardized terminology on oxygen transport to tissue. Adv. Exp. Med. Biol. **1985**, *191*, 965–970.
10. Thomlinson, R.H.; Gray, L.H. The histological structure of some human lung cancers and the possible implications for radiotherapy. Brit. J. Cancer **1955**, *9*, 539–549.
11. Brown, J.M. Evidence for acutely hypoxic cells in mouse tumours and a possible mechanism of reoxygenation. Brit. J. Radiol. **1979**, *52*, 650–656.
12. Chaplin, D.J.; Olive, P.L.; Durand, R.E. Intermittent blood flow in a murine tumor: radiobiological effects. Cancer Res. **1987**, *47*, 597–601.
13. Kimura, H.; Braun, R.D.; Ong, E.T.; Hsu, R.; Secomb, T.W.; Papahadjopoulos, D.; Hong, K.; Dewhirst, M.W. Fluctuations in red cell flux in tumor microvessels can lead to transient hypoxia and reoxygenation in tumor parenchyma. Cancer Res. **1996**, *56*, 5522–5528.
14. Hill, S.A.; Pigott, K.H.; Saunders, M.I.; Powell, M.E.; Arnold, S.; Obeid, A.; Ward, G.; Leahy, M.; Hoskin, P.J.; Chaplin, D.J. Microregional blood flow in murine and human tumours assessed using laser Doppler microprobes. Brit. J. Cancer Suppl. **1996**, *27*, S260–S263.
15. Brizel, D.M.; Sibley, G.S.; Prosnitz, L.R.; Scher, R.L.; Dewhirst, M.W. Tumor hypoxia adversely affects the prognosis of carcinoma of the head and neck. Int. J. Radiat. Oncol. Biol. Phys. **1997**, *38*, 285–289.
16. Raleigh, J.A.; Calkins-Adams, D.P.; Rinker, L.H.; Ballenger, C.A.; Weissler, M.C.; Fowler, W.C., Jr.; Novotny, D.B.; Varia, M.A. Hypoxia and vascular endothelial growth factor expression in human squamous cell carcinomas using pimonidazole as a hypoxia marker. Cancer Res. **1998**, *58*, 3765–3768.
17. Vaupel, P.; Hockel, M. Oxygenation of human tumours. In *Blood perfusion and microenvironment of human tomours*; Molls, M., Vaupel, P., Eds.; Springer-Verlag: Berlin, 1998; 63–72.

18. Becker, A.; Hansgen, G.; Bloching, M.; Weigel, C.; Lautenschlager, C.; Dunst, J. Oxygenation of squamous cell carcinoma of the head and neck: comparison of primary tumors, neck node metastases, and normal tissue. Int. J. Radiat. Oncol. Biol. Phys. **1998**, *42*, 35–41.
19. Teicher, B.; Lazo, J.; Sartorelli, A. Classification of antineoplastic agents by their selective toxicities toward oxygenated and hypoxic tumor cells. Cancer Res. **1981**, *41*, 73–81.
20. Gatenby, R.; Kessler, H.; Rosenblum, J.; Coia, L.; Moldofsky, P.; Hartz, W.; Broder, G. Oxygen distribution in squamous cell carcinoma metastases and its relationship to outcome of radiation therapy. Int. J. Radiat. Oncol. Biol. Phys. **1988**, *14*, 831–838.
21. Teicher, B.; Lazo, J.; Sartorelli, A. Hypoxia and drug resistance. Cancer Metastasis Rev. **1994**, *13*, 139–168.
22. Brizel, D.M.; Scully, S.P.; Harrelson, J.M.; Layfield, L.J.; Bean, J.M.; Prosnitz, L.R.; Dewhirst, M.W. Tumor oxygenation predicts for the likelihood of distant metastasis in human soft tissue sarcoma. Cancer Res. **1996**, *56*, 941–943.
23. Brizel, D.M.; Sibley, G.S.; Prosnitz, L.R.; Scher, R.L.; Dewhirst, M.W. Tumor hypoxia adversely affects the prognosis of carcinoma of the head and neck. Int. J. Radiat. Oncol. Biol. Phys. **1997**, *38*, 285–289.
24. Koong, A.C.; Denko, N.C.; Hudson, K.M.; Schindler, C.; Swiersz, L.; Koch, C.; Evans, S.; Ibrahim, H.; Le, Q.T.; Terris, D.J.; Giaccia, A.J. Candidate genes for the hypoxic tumor phynotype. Cancer Res. **2000**, *60*, 883–887.
25. Young, S.D.; Hill, R.F. Effects of reoxigenation on cells from hypoxic regions of solid tumors: anticancer drug sensitivity and metastatic potential. J. Natl. Cancer Inst. **1990**, *82*, 371–380.
26. Graeber, T.G.; Osmanian, C.; Jacks, T.; Housman, D.E.; Koch, C.J.; Lowe, S.W.; Giaccia, A.J. Hypoxia mediated selection of cells with diminished apoptotic potential in solid tumors. Nature (London) **1996**, *379*, 88–91.
27. Rofstad, E.K.; Danielson, T. Hypoxia-induced metastasis of human melanoma cells: involvement of vascular endothelial growth factor mediated angiogenesis. Brit. J. Cancer **1990**, *80*, 1697–1707.
28. Schwickert, G.; Walenta, S.; Sundfor, K.; Rofstad, E.K.; Mueller-Klieser, W. Correlation of high lactate levels in human cervical cancer with incidence of metastasis. Cancer Res. **1995**, *55*, 4757–4759.
29. Yang, W.; Block, E.R. Effect of hypoxia and reoxygenation on the formation and release of reactive oxygen species by porcine pulmonary artery endothelial cells. J. Cell Physiol. **1995**, *164*, 414–423.
30. Littauer, A.; de Groot, H. Release of reactive oxygen by hepatocytes on reoxygenation: three phases and role of mitochondria. Am. J. Physiol. **1992**, *262* (6 Pt 1), G1015–G1020.
31. Becker, L.B.; vanden Hoek, T.L.; Shao, Z.H.; Li, C.Q.; Schumacker, P.T. Generation of superoxide in cardiomyocytes during ischemia before reperfusion. Am. J. Physiol. **1999**, *277* (6 Pt 2), H2240–H2246.
32. Chandel, N.S.; McClintock, D.S.; Feliciano, C.E.; Wood, T.M.; Melendez, J.A.; Rodriguez, A.M.; Schumacker, P.T. Reactive oxygen species generated at mitochondrial complex III stabilize hypoxia-inducible factor-1-alpha during hypoxia: a mechanism of O_2 sensing. J. Biol. Chem. **2000**, *275*, 25130–25138.
33. Paddenberg, R.; Goldenberg, A.; Faulhammer, P.; Braun-Dullaeus, R.C.; Kummer, W. Mitochondrial complex II is essential for hypoxia-induced ROS

generation and vasoconstriction in the pulmonary vasculature. Adv. Exp. Med. Biol. **2003**, *536*, 163–169.
34. Barford, D. The role of cysteine residues as redox-sensitive regulatory switches. Curr. Opin. Struct. Biol. **2004**, *14*, 679–686.
35. Dong, Y.; Zhang, H.; Hawthorn, L.; Ganther, H.E.; Ip, C. Delineation of the molecular basis for selenium-induced growth arrest in human prostate cancer cells by oligonucleotide array. Cancer Res. **2003**, *63*, 52–59.
36. Baek, S.H.; Lee, U.Y.; Park, E.M.; Han, M.Y.; Lee, Y.S.; Park, Y.M. Role of protein kinase C delta in transmitting hypoxia signal to HSF and HIF-1. J. Cell Physiol. **2001**, *188*, 223–235.
37. LeBel, C.P.; Ischiropoulos, H.; Bondy, S.C. Evaluation of the probe 2′,7′-dichlorofluorescin as an indicator of reactive oxygen species formation and oxidative stress. Chem. Res. Toxicol. **1992**, *5*, 227–231.
38. Lowry, O.H.; Rosebrough, N.J.; Farr, A.L.; Randall, R.J. Protein measurement with the Folin phenol reagent. J. Biol. Chem. **1951**, *193*, 265–275.
39. Park, E.M.; Choi, K.S.; Park, S.Y.; Kong, E.S.; Zu, K.; Wu, Y.; Zhang, H.; Ip, C.; Park, Y.M. A display thiol-proteomics approach to characterize global redox modification of proteins by selenium: Implications for the anticancer action of selenium. Cancer Genom. Proteom. **2005**, *2*, 25–36.
40. Tamayo, P.; Slonim, D.; Mesirov, J.; Zhu, Q.; Dmitrovsky, E.; Lander, E.S.; Golub, T.R. Intepreting gene expression with self-organizing maps: Methods and application to hematopoeitic differentiation. Proc. Natl. Acad. Sci. USA **1999**, *96*, 2907–2912.
41. Golub, T.R.; Slonim, D.K.; Tamayo, P.; Huard, C.; Gaasenbeek, M.; Mesirov, J.P.; Coller, H.; Loh, M.L.; Downing, J.R.; Caligiuri, M.A.; Bloomfield, C.D.; Lander, E.S. Molecular classification of cancer: Class discovery and class prediction by gene expression monitoring. Science **1999**, *286*, 531–537.
42. Jung, C.H.; Thomas, J.A. S-glutathiolated hepatocyte proteins and insulin disulfides as substrates for reduction by glutaredoxin, thioredoxin, protein disulfide isomerase, and glutathione. Arch. Biochem. Biophys. **1996**, *335*, 61–72.
43. Ghezzi, P.; Romines, B.; Fratelli, M.; Eberini, I.; Gianazza, E.; Casagrande, S.; Laragione, T.; Mengozzi, M.; Herzenberg, L.A. Protein glutathionylation: coupling and uncoupling of glutathione to protein thiol groups in lymphocytes under oxidative stress and HIV infection. Mol. Immunol. **2002**, *38*, 773–780.
44. Eaton, P.; Byers, H.L.; Leeds, N.; Ward, M.A.; Shattock, M.J. Detection, quantitation, purification, and identification of cardiac proteins S-thiolated during ischemia and reperfusion. J. Biol. Chem. **2002**, *277*, 9806–9811.
45. Di Simplicio, P.; Franconi, F.; Frosali, S.; Di Giuseppe, D. Thiolation and nitrosation of cysteines in biological fluids and cells. Amino Acids **2003**, *25*, 323–339.
46. Shenton, D.; Grant, C.M. Protein S-thiolation targets glycolysis and protein synthesis in response to oxidative stress in the yeast Saccharomyces cerevisiae. Biochem. J. **2003**, *374* (Pt2), 513–519.
47. Eaton, P.; Fuller, W.; Shattock, M.J. S-thiolation of HSP27 regulates its multimeric aggregate size independently of phosphorylation. J. Biol. Chem. **2002**, *277*, 21189–21196.

Received June 20, 2005
Accepted August 5, 2005
Manuscript 7450

Preparative Biochemistry & Biotechnology, 36: 37–64, 2006

ISSN 1082-6068 print/1532-2297 online
DOI: 10.1080/10826060500388512

Neural Network-Based Analysis of Thiol Proteomics Data in Identifying Potential Selenium Targets

Jong-Sik Lee and Yong-Beom Ma
School of Computer Science & Engineering, Inha University, Korea

Kyoung-Soo Choi, Soo-Yeon Park, Sun-Hee Baek, and Young-Mee Park
Department of Cellular Stress Biology, Roswell Park Cancer Institute, Buffalo, NY, USA

Ke Zu, Haitao Zhang, and Clement Ip
Department of Cancer Chemoprevention, Roswell Park Cancer Institute, Buffalo, NY, USA

Yeul Hong Kim
Genomic Research Center for Lung and Breast/Ovarian Cancer, Korea University Medical School, Korea

Eun-Mi Park
Department of Chemistry, University of Incheon, Incheon, Korea

Abstract: Generation of a monomethylated selenium metabolite is critical for the anticancer activity of selenium. Because of its strong nucleophilicity, the metabolite can react directly with protein thiols to cause redox modification. Here, we report a neural network-based analysis to identify potential selenium targets. A reactive thiol specific reagent, BIAM, was used to monitor thiol proteome changes on 2D gel. We constructed a dynamic model and evaluated the relative importance of proteins mediating the cellular responses to selenium. Information from this study will

Address correspondence to Young-Mee Park, Department of Cellular Stress Biology, Roswell Park Cancer Institute, Elm & Carlton Streets, Buffalo, NY 14263, USA. E-mail: young-mee.park@roswellpark.org

provide new clues to unravel mechanisms of anticancer action of selenium. High impact selenium targets could also serve as biomarkers to gauge the efficacy of selenium chemoprevention.

Keywords: Neural-network, Dynamic modeling, Display thiol proteomics, Redox modification, Selenium, Anticancer action

INTRODUCTION

The anticancer activity of selenium is well documented.[1] Both inorganic and organic selenium compounds, as exemplified by selenite and selenomethionine, respectively, are effective in suppressing tumorigenesis in animal models. As proposed originally by Ip and coworkers,[2–4] the metabolism of selenite or selenomethionine to methylselenol (CH_3SeH) is important for their anticancer activities. Methylselenol is highly reactive, difficult to prepare, and cannot be tested as is, in vitro. In order to obviate this problem, a stable metabolite called methylseleninic acid (CH_3SeO_2H, abbreviated to MSA) was developed specifically for cell culture studies. Once taken up by cells, MSA is reduced rapidly to CH_3SeH through non-enzymatic reactions.[5] In vitro studies with human prostate cancer cells showed that exposure to MSA results in cell cycle arrest and induction of apoptosis.[6–11]

At physiological pH, methylselenol is present as anionic methylselenolate. Most protein cysteine residues would not react with methylselenolate because they generally exhibit a pK_a value of 8.0–8.5. But, some protein cysteine residues exist as thiolate anions at neutral pH, because their pK_a value is lowered as a result of the influence of neighboring nucleophilic groups, and the thiolate is often stabilized by salt bridges to positively charged moieties.[12,13] By virtue of the negative charge, thiolates have enhanced reactivity and are called “reactive thiols.” Many vicinal thiols are reactive thiols. Under oxidative stress conditions, a reactive thiol could easily lose an electron to become a thiyl radical,[14,15] which can then react with methylselenolate to form an activated selenenylsulfide intermediate. The latter is susceptible to attack by a second thiol to form an intramolecular disulfide.[16] Due to its strong nucleophilic nature, methylselenolate also readily reacts with protein disulfides and converts them to sulfhydryl groups. From the above description, it is apparent that the interaction of proteins with methylselenolate could result in either a gain or a loss of reactive thiols, depending on the reduction potential of the redox couple. Using a biotinylated iodoacetamide-based display thiol proteomics approach, we recently reported global proteome redox changes of human prostate cancer PC-3 cells by selenium.[17]

In order to identify novel diagnostic and therapeutic targets, there is a great need to develop technologies that allow the systematic analysis of proteomics data. Several computer algorithms have been developed to this end.

However, time-based transitions are not captured in pattern recognition approaches. Furthermore, conventional bioinformatics approaches do not offer clues to the relative importance of proteins in mediating the cellular responses to given stimuli.

Given that a composite of protein-to-protein interactions and dynamic changes of their interactions during the time-transition would determine the cellular responses to selenium, we undertook a neural network-based dynamic modeling approach. Dynamic modeling is based on machine learning algorithms of neural networks.[18–22]

Using the dynamic modeling, time-based changes of redox-status of thiol-containing proteins can be specified and their time-based transitions can be simultaneously analyzed. The weight values of each protein can be computed with respect to their relative contribution in dictating the transition, i.e., cellular responses to selenium.

In this paper, we report thiol proteome data mining for potential selenium target proteins. A neural network-based dynamic model was constructed and the relative importance of proteins was computed using the dynamic model.

EXPERIMENTAL

Cell Culture and Treatment Condition

PC-3 human prostate cancer cells were obtained from the American Type Culture Collection (Manassas, VA). They were cultured in RPMI 1640 medium supplemented with 10% fetal bovine serum, 2 mM glutamine, 100 units/mL of penicillin, and 100 μg/mL of streptomycin.[6] MSA, synthesized as described previously,[5] was added to the culture medium at a final concentration of 10 μM. Cells were processed for protein reactive thiol labeling after 0.5, 1, 2, 3, 6, 12, or 24 h of exposure to MSA. In a parallel experiment, control cultures without MSA treatment were processed similarly.

Reactive Thiol Labeling with N-(Biotinyl)-N′-(Iodoacetyl) Ethylenediamine (BIAM)

Proteins with reactive thiols were labeled with a thiol specific reagent, BIAM, as previously described.[17] Briefly, cells were exposed directly to 100 μL of lysis buffer containing 20 μM BIAM (Molecular Probes, Eugene, OR) in a hypoxic chamber. The lysis buffer consisted of 50 mM 2-(N-morpholino) ethanesulfonic acid (pH 6.5), 100 mM NaCl, 0.5% (v/v) Triton X-100, 1 μg/mL leupeptin, and 10 μM phenylmethylsulfonyl fluoride; the buffer was rendered free of oxygen by bubbling with argon gas at a low flow rate for 1 h. Cells were detached from the dish with a cell scraper and homogenized with a glass/glass homogenizer with 10 strokes in an anoxic condition.

The labeling reaction was terminated by adding β-mercaptoethanol to a final concentration of 20 mM. The reaction mixture was centrifuged at 10,000 g for 10 min at 4°C. The supernatant was subjected to 2D gel electrophoresis.

Display of BIAM-Labeled Reactive Thiols on 2D Gel

The supernatant obtained as above was subjected to a display thiol proteomics approach, as described in our previous work.[17] In brief, the reagent, BIAM, is biotinylated so that the biotin group now linked to the protein thiol (–S-IAM-biotin) can later react with HRP-conjugated streptavidin to locate the spot on the 2D gel. Since BIAM preferentially reacts with thiolates and not with cysteine sulfhydryl groups (Cys-SH), only proteins with reactive thiols are visualized by HRP-conjugated streptavidin and enhanced chemiluminescence. Approximately 35% of total protein spots are consistently labeled by BIAM in our hands.

2D Gel Electrophoresis and Image Analysis

The supernatant was mixed with a rehydration buffer (8 M urea, 2% CHAPS, 1% IPG buffer, and 50 mM DTT) for 2 h at room temperature. It was electrofocused in DryStryps (pH 3–10 NL) with the IPGphore (both from Amersham Biosciences). After electrofocusing, the gel was equilibrated for 15 min with a buffer containing 10 mg/mL DTT, 8 M urea, 2% (w/v) SDS and 30% (v/v) glycerol, and then for another 15 min with a second buffer containing the same ingredients, with the exception that DTT was replaced with 25 mg/mL iodoacetamide. Second-dimensional SDS-PAGE was performed on a 12% polyacrylamide gel. Proteins labeled with BIAM were transferred to a PVDF membrane and detected with HRP-conjugated streptavidin (Amersham) and enhanced chemiluminescence. The image of the thiol specific-stained blots was analyzed by PDQuest (version 7.1, Bio-Rad) to extract the raw intensity data. The total quantity of internal control spots was used for normalization. A separate portion of the protein extract was subjected to 2D gel electrophoresis, stained with SyproRuby (Bio-Rad), and processed for the subsequent identification of labeled proteins.

Protein Identification by Mass Spectrometry

Protein spots were analyzed by mass spectrometry after tryptic in-gel digestion. For the initial analysis, we carried out MALDI-TOF mass spectrometry using M@LDI^{TM}-LR (Micromass, Beverly, MA). The raw mass spectra were analyzed to obtain a list of monoisotopic peaks using ProteinLynx

Global SERVER 2.0 program from Waters (http://www.waters.com). The peptide mass error was limited to 50 ppm. The protein candidates were identified using the National Center for Biotechnology Information (NCBI) database as the search engine. When the search results were ambiguous, the remaining tryptic mixture after MALDI-TOF Mass Spectrometry was subjected to ESI-tandem mass spectrometry using Q-TOF API US (Micromass).

Protein Annotation and Retrieval of Information on Vicinal Thiols

The sequences and annotations of the identified proteins were retrieved from the Protein database at the NCBI by querying the database with the protein accession numbers. The sequences were analyzed for the presence of vicinal thiols using regular expression. The above analyses were performed with custom PERL scripts.

RESULTS

Effect of MSA Treatment on Protein Redox Modification and Construction of Neural Network-Based Dynamic Model

Cells were treated with 10 μM MSA for 0.5, 1, 2, 3, 6, 12, or 24 h. MSA did not affect growth or apoptosis of PC-3 cells within this time frame.[6] The purpose of the experiment was to quantify the subset of proteins sensitive to redox modification by MSA and the manner in which these changes occurred. At each time point, we identified the spots of which the BIAM labeling intensity was either decreased or increased, respectively, in response to MSA. We identified a total of 194 proteins labeled by BIAM in MSA-exposed cells. For comparison, we ran control samples harvested at the same time points as MSA-treated cells. This data set did not cause any distinguishing changes of BIAM-labeled spots.[17] In order to facilitate a comparison of the image intensity of each spot at different time points standardized against the zero hour data, we performed a scatter plot analysis to study the variations as a function of time. Based on the Pearson's correlation coefficient, it was evident that there were minimal changes in redox modification of proteins during this period.

In order to obtain insight into the manner of protein thiol redox changes induced by MSA, we employed a neural network-based dynamic model. Cellular response to MSA would, at least in part, be mediated by the changes of redox status and function of thiol-containing proteins at a given time point. To design the structure of time-related data features in a dynamic model, each BIAM-labeled protein spot in 2D gels was designated as a single element. A composite of these elements (multi-element) was

designated as a "state". Influence of an element is not likely to be a one-to-one protein relationship. Rather, each element is likely to be cross-influenced by each other as schematized in Figure 1. A neural network-based dynamic model represents the relationship between states, each state containing multiple interactive elements, i.e., proteome. The dynamic model computes the fully connected network of neural network and assigns its "weight value" to each connection. The weight value is a quantitative representation of an influence of an element (protein) to another element in the next time point in a fully connected neural network. The weight value of one protein to other proteins would change during the time transition following the learning rule of the neural network. The dynamic model keeps a trace of a time-based transition of cellular state and identifies dominant proteins that influence the state-transition.

Model Input, Output, and Execution

To execute the neural network-based dynamic model, signal intensities of BIAM-labeled protein spots were used as input values. Input values of spots represent the $\log_2$ transformation of the treatment to control signal

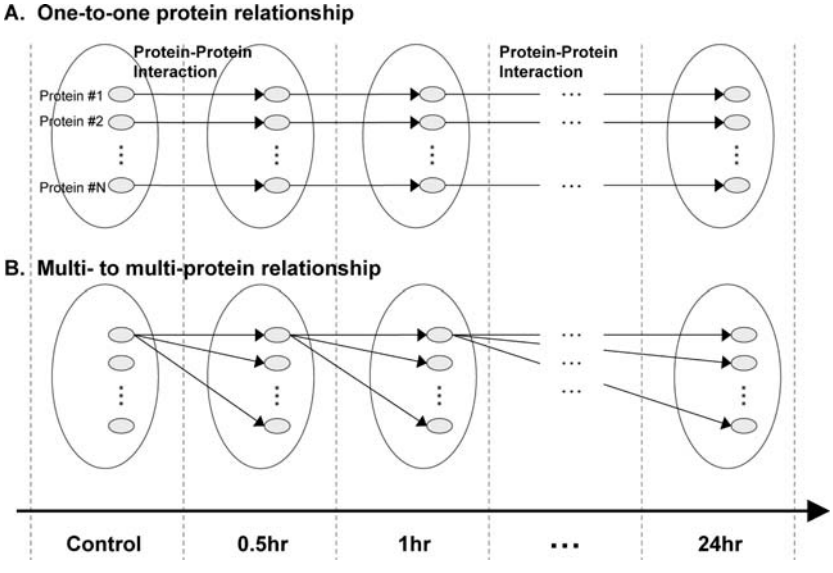

Figure 1. Dynamic model with state transition in time series. Panel A. dynamic model with one-to-one protein interaction in multi-element state transition; Panel B. neural network-based dynamic model with multi-to-multi interaction in multi-element state transition.

ratios at each time point. Figure 2 illustrates an object diagram of the neural network-based dynamic model. For weight value training, Delta-learning rule[23] (also called the Widrow-Hoff rule) was employed. The inputs are the signal intensities of BIAM-labeled protein spots in 2D gels. The outputs are the weight values computed based on the weight training by the Delta-learning rule. The Delta-Learning rule trains the network weight values (relative importance) by reducing the error between the computed signal intensities from the dynamic model and the actual signal intensities obtained from the BIAM-labeled protein spots.

To obtain a cumulative significance of BIAM-labeled protein spots in influencing cellular responses and state-transition during exposure to selenium, we employed forward- and backward-weight rank determination methods using the trained weight values (Figure 3). The forward-weight rank method determines the influence of a BIAM-labeled spot (an element) in a current time point (state) on the cell state transition in the next time point. A cumulative weight value of an element was obtained by combining its weight values in a given time point to all elements in the next state ($\text{Sum}_{a0} = \sum a_0 a_1$). Forward rank was determined by combining the forward-weight values of each BIAM-labeled spot, $\text{Rank}_{a0} = \text{Ranking}(\text{Sum}_{a0})$, in our display thiol proteomics approach. The backward-weight rank was determined similarly to the forward-weight rank, but by evaluating the influence of each element in previous cell state on an element in the current cell state. A cumulative significance of a BIAM-labeled protein spot was obtained as schematized in Figure 4.

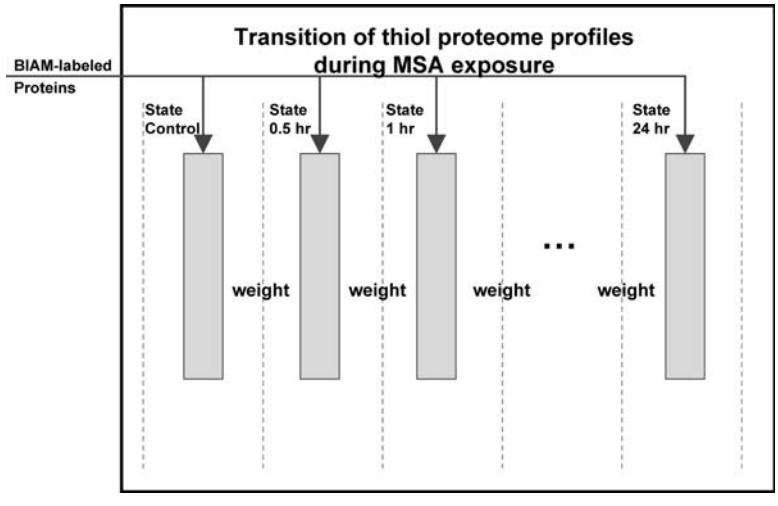

Figure 2. Object diagram of neural network-based dynamic model. Transition of thiol proteome profiles during MSA exposure is schematized in an object diagram.

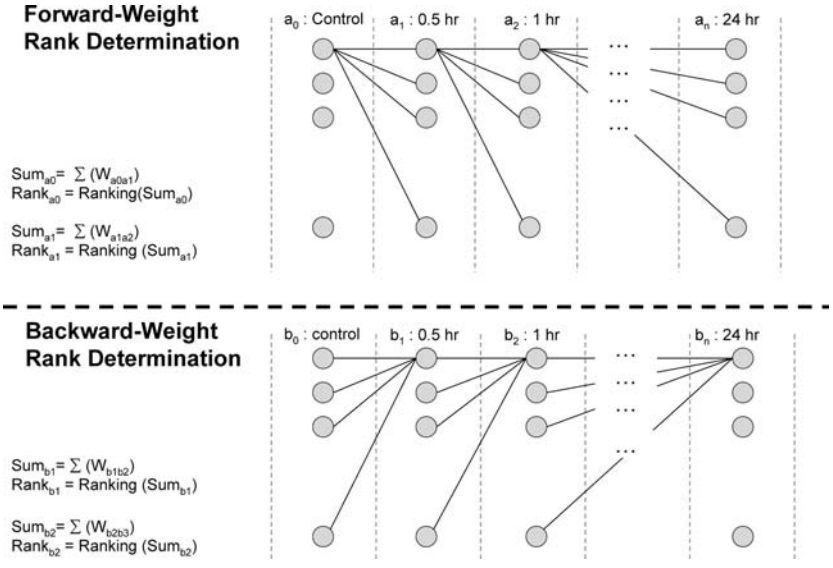

Figure 3. Forward- and backward-weight rank determination.

Rank Determination and Protein Identification by Mass Spectrometry

Based on the hierarchical ranking determination method, early-state, late-state, and all time-series ranking were hierarchically determined. Out of a total of 195 protein spots displayed in the 2D gel, we identified 85 proteins using MALDI-TOF and ESI-tandem mass spectrometry. Tables 1–3 show the identities of 85 proteins in the order of relative importance from top to bottom in early-state (Table 1), late state (Table 2), and all time-series (Table 3). The tables also show information on the accession number, protein name, subcellular localization, and vicinal thiols. The identified proteins are present in various subcellular compartments, including nucleus, cytoplasm, mitochondria, endoplasmic reticulum (ER), and lysosome. Their ubiquity is consistent with the pervasive nature of a small selenium metabolite capable of striking many sensitive targets in a cell. Individually, there could be changes in the functions of these proteins when their redox status is altered. On a global scale, redox modification of these proteins is likely to play an important role in mediating the cellular responses to selenium.

DISCUSSION

This is the first study to describe using a neural network-based data mining tool to evaluate the relative importance of potential selenium targets identified

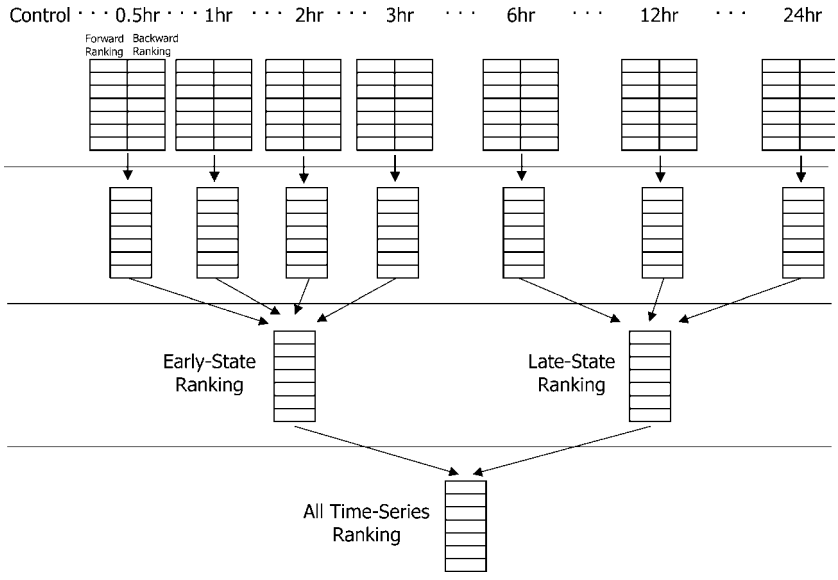

Figure 4. Early-state, late-state and all time series ranking determination.

in a display thiol-proteomics approach. The information obtained from this study is expected to provide new clues in elucidating the mechanisms of the anticancer action of selenium. In our previous publication,[17] the $\log_2$-transformed signal intensities of the BIAM-labeled protein spots were subjected to clustering analysis by using the self-organizing maps (SOM) algorithm. The SOM algorithm is designed for pattern recognition in grouping proteins according to the similarities in their redox profiles as a function of time. Four distinct patterns emerged from the analysis; these patterns provide valuable insight into the dynamics of thiol redox modification by selenium. However, the clustering analysis does not offer answers to the more biologically relevant question: which protein(s) are functionally important for the effect of selenium? The neural network-based modeling, coupled to a hierarchical ranking determination, is a novel concept in bioinformatics data mining because it prioritizes the relative importance of a particular protein in mediating the cellular responses to selenium.

Heat shock 70 kDa protein 5, also known as GRP78, is one of the high ranking proteins in the early-state, late-state, as well as all-time series. GRP78 is an ER-resident chaperone; it binds to, and maintains, nascent proteins in a folding-competent state, preventing protein aggregation. Accumulation of unfolded/misfolded proteins in the ER lumen elicits self-protective signaling events known as unfolded protein response (UPR). As the master regulator of the UPR, GRP78 sequesters the ER stress transducers on the ER membrane by binding to their lumenal domains. There is also free

Table 1. Early state rank determination and protein identification

SSP	Accession no.	Protein name	Subcellualar localization	Vicinal thiol
6402	BAA22860	A + U-rich element RNA binding factor		
6301	Q13490	Inhibitor of apoptosis protein 2(HIAP2)	Cytoplasmic (Potential)	83-CFCC, 220-CFAC, 306-CFCC, 571-CKVC, 592-CQEC, 602-CPIC
1601	P43329	ATP dependent helicase hrpA		1112-CISC
2501	Q10250	Hypothetical 170 7 kDa protein C56F8 02 in chromos		770-CVEC
3205	P32119	Peroxiredoxin 2	Cytoplasmic	
4301	P30084	Enoyl-CoA hydratase, Mitochondrial precursor	Mitochondrial matrix	
2103	P32485	Mitogen activated protein kinase HOG1 EC 2 7 1		
4501	P17545	DNA directed RNA polymerase II largest subunit EC		69-CETC, 107-CVCKTC
6604	P50995	Annexin A11 Annexin XI Calcyclin associated ann		
3303	O65607	DNA mismatch repair protein MSH3 AtMsh3		
3701	NP_005304	Glucose regulated protein, 58kDa		57-CGHC, 406-CGHC
2304	4505773	Prohibitin		
5301	NP_005338	Heat shock 70 kDa protein 5	Endoplasmic reticulum	
106	Q20799	Probable calcium binding mitochondrial carrier F55		448-CGTC
3304	P05164	Myeloperoxidase precursor(MPO) C-1-tetrahydrofolate synthase, cytoplasmic(methylenetetrahydrofolate dehydrogenase)	Lysosomal	316-CPAC
6304	Q9UPN3	Microtubule-actin crosslinking factor 1, isoforms 1/2/3 (Actin cross-linking family protein 7) (Macrophin 1)	Cytoplasmic	775-CLC, 5175-CKC

4504	P48681	Nestin		
6810	NP_228019	ABC transporter, ATP-binding protein		
6701	P78527	DNA-dependent protein kinase catalytic subunit (DNA-PKcs) (DNPK1) (p460)	Nuclear	1029-CGRC
3402	Q9UY36	Alanyl tRNA synthetase EC 6 1 1 7 Alanine tRNA		20-CKVC
1304	P40939	Mitochondrial trifunctional enzyme alpha subunit precusor(containing chain Enoyl-CoA hydratase/ Long chain 3-hydroxyacyl-CoA dehydrogenase)	Mitochondrial matrix	
7201	NP_002565	Peroxiredoxin 1	Cytoplasmic	
7301	P25388	Guanine nucleotide binding protein beta subunit li		
1801	NP_004125	Heat shock 70 kDa		
3305	Q16658	Fascin(actin bundling protein)		
4401	BAB84979	FLJ0226 protein		
3302	P31937	3 hydroxyisobutyrate dehydrogenase mito	Mitochondrial	
3801	P38646	Mitochondrial stress-70 protein precusor(75kD glucose regulated proein)(GRP75)	Mitochondrial	
4208	P30048	Thioredoxin dependent peroxide reductase mitochon		
4608	P78371	T-complex protein 1, beta subunit	Cytoplasmic	
6801	P00558	Phosphoglycerate kinase 1 EC 2 7 2 3 Primer rec		
4304	P06713	Nitrogen regulation protein NR I		
2404	AAQ10304	IL1RAPL1-dystrophin fusion prtoein		
302	AAL84570	TPMsk3		
3702	P30101	Protein disulfide isomerase A3 precusor EC534	Endoplasmic reticulum lumen (By similarity)	57-CGHC, 406-CGHC
7303	229674	Aldolase A		
6401	P03519	Matrix protein		

(*continued*)

Table 1. Continued

SSP	Accession no.	Protein name	Subcellualar localization	Vicinal thiol
8501	P07954	Fumarate hydratase	Mitochondrial & cytoplasmic	
107	P08968	DNA directed RNA polymerase III largest subunit E		74-CETC, 114-CKRC, 161-CLKC, 495-CCC
2807	P38646	Stress-70 protein, mitochondrial precursor (75 kDa glucose regulated protein) (GRP 75) (Peptide-binding protein 74) (PBP74) (Mortalin) (MOT)	Mitochondrial	
3306	Q10451	Hypothetical 141 9 kDa protein C12B10 18 in chromo		
7702	O60701	UDP glucose 6 dehydrogenase EC 1 1 1 22 UDP Glc		
2102	P47768	DNA directed RNA polymerase beta chain EC 2 7 7 6		
202	P33459	POL polyprotein contains protease retropepsin		869-CEIC
3307	Q45388	TEX protein		
5202	P52111	Glycerol 3 phosphate dehydrogenase EC 1 1 99 5		
5303	O31047	Adenylosuccinate synthetase EC 6 3 4 4 IMP asp	Cytoplasmic	
3204	P41958	Apoptosis regulator ced 9 Cell death protein 9		
5806	Q15942	Zyxin	Cytoplasmic; associates with the actin cytos-keleton near the adhesion plaques	384-CGRC, 409-CFTCHQC, 433-CEGC, 444-CNTC, 467-CFTCVVC, 504-CSVC, 534-CYKCEDC, 562-CRKC
7302	Q99714	3 hydroxyacyl CoA dehydrogenase type II EC 1 1 1		

5401	P06733	Alpha enolase (EC 4.2.1.11)	Cytoplasmic	337-CNC
7101	P04080	Cystatin B liver thiol proteinase inhibitor CPI	Cytoplasmic and nuclear	
201	KIAA1723 protein			
2401	NP_000909	Proline 4 hydroxylase	Cytoplasmic	53-CGHC, 397-CGHC
4802	P13433	DNA directed RNA polymerase mitochondrial precurs		
5805	NP_005496	Scavenger receptor class B, member 1; CD36 antigen-like 1		
7402	P04406	Glyceraldehyde 3-phosphate dehydrogenase, liver (GAPDH)	Cytoplasmic	
4206	P28649	Cytochrome P450 11B1 mitochondrial precursor EC	Membrane-bound	
3805	O65607	DNA mismatch repair protein MSH3 AtMsh3		
105	P39975	Hypothetical 26 8 kDa protein in DLD3 5 region		4-CPC
4201	NP_000260	Nucleoside-diphosphate kinase 1 isoform b		
3404	P15531	Nucleoside diphosphate kinase A EC 2 7 4 6 NDK		
7504	Q91187	V D J recombination activating protein 1 RAG 1		110-CLCRLC, 176-CQRC, 207-CLLC, 310-CQVC, 330-CRSC, 345-CPAC, 762-CTLC
8201	P37802	Transgelin 2 SM22 alpha homolog		
3604	Q10970	Chromosome partition protein smc		
4805	O19048	DNA directed RNA polymerase II largest subunit EC		
1103	Q04832	DNA binding protein HEXBP Hexamer binding protein		
5601	O33369	DNA gyrase subunit B EC 5 99 1 3		

(*continued*)

Table 1. Continued

SSP	Accession no.	Protein name	Subcellualar localization	Vicinal thiol
2701	P05209	Tubulin alpha 1 chain		
2305	PMHUYM	Phosphoglycerate mutase EC 5 4 2 1		
7704	Q03265	ATP synthase alpha chain mitochondrial precursor	Mitochondrial	
4103	P05092	Peptidyl prolyl cis trans isomerase A EC 5 2 1 8	Cytoplasmic	
3207	P16666	Inclusion body matrix protein Viroplasmin	Cytoplasmic inclusion bodies	477-CHHC
1201	P14742	Glucosamine fructose 6 phosphate aminotransferase		183-CKSC
1102	Q15181	Inorganic pyrophosphatase EC 3 6 1 1 Pyrophosph		
5101	P20228	Glutamate decarboxylase EC 4 1 1 15 GAD		
7801	P78332	RNA binding protein 6 RNA binding motif protein 6		
404	P78621	Cytokinesis protein sepA FH1 2 protein Forced e		
2809	Q60577	Heterogeneous nuclear ribonucleoprotein K hnRNP K		
3405	NP_003748	Eukaryotic translation initiation factor 3, subunit 2 beta; TNF beta receptor interacting protein 1		
5702	NP_000427	3-oxoacidCoA transferase	Mitochondrial	28-CVC
7404	Q9TT14	Voltage dependent anion selective channel protein		
602	Q05022	rRNA biogenesis protein RRP5		
1704	P25328	Probable RNA directed RNA polymerase in W dsRNA E		
8104	O18017	Probable blooms syndrome protein homolog EC 3 6		640-CDIC

Table 2. Late state rank determination and protein identification

SSP	Accession no.	Protein name	Subcellualar localization	Vicinal thiol
2404	AAQ10304	IL1RAPL1-dystrophin fusion prtoein		
1601	P43329	ATP dependent helicase hrpA		1112-CISC
2501	Q10250	Hypothetical 170 7 kDa protein C56F8 02 in chromos		770-CVEC
3302	P31937	3 hydroxyisobutyrate dehydrogenase mito	Mitochondrial	
4504	P48681	Nestin		
1801	NP_004125	Heat shock 70 kDa		
2807	P38646	Stress-70 protein, mitochondrial precursor (75 kDa glucose regulated protein) (GRP 75) (Peptide-binding protein 74) (PBP74) (Mortalin) (MOT)	Mitochondrial	
5301	NP_005338	Heat shock 70 kDa protein 5	Endoplasmic reticulum	
4608	P78371	T-complex protein 1, beta subunit	Cytoplasmic	
3402	Q9UY36	Alanyl tRNA synthetase EC 6 1 1 7 Alanine tRNA		20-CKVC
1304	P40939	Mitochondrial trifunctional enzyme alpha subunit precusor(containing chain Enoyl-CoA hydratase/ Long chain 3-hydroxyacyl-CoA dehydrogenase)	Mitochondrial matrix	
6701	P78527	DNA-dependent protein kinase catalytic subunit (DNA-PKcs) (DNPK1) (p460)	Nuclear	1029-CGRC
3701	NP_005304	Glucose regulated protein, 58 kDa		57-CGHC, 406-CGHC
7301	P25388	Guanine nucleotide binding protein beta subunit li		
3205	P32119	Peroxiredoxin 2	Cytoplasmic	

(*continued*)

Table 2. Continued

SSP	Accession no.	Protein name	Subcellualar localization	Vicinal thiol
7504	Q91187	V D J recombination activating protein 1 RAG 1		110-CLCRLC, 176-CQRC, 207-CLLC, 310-CQVC, 330-CRSC, 345-CPAC, 762-CTLC
6301	Q13490	Inhibitor of apoptosis protein 2(HIAP2)	Cytoplasmic (Potential)	83-CFCC, 220-CFAC, 306-CFCC, 571-CKVC, 592-CQEC, 602-CPIC
3303	O65607	DNA mismatch repair protein MSH3 AtMsh3		
3702	P30101	Protein disulfide isomerase A3 precusor EC534	Endoplasmic reticulum lumen (By similarity)	57-CGHC, 406-CGHC
5401	P06733	Alpha enolase (EC 4.2.1.11)	Cytoplasmic	337-CNC,
4301	P30084	Enoyl-CoA hydratase, Mitochondrial precursor	Mitochondrial matrix	
2304	4505773	Prohibitin		
4501	P17545	DNA directed RNA polymerase II largest subunit EC		69-CETC, 107-CVCKTC
3207	P16666	Inclusion body matrix protein Viroplasmin	Cytoplasmic inclusion bodies	477-CHHC
4401	BAB84979	FLJ0226 protein		
7402	P04406	Glyceraldehyde 3-phosphate dehydrogenase, liver (GAPDH)	Cytoplasmic	

6801	P00558	Phosphoglycerate kinase 1 EC 2 7 2 3 Primer rec		
6401	P03519	Matrix protein		
6304	Q9UPN3	Microtubule-actin crosslinking factor 1, isoforms 1/2/3 (Actin cross-linking family protein 7) (Macrophin 1)	Cytoplasmic	775-CLC, 5175-CKC
8501	P07954	Fumarate hydratase	Mitochondrial & cytoplasmic	
7303	229674	Aldolase A		
7702	O60701	UDP glucose 6 dehydrogenase EC 1 1 1 22 UDP Glc		
6604	P50995	Annexin A11 Annexin XI Calcyclin associated ann		
7201	NP_002565	Peroxiredoxin 1	Cytoplasmic	
5601	O33369	DNA gyrase subunit B EC 5 99 1 3		
6402	BAA22860	A + U-rich element RNA binding factor		
3801	P38646	Mitochondrial stress-70 protein precusor(75kD glucose regulated proein)(GRP75)	Mitochondrial	
2102	P47768	DNA directed RNA polymerase beta chain EC 2 7 7 6		
302	AAL84570	TPMsk3		
5806	Q15942	Zyxin	Cytoplasmic; associates with the actin cytos-keleton near the adhesion plaques	384-CGRC, 409-CFTCHQC, 433-CEGC, 444-CNTC, 467-CFTCVVC, 504-CSVC, 534-CYKCEDC, 562-CRKC
7704	Q03265	ATP synthase alpha chain mitochondrial precursor	Mitochondrial	
3305	Q16658	Fascin(actin bundling protein)		
5303	O31047	Adenylosuccinate synthetase EC 6 3 4 4 IMP asp	Cytoplasmic	

(*continued*)

Table 2. Continued

SSP	Accession no.	Protein name	Subcellualar localization	Vicinal thiol
7101	P04080	Cystatin B liver thiol proteinase inhibitor CPI	Cytoplasmic and nuclear	
201	KIAA1723 protein			
2809	Q60577	Heterogeneous nuclear ribonucleoprotein K hnRNP K		
4208	P30048	Thioredoxin dependent peroxide reductase mitochon		
7404	Q9TT14	Voltage dependent anion selective channel protein		
3204	P41958	Apoptosis regulator ced 9 cell death protein 9		
2701	P05209	Tubulin alpha 1 chain		
7302	Q99714	3 hydroxyacyl CoA dehydrogenase type II EC 1 1 1		
3304	P05164	Myeloperoxidase precursor(MPO) C-1-tetrahydrofolate synthase, cytoplasmic(methylenetetrahydrofolate dehydrogenase)	Lysosomal	316-CPAC
202	P33459	POL polyprotein contains protease retropepsin		869-CEIC
106	Q20799	Probable calcium binding mitochondrial carrier F55		448-CGTC
2103	P32485	Mitogen activated protein kinase HOG1 EC 2 7 1		
4201	NP_000260	Nucleoside-diphosphate kinase 1 isoform b		
2305	PMHUYM	Phosphoglycerate mutase EC 5 4 2 1		
5202	P52111	Glycerol 3 phosphate dehydrogenase EC 1 1 99 5		
6810	NP_228019	ABC transporter, ATP-binding protein		
3307	Q45388	TEX protein		
404	P78621	Cytokinesis protein sepA FH1 2 protein Forced e		
1201	P14742	Glucosamine fructose 6 phosphate aminotransferase		183-CKSC
105	P39975	Hypothetical 26 8 kDa protein in DLD3 5 region		4-CPC

4802	P13433	DNA directed RNA polymerase mitochondrial precurs		
4304	P06713	Nitrogen regulation protein NR I		
1704	P25328	Probable RNA directed RNA polymerase in W dsRNA E		
8201	P37802	Transgelin 2 SM22 alpha homolog		
3604	Q10970	Chromosome partition protein smc		
1102	Q15181	Inorganic pyrophosphatase EC 3 6 1 1 Pyrophosph		
2401	NP_000909	Proline 4 hydroxylase	Cytoplasmic	53-CGHC, 397-CGHC
107	P08968	DNA directed RNA polymerase III largest subunit E		74-CETC, 114-CKRC, 161-CLKC, 495-CCC
7801	P78332	RNA binding protein 6 RNA binding motif protein 6		
3306	Q10451	Hypothetical 141 9 kDa protein C12B10 18 in chromo		
4206	P28649	Cytochrome P450 11B1 mitochondrial precursor EC	Membrane-bound	
1103	Q04832	DNA binding protein HEXBP Hexamer binding protein		
3405	NP_003748	Eukaryotic translation initiation factor 3, subunit 2 beta; TNF beta receptor interacting protein 1		
3404	P15531	Nucleoside diphosphate kinase A EC 2 7 4 6 NDK		
5702	NP_000427	3-oxoacidCoA transferase	Mitochondrial	28-CVC
5805	NP_005496	Scavenger receptor class B, member 1; CD36 antigen-like 1		
4805	O19048	DNA directed RNA polymerase II largest subunit EC		
4103	P05092	Peptidyl prolyl cis trans isomerase A EC 5 2 1 8	Cytoplasmic	
5101	P20228	Glutamate decarboxylase EC 4 1 1 15 GAD		
602	Q05022	rRNA biogenesis protein RRP5		
3805	O65607	DNA mismatch repair protein MSH3 AtMsh3		
8104	O18017	Probable blooms syndrome protein homolog EC 3 6		640-CDIC

Table 3. Total rank determination and protein identification

SSP	Accession no.	Protein name	Subcellualar localization	Vicinal thiol
1601	P43329	ATP dependent helicase hrpA		1112-CISC
2501	Q10250	Hypothetical 170 7 kDa protein C56F8 02 in chromos	Integral membrane protein (Potential)	770-CVEC
4504	P48681	Nestin		
5301	NP_005338	Heat shock 70 kDa protein 5	Endoplasmic reticulum	
3205	P32119	Peroxiredoxin 2	Cytoplasmic	
3302	P31937	3 hydroxyisobutyrate dehydrogenase mito	Mitochondrial	
6301	Q13490	Inhibitor of apoptosis protein 2(HIAP2)	Cytoplasmic (Potential)	83-CFCC, 220-CFAC, 306-CFCC, 571-CKVC, 592-CQEC, 602-CPIC
1801	NP_004125	Heat shock 70 kDa		
2404	AAQ10304	IL1RAPL1-dystrophin fusion prtoein		
3701	AAP36370	Glucose regulated protein, 58 kDa		57-CGHC, 406-CGHC
6402	BAA22860	A + U-rich element RNA binding factor		
4301	P30084	Enoyl-CoA hydratase, Mitochondrial precursor	Mitochondrial matrix	
3303	O65607	DNA mismatch repair protein MSH3 AtMsh3		
4501	P17545	DNA directed RNA polymerase II largest subunit EC		69-CETC, 107-CVCKTC
3402	Q9UY36	Alanyl tRNA synthetase EC 6 1 1 7 Alanine tRNA		20-CKVC
6701	P78527	DNA-dependent protein kinase catalytic subunit (DNA-PKcs) (DNPK1) (p460)	Nuclear	1029-CGRC
1304	P40939	Mitochondrial trifunctional enzyme alpha subunit precusor(containing chain Enoyl-CoA hydratase/ Long chain 3-hydroxyacyl-CoA dehydrogenase)	Mitochondrial matrix	
2304	4505773	Prohibitin		

4608	P78371	T-complex protein 1, beta subunit	Cytoplasmic	
7301	P25388	Guanine nucleotide binding protein beta subunit li		
2807	P38646	Stress-70 protein, mitochondrial precursor (75 kDa glucose regulated protein) (GRP 75) (Peptide-binding protein 74) (PBP74) (Mortalin) (MOT)	Mitochondrial	
6604	P50995	Annexin A11 Annexin XI Calcyclin associated ann		
6304	Q9UPN3	Microtubule-actin crosslinking factor 1, isoforms 1/2/3 (Actin cross-linking family protein 7) (Macrophin 1)	Cytoplasmic	775-CLC, 5175-CKC
4401	BAB84979	FLJ0226 protein		
7201	NP_002565	Peroxiredoxin 1	Cytoplasmic	
3702	P30101	Protein disulfide isomerase A3 precusor EC534	Endoplasmic reticulum lumen (By similarity)	57-CGHC, 406-CGHC
6801	P00558	Phosphoglycerate kinase 1 EC 2 7 2 3 Primer rec		
2103	P32485	Mitogen activated protein kinase HOG1 EC 2 7 1		
3304	P05164	Myeloperoxidase precursor(MPO) C-1-tetrahydrofolate synthase, cytoplasmic(methylenetetrahydrofolate dehydrogenase)	Lysosomal	316-CPAC
3305	Q16658	Fascin(actin bundling protein)		
3801	P38646	Mitochondrial stress-70 protein precusor(75 kD glucose regulated protein)(GRP75)	Mitochondrial	
6401	P03519	Matrix protein		
106	Q20799	Probable calcium binding mitochondrial carrier F55		448-CGTC
7303	229674	Aldolase A		
302	AAL84570	TPMsk3		

(*continued*)

Table 3. Continued

SSP	Accession no.	Protein name	Subcellualar localization	Vicinal thiol
8501	P07954	Fumarate hydratase	Mitochondrial & cytoplasmic	
4208	P30048	Thioredoxin dependent peroxide reductase mitochon		
6810	NP_228019	ABC transporter, ATP-binding protein		
7702	O60701	UDP glucose 6 dehydrogenase EC 1 1 1 22 UDP Glc		
5401	P06733	Alpha enolase (EC 4.2.1.11)	Cytoplasmic	337-CNC
2102	P47768	DNA directed RNA polymerase beta chain EC 2 7 7 6		
7402	P04406	Glyceraldehyde 3-phosphate dehydrogenase, liver (GAPDH)	Cytoplasmic	
7504	Q91187	V D J recombination activating protein 1 RAG 1		110-CLCRLC, 176-CQRC, 207-CLLC, 310-CQVC, 330-CRSC, 345-CPAC, 762-CTLC
5303	O31047	Adenylosuccinate synthetase EC 6 3 4 4 IMP asp	Cytoplasmic	
5806	Q15942	Zyxin	Cytoplasmic; associates with the actin cytoskeleton near the adhesion plaques	384-CGRC, 409-CFTCHQC, 433-CEGC, 444-CNTC, 467-CFTCVVC, 504-CSVC, 534-CYKCEDC, 562-CRKC
202	P33459	POL polyprotein contains protease retropepsin		869-CEIC
3204	P41958	Apoptosis regulator ced 9 cell death protein 9		
7101	P04080	Cystatin B liver thiol proteinase inhibitor CPI	Cytoplasmic and nuclear	
4304	P06713	Nitrogen regulation protein NR I		

201	KIAA1723 protein			
5202	P52111	Glycerol 3 phosphate dehydrogenase EC 1 1 99 5		
7302	Q99714	3 hydroxyacyl CoA dehydrogenase type II EC 1 1 1		
3307	Q45388	TEX protein		
5601	O33369	DNA gyrase subunit B EC 5 99 1 3		
3207	P16666	Inclusion body matrix protein Viroplasmin	Cytoplasmic inclusion bodies	477-CHHC
107	P08968	DNA directed RNA polymerase III largest subunit E		74-CETC, 114-CKRC, 161-CLKC, 495-CCC
3306	Q10451	Hypothetical 141 9 kDa protein C12B10 18 in chromo		
4201	NP_000260	Nucleoside-diphosphate kinase 1 isoform b		
7704	Q03265	ATP synthase alpha chain mitochondrial precursor	Mitochondrial	
105	P39975	Hypothetical 26 8 kDa protein in DLD3 5 region		4-CPC
4802	P13433	DNA directed RNA polymerase mitochondrial precurs		
2701	P05209	Tubulin alpha 1 chain		
2401	NP_000909	Proline 4 hydroxylase	Cytoplasmic	53-CGHC, 397-CGHC
4206	P28649	Cytochrome P450 11B1 mitochondrial precursor EC	Membrane-bound	
2305	PMHUYM	Phosphoglycerate mutase EC 5 4 2 1		
8201	P37802	Transgelin 2 SM22 alpha homolog		
3604	Q10970	Chromosome partition protein smc		
5805	NP_005496	Scavenger receptor class B, member 1; CD36 antigen-like 1		
3404	P15531	Nucleoside diphosphate kinase A EC 2 7 4 6 NDK		
2809	Q60577	Heterogeneous nuclear ribonucleoprotein K hnRNP K		

(*continued*)

Table 3. Continued

SSP	Accession no.	Protein name	Subcellualar localization	Vicinal thiol
1201	P14742	Glucosamine fructose 6 phosphate aminotransferase		183-CKSC
1103	Q04832	DNA binding protein HEXBP Hexamer binding protein		
7404	Q9TT14	Voltage dependent anion selective channel protein		
4805	O19048	DNA directed RNA polymerase II largest subunit EC		
404	P78621	Cytokinesis protein sepA FH1 2 protein Forced e		
1102	Q15181	Inorganic pyrophosphatase EC 3 6 1 1 Pyrophosph		
7801	P78332	RNA binding protein 6 RNA binding motif protein 6		
3805	O65607	DNA mismatch repair protein MSH3 AtMsh3		
4103	P05092	Peptidyl prolyl cis trans isomerase A EC 5 2 1 8	Cytoplasmic	
3405	NP_003748	Eukaryotic translation initiation factor 3, subunit 2 beta; TNF beta receptor interacting protein 1		
5101	P20228	Glutamate decarboxylase EC 4 1 1 15 GAD		
5702	NP_000427	3-oxoacidCoA transferase	Mitochondrial	28-CVC
1704	P25328	Probable RNA directed RNA polymerase in W dsRNA E		
602	Q05022	rRNA biogenesis protein RRP5		
8104	O18017	Probable blooms syndrome protein homolog EC 3 6		640-CDIC

GRP78 in the ER lumen, cycling between a monomeric and an oligomeric state. Only the monomeric GRP78 associates with the newly synthesized proteins to facilitate their folding. The oligomeric GRP78 might serve as a storage pool, from which monomeric GRP78 is recruited in the presence of unfolded protein accumulation. Depleting this reservoir during ER stress causes GRP78 to dissociate from the transducers and leads to downstream UPR signaling. Our unpublished data showed that selenium treatment activates the signature UPR signaling molecules. The thiol redox modification by selenium may change the conformational structure of GRP78, and, thus, may affect its ability to oligomerize, and disrupt the balance between the monomeric and oligomeric GRP78 and/or facilitate the dissociation of GRP78 from the transducers.

Nestin, a protein with high rank points in all three groups, is a type VI intermediate filament (IF). In general, intermediate filament proteins are components of the cytoskeleton; their expression is tissue specific and developmentally regulated. Tumor cells exhibit differential patterns of IF expression, regardless of their cell origin. Nestin is primarily found in neuroectodermal progenitor cells and skeletal muscle progenitor cells. It is also widely used as a marker for angiogenesis. Recently, nestin has been implicated in the development of androgen independence in human prostate cancer cells. This study is the first to report nestin as a target of selenium. However, the protein functions and downstream signaling of nestin remain unclear. We will direct part of our future effort to elucidate the role of nestin in mediating the anticancer effects of selenium.

Redox regulation of proteins has a profound effect on their functions/activities. Two examples are cited below to illustrate how selenium causes defined redox changes which are accompanied by either a gain or loss of function/activity of the protein. Full length human p53 contains 10 cysteine residues. Using a 20 kDa carboxyl-terminal fragment of p53 with two cysteines at codons 275 and 277, Seo et al.[24] reported that a reduction of these two thiols by selenium significantly increases sequence specific DNA binding and transactivation of p53. MSA and selenite are more potent than selenomethionine in inducing p53 redox changes.[25] This finding is congruent with the interpretation that MSA and selenite are converted to the reactive monomethylated metabolite much more efficiently than selenomethionine. A second example is provided by the work of Gopalakrishna et al.[26] regarding the redox modification of protein kinase C by selenite. There are two cysteine-rich regions in protein kinase C; the regulatory domain contains 12 cysteine residues, and the catalytic domain contains 6 or 7 cysteine residues. At low concentrations, selenite converts four cysteine residues to two disulfides; and at high concentrations, it converts eight cysteine residues to four disulfides. The former modification is associated with a loss of affinity to ATP, while the latter with a lower Vmax of the enzyme. Without doing similarly sophisticated biochemistry with the proteins identified in this study, there is no way to predict how their

functions or activities will influence the cellular responses to selenium. Part of our future effort will be focused on this area of research. Depending on the redox milieu of the tissue, as well as that of the cellular and subcellular environment, selenium might act as a chemical switch to turn a protein on or off without affecting the expression level of the protein.

In spite of the novelty of our study, there is a caveat to our research finding. Our methodology is limited to the detection of high abundance proteins. With few exceptions, low abundance proteins, proteins with extreme pI, or proteins with poor to solubility, are generally not well resolved. Thus, in reality, the present approach is likely to under-estimate the number of redox-sensitive proteins. Further, it is unlikely that all reactive thiol-containing proteins are targets of selenium. On a grander scale, there is increasing recognition that many cellular processes are sensitive to the integration of redox signals. In this regard, it will be of great potential importance to develop a future study to investigate these proteins identified as high impact proteins that influence the state transition during MSA exposure. We believe that a novel combination of display thiol proteomics approach and the neural network-based dynamic modeling will provide new clues that are otherwise unavailable. Given what we know about cellular responses to selenium, we are currently pursuing the idea that redox modification of key proteins will play a critical role in determining how cells respond to treatment with selenium.

ABBREVIATIONS

MSA, methylseleninic acid; BIAM, N-(biotinyl)-N′-(iodoacetyl) ethylenediamine

ACKNOWLEDGMENTS

This work was supported by NIH CA109480, CA111846, CA09796, U.S. Army PC050127, Korea Health 21 R & D project 01-PJ3-PG6-01GN07, and Inha University.

REFERENCES

1. Combs, G.F.; Clark, L.C. Selenium and cancer prevention. In *Antioxidant Nutrients and Disease Prevention*; CRC Press: Boca Raton, FL, 1997.
2. Ip, C.; Ganther, H.E. Activity of methylated forms of selenium in cancer prevention. Cancer Res. **1990**, *50* (4), 1206–1211.
3. Ip, C.; Hayes, C.; Budnick, R.M.; Ganther, H.E. Chemical form of selenium, critical metabolites, and cancer prevention. Cancer Res. **1991**, *51* (2), 595–600.
4. Ip, C. Lessons from basic research in selenium and cancer prevention. J. Nutr. **1998**, *128* (11), 1845–1854.

5. Ip, C.; Thompson, H.J.; Zhu, Z.; Ganther, H.E. In vitro and in vivo studies of methylseleninic acid: evidence that a monomethylated selenium metabolite is critical for cancer chemoprevention. Cancer Res. **2000**, *60* (11), 2882–2886.
6. Dong, Y.; Zhang, H.; Hawthorn, L.; Ganther, H.E.; Ip, C. Delineation of the molecular basis for selenium-induced growth arrest in human prostate cancer cells by oligonucleotide array. Cancer Res. **2003**, *63* (1), 52–59.
7. Zu, K.; Ip, C. Synergy between selenium and vitamin E in apoptosis induction is associated with activation of distinctive initiator caspases in human prostate cancer cells. Cancer Res. **2003**, *63* (20), 6988–6995.
8. Dong, Y.; Lee, S.O.; Zhang, H.; Marshall, J.; Gao, A.C.; Ip, C. Prostate specific antigen expression is down-regulated by selenium through disruption of androgen receptor signaling. Cancer Res. **2004**, *64* (1), 19–22.
9. Jiang, C.; Wang, Z.; Ganther, H.; Lu, J. Caspases as key executors of methyl selenium-induced apoptosis (anoikis) of DU-145 prostate cancer cells. Cancer Res. **2001**, *61* (7), 3062–3070.
10. Jiang, C.; Wang, Z.; Ganther, H.; Lu, J. Distinct effects of methylseleninic acid versus selenite on apoptosis, cell cycle, and protein kinase pathways in DU145 human prostate cancer cells. Mol. Cancer Ther. **2002**, *1* (12), 1059–1066.
11. Wang, Z.; Jiang, C.; Lu, J. Induction of caspase-mediated apoptosis and cell-cycle G1 arrest by selenium metabolite methylselenol. Mol. Carcinog. **2002**, *34* (3), 113–120.
12. Polgar, L.; Halasz, P. Evidence for multiple reactive forms of papain. Eur. J. Biochem. **1978**, *88* (2), 513–521.
13. Page, M.G.; West, I.C. Characterisation in vivo of the reactive thiol groups of the lactose permease from Escherichia coli and a mutant; exposure, reactivity and the effects of substrate binding. Biochim. Biophys. Acta **1986**, *858* (1), 67–82.
14. Wefers, H.; Sies, H. Oxidation of glutathione by the superoxide radical to the disulfide and the sulfonate yielding singlet oxygen. Eur. J. Biochem. **1983**, *137* (1–2), 29–36.
15. Medeiros, M.H.; Wefers, H.; Sies, H. Generation of excited species catalyzed by horseradish peroxidase or hemin in the presence of reduced glutathione and H_2O_2. Free Radical Biol. Med. **1987**, *3* (2), 107–110.
16. Ganther, H.E. Selenium metabolism, selenoproteins and mechanisms of cancer prevention: complexities with thioredoxin reductase. Carcinogenesis **1999**, *20* (9), 1657–1666.
17. Park, E.M.; Choi, K.S.; Park, S.Y.; Kong, E.S.; Zu, K.; WU, Y.; Zhang, H.; Ip, C.; Park, Y.M. A display thiol-proteomics approach to characterize global redox modification of proteins by selenium: Implications for the anticancer action of selenium. Cancer Genom. Proteom. **2005**, *2*, 25–36.
18. Barto, A.G.; Bradtke, S.J.; Singh, S.P. Learning to act using real-time dynamic programming. Artif. Intell. **1995**, *72* (1–2), 81–138.
19. Zeigler, B.P.; Praehofer, H.; Kim, T.G. *Theory of Modeling and Simulation*, 2nd ed.; Academic Press: New York, 1999.
20. Guyon, I.; Matic, N.; Vapnik, V. Discovering informative patterns and data cleaning. In *Advances in Knowledge Discovery and Data Mining*; MIT Press: Cambridge, 1996; 181–203.
21. Lee, J.; Chung, J. Recognition of digits using spatio-temperal neural network. *SPIE Application and Science of Artificial N.N. Conference*, Proceedings of the SPIE – The International Society for Optical Engineering, 2492, pt. 2, 1995; 928–938.
22. Lee, J.; Chung, J. Continuous digit recognition using spatio-temporal neural network. J. Korean Comm. Elect. Eng. **1996**.

23. Breiman, L.; Friedman, J.; Olshen, R.; Stone, C. *Classification and Regression Tree*; Wadsworth International Group, 1984.
24. Seo, Y.R.; Kelley, M.R.; Smith, M.L. Selenomethionine regulation of p53 by a ref1-dependent redox mechanism. Proc. Natl. Acad. Sci. USA **2002**, *99* (22), 14548–14553.
25. Smith, M.L.; Lancia, J.K.; Mercer, T.I.; Ip, C. Selenium compounds regulate p53 by common and distinctive mechanisms. Anticancer Res. **2004**, *24* (3a), 1401–1408.
26. Gopalakrishna, R.; Gundimeda, U.; Chen, Z.H. Cancer-preventive selenocompounds induce a specific redox modification of cysteine-rich regions in Ca(2+)-dependent isoenzymes of protein kinase C. Arch. Biochem. Biophys. **1997**, *348* (1), 25–36.

Received June 20, 2005
Accepted August 5, 2005
Manuscript 7449

Oncogene (2006) 25, 546–554

www.nature.com/onc

ORIGINAL ARTICLE

Enhanced selenium effect on growth arrest by BiP/GRP78 knockdown in p53-null human prostate cancer cells

K Zu[1], T Bihani[2], A Lin[2], Y-M Park[3], K Mori[4] and C Ip[1]

[1]*Department of Cancer Chemoprevention, Roswell Park Cancer Institute, Buffalo, NY, USA;* [2]*Department of Pharmacology and Therapeutics, Roswell Park Cancer Institute, Buffalo, NY, USA;* [3]*Department of Cell Stress Biology, Roswell Park Cancer Institute, Buffalo, NY, USA and* [4]*Department of Biophysics, Graduate School of Science, Kyoto University, Kyoto, Japan*

Redox modification of thiol/disulfide interchange in proteins by selenium could lead to protein unfolding. When this occurs in the endoplasmic reticulum (ER), a process known as unfolded protein response (UPR) is orchestrated for survival through activation of PERK–eIF2α (PERK: double-stranded RNA-activated protein kinase-like ER kinase; eIF2α: eucaryotic initiation factor 2α), ATFα (ATFα: activating transcription factor 6) and inositol requiring 1 (IRE1)-x-box-binding protein 1 (XBP1) signalings. All three UPR transducer pathways were upregulated very rapidly when PC-3 cells were exposed to selenium. These changes were accompanied by increased expression of UPR target genes, including immunoglobulin heavy chain-binding protein/glucose-regulated protein, 78 kDa and CCAAT/enhancer binding protein-homologous protein/growth arrest- and DNA damage-inducible gene (CHOP/GADD153). Induction of BiP/GRP78, an ER-resident chaperone, is part of the damage control mechanism, while CHOP/GADD153 is a transcription factor associated with growth arrest and apoptosis in the event of prolonged ER stress. Knocking down BiP/GRP78 induction by small interference RNA produced a differential response of the three transducers to selenium, suggesting that the signaling intensity of each transducer could be fine-tuned depending on BiP/GRP78 availability. In the presence of selenium, CHOP/GADD153 expression was raised even higher by BiP/GRP78 knockdown. Under this condition, the selenium effect on wild-type p53-activated fragment p21 ($p21^{WAF}$), cyclin-dependent kinase (CDK)1 and CDK2 was also magnified in a manner consistent with enhanced cell growth arrest. Additional experiments with CHOP/GADD153 siRNA knockdown strongly suggested that CHOP/GADD153 may play a positive role in upregulating the expression of $p21^{WAF}$ in a p53-independent manner (PC-3 cells are p53 null). Collectively, the above findings support the idea that UPR could be an important mechanism in mediating the anticancer activity of selenium.
Oncogene (2006) **25,** 546–554. doi:10.1038/sj.onc.1209071; published online 3 October 2005

Correspondence: Dr C Ip, Department of Cancer Chemoprevention, Roswell Park Cancer Institute, Elm & Carlton Streets, Buffalo, NY 14263, USA.
E-mail: clement.ip@roswellpark.org
Received 27 June 2005; revised 1 August 2005; accepted 1 August 2005; published online 3 October 2005

Keywords: selenium; unfolded protein response; BiP/GRP78 knockdown; ER stress signalings

Introduction

The anticancer activity of selenium is well documented (Ip *et al*., 2002; El Bayoumy and Sinha, 2004). Selenomethionine is the reagent of choice in a number of human intervention trials with prostate cancer. As proposed originally by Ip and Ganther (1990) and Ip *et al*. (1991), the metabolism of selenomethionine to methylselenol (CH_3SeH) is essential for anticancer activity. For reasons that have been elaborated in detail previously, neither selenomethionine nor methylselenol is suitable for use, as in cell culture experiments, to investigate the mechanism of action of selenium (Ip, 1998). A stable metabolite called methylseleninic acid (CH_3SeO_2H, abbreviated to MSA) was developed specifically for *in vitro* studies (Ip *et al*., 2000). Once taken up by cells, MSA is reduced rapidly to CH_3SeH through nonenzymatic reactions. Exposure of human prostate cancer cells to physiological concentrations of MSA results in cell cycle arrest and apoptosis (Dong *et al*., 2003; Zu and Ip, 2003).

Owing to its strong nucleophilicity, methylselenolate (the anion of methylselenol) readily reacts with protein sulfhydryl groups to cause thiol/disulfide interchange. By using a thiol-proteomics approach coupled to matrix-assisted laser desorption ionization-time-of-flight (MALDI-TOF) and electrospray ionization (ESI)-tandem mass spectrometry, we recently showed that MSA caused global thiol/disulfide redox modification of numerous proteins that are distributed in various subcellular compartments, including cytosol, mitochondria, nucleus, and endoplasmic reticulum (ER) (Park *et al*., 2005). These changes are expected to lead to protein unfolding or misfolding, especially for the newly synthesized proteins.

The ER is an intracellular organelle where newly synthesized proteins undergo post-translational modifications to form their proper tertiary structure. This process is tightly supervised by a host of ER-resident molecules, which are charged with performing specific

tasks, as exemplified by immunoglobulin heavy chain-binding protein/glucose-regulated protein, 78 kDa (BiP/GRP78) for maintaining proteins in a folding-competent state (Kuznetsov *et al*., 1994), protein disulfide isomerase for catalysing the protein folding reaction (Jessop *et al*., 2004; Tu and Weissman, 2004), as well as calnexin and calreticulin for quality control monitoring (Ellgaard and Helenius, 2003). Normal functions of the ER could be impaired under various stressful conditions, including suppression of protein glycosylation, disruption of calcium homeostasis, or alterations in redox status. These ER stress signals cause accumulation of misfolded/unfolded proteins in the ER lumen, and in turn initiate a series of transducer pathways as a self-protective mechanism. This so-called unfolded protein response (UPR) is characterized by an immediate stoppage of new protein synthesis and growth arrest, followed by adaptive survival, or apoptosis if stress is prolonged (Kadowaki *et al*., 2004; Ma and Hendershot, 2004; Shen *et al*., 2004).

The UPR is mediated primarily by one protein chaperone, BiP/GRP78, and three transmembrane ER stress transducers: double-stranded RNA-activated protein kinase-like ER kinase (PERK), inositol requiring 1 (IRE1), and activating transcription factor 6 (ATF6). In the unstressed ER, BiP/GRP78 binds to the ER luminal domains of the transducers and keeps them inactive in sequestration. Upon sensing the accumulation of misfolded/unfolded proteins, BiP/GRP78 dissociates from its clients and translocates to the ER lumen to help protein folding (Bertolotti *et al*., 2000; Liu *et al*., 2000, 2002, 2003). Once released from sequestration, PERK is activated by oligomerization and autophosphorylation. It then phosphorylates eucaryotic initiation factor 2α (eIF2α), thereby shutting off general protein translation (Harding *et al*., 1999). Similar to PERK, IRE1 is fully activated after dimerization and autophosphorylation. The site-specific endoribonuclease (RNase) activity of IRE1 mediates the removal of a 26-nucleotide intron from x-box-binding protein 1 (XBP1) mRNA (Tirasophon *et al*., 1998, 2000; Yoshida *et al*., 2001; Calfon *et al*., 2002; Lee *et al*., 2002). The spliced form of XBP1 subsequently binds to the ER stress response element (ERSE) and upregulates the transcription of UPR target genes, such as BiP/GRP78 and endoplasmic reticulum degradation-enhancing alpha-mannosidase-like protein (EDEM). The latter is meant to accelerate the degradation of misfolded proteins (Yoshida *et al*., 1998, 2003). After dissociation from BiP/GRP78, ATF6 translocates to the Golgi, where the active form of ATF6, ATF6 p50, is generated by proteolysis (Haze *et al*., 1999; Chen *et al*., 2002; Shen *et al*., 2002; Okada *et al*., 2003). As a transcription factor, ATF6 p50 binds to ERSE, resulting in the induction of BiP/GRP78, XBP1, CCAAT/enhancer binding protein-homologous protein/growth arrest- and DNA damage-inducible gene (CHOP/GADD153), and protein kinase inhibitor p58 ($p58^{IPK}$) (Yoshida *et al*., 1998, 2000; van Huizen *et al*., 2003). In summary, a circuitry of signaling molecules are functioning cooperatively to alleviate the accumulation of unfolded/misfolded proteins in the ER lumen. When the survival response fails to adapt under prolonged ER stress, cells will eventually undergo apoptosis, although the mechanism behind this decision has not been elucidated.

The objectives of the present study were (i) to examine systemically the activation of signature UPR transducers and target genes by MSA in PC-3 human prostate cancer cells, (ii) to investigate the sensitivity of various UPR transducers to knockdown of BiP/GRP78 induction by MSA, and (iii) to study how BiP/GRP78 availability might modulate the growth arrest effect of MSA. These experiments were designed to test the hypothesis that UPR is an important mechanism in mediating the anticancer action of selenium.

Results

Induction of signature UPR transducer pathways and target genes by MSA

To assess the effect of MSA on UPR, all three transducer pathways were examined systematically in PC-3 cells with or without MSA treatment. As shown in Figure 1a, signal transduction of the PERK–eIF2α pathway and activation of ATF6 were evaluated by Western blot analysis. At the 6 h time point, MSA treatment increased the levels of phospho-PERK and cleaved ATF6, that is, ATF6 p50. The active forms of both PERK and ATF6 remained elevated at 12 h, but returned to their basal level or below by 24 h. Phospho-eIF2α changed in a direction similar to that of phospho-PERK, although the former still remained above its basal level at the 24 h time point. The total protein level of eIF2α was not affected by MSA. Phosphorylation of eIF2α by PERK inhibits its activity as an initiation factor in protein translation. Since total eIF2α did not change while phospho-eIF2α (inactive) increased with MSA treatment, the inference is that there would be less unphosphorylated eIF2α (active), thus leading to suppression of protein translation.

The antibody to phospho-IRE1 is not available commercially. The effect of MSA on IRE1 activation was assessed by using IRE1-mediated XBP1 splicing as a surrogate marker (Calfon *et al*., 2002). A schematic illustration of the principle of this analysis is presented in the left panel of Figure 1b. The PCR fragments of XBP1 cDNA contain a 473-bp unspliced form and a 447-bp spliced form. The unspliced form encompasses a *Pst*I restriction site, which is lost in the spliced form. After digestion of the PCR fragments with *Pst*I, the unspliced XBP1 cDNA is detected as two digestion products of 290 and 183 bp, whereas the spliced form remains as a 447-bp fragment due to its resistance to *Pst*I. The results of MSA-induced XBP1 splicing are shown in the right panel of Figure 1b. The unspliced XBP1 fragment was the dominant form in the control. With MSA treatment, almost all XBP1 cDNAs became spliced at the 6 h time point. The appearance of spliced XBP1 suggested that the IRE1 pathway was activated. The level of spliced XBP1 decreased gradually

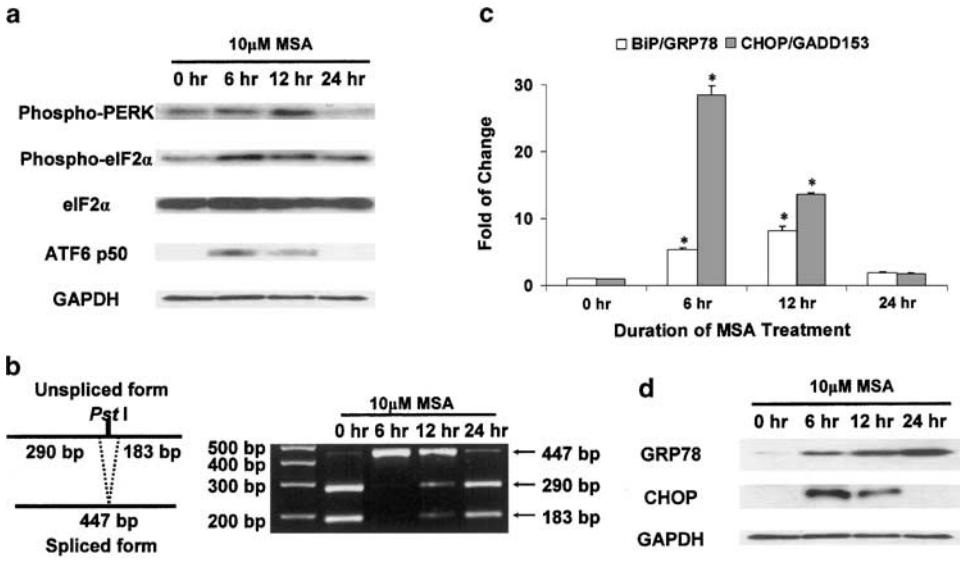

Figure 1 Induction of signature UPR transducer pathways and target genes by MSA. The Western blot and DNA electrophoresis data are representative of the results from three independent experiments. The real-time RT–PCR results are presented as mean ± standard error ($n = 3$). *statistically different ($P < 0.05$) compared to the untreated control. (**a**) MSA-induced signal transduction of the PERK–eIF2α pathway and activation of ATF6 by Western blot analysis. Phosphorylation of PERK and eIF2α was determined by phosphospecific antibodies. (**b**) Analysis of XBP1 splicing as a surrogate marker for activation of the IRE1 pathway. The principle of this analysis (Calfon *et al*., 2002) is presented in a schematic illustration (left panel). XBP1 cDNA fragments were amplified by RT–PCR using XBP1-specific primers. After digestion with the *Pst*I restriction enzyme at 37°C for 3 h, the cDNA fragments were separated on a 2% agarose gel (right panel). (**c**) MSA induction of UPR target genes, BiP/GRP78 and CHOP/GADD153, as determined by real-time RT–PCR. The relative quantitation of gene expression (fold of change) was calculated as described in Materials and methods. (**d**) MSA induction of BiP/GRP78 and CHOP/GADD153 as determined by Western blot analysis.

as the unspliced form recovered steadily with longer treatment.

In order to assess the transcriptional control of target genes by activated ATF6 and XBP1, the expression of BiP/GRP78 and CHOP/GADD153 was examined at the mRNA level by quantitative real-time reverse transcription–polymerase chain reaction (RT–PCR) (Figure 1c), and at the protein level by Western blot analysis (Figure 1d). Similar to the activation of UPR transducers, the mRNA level of BiP/GRP78 and CHOP/GADD153 increased markedly following a short exposure to MSA, and returned to the basal level by 24 h. The change in CHOP/GADD153 protein level was consistent with the change in mRNA. However, the accumulation of BiP/GRP78 protein continued to rise with the duration of treatment, despite the drop in mRNA level at 24 h. This discrepancy between mRNA and protein levels may reflect the long half-life of BiP/GRP78 protein (Satoh *et al*., 1993).

Differential sensitivity of UPR transducers to knockdown of BiP/GRP78 induction by MSA

As a master negative regulator of UPR, BiP/GRP78 binds to PERK, ATF6, and IRE1 to keep them inactive. BiP/GRP78 also exists in a free form to facilitate protein folding in the ER lumen. UPR signal transduction is regulated through a delicate balance between free and bound BiP/GRP78. During ER stress, BiP/GRP78 is induced in order to increase the folding capacity of the ER and to compensate for the depletion of free BiP/GRP78. In an attempt to investigate the role of BiP/GRP78 induction by MSA, small interference RNA (siRNA) technique was used to knock down the increased expression of BiP/GRP78. A concentration of 75 nM siRNA was used since it was the highest nontoxic dose based on preliminary titration experiments. As shown in Figure 2a, transient transfection with siRNA against BiP/GRP78 was able to tone down significantly the robust induction of this gene by MSA at both the mRNA (upper panel) and protein levels (lower panel). The comparison was made against control cells transfected with scramble siRNA and similarly treated with MSA. The UPR transducer pathways and downstream signalings were then examined in this BiP/GRP78 knockdown model.

As shown in Figure 2b, the level of phospho-PERK in both the control and BiP/GRP78 knockdown samples was increased by MSA treatment. However, at the later time points (12 and 24 h), the magnitude of the increase was dampened in the BiP/GRP78 knockdown samples. Likewise, the modulation of eIF2α followed a similar pattern of a lesser amount of phospho-eIF2α in the GRP78 siRNA-transfected cells. In contrast, the induction of ATF6 p50 was maintained for a longer period of time by reduced expression of BiP/GRP78.

Analysis of IRE1-mediated XBP1 splicing in the GRP78 siRNA-transfected cells is shown in Figure 2c. After 6 h of MSA treatment, XBP1 mRNA was present primarily in the spliced form. As observed previously, the unspliced form recovered gradually with time. However, there was no significant difference in XBP1

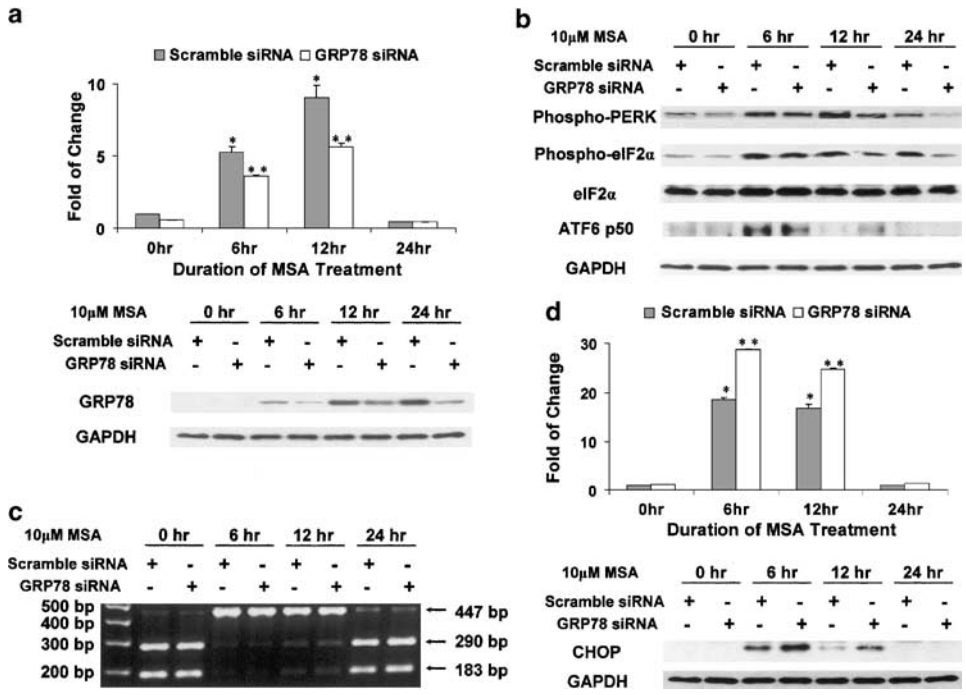

Figure 2 Differential sensitivity of UPR transducers to knockdown of BiP/GRP78 induction by MSA. The Western blot and DNA electrophoresis data are representative of the results from three independent experiments. The real-time RT–PCR results are presented as mean $\pm$ standard error ($n=3$). *statistically different ($P<0.05$) compared to the untreated control. ** BiP/GRP78 knockdown results are statistically different ($P<0.05$) compared to the scramble control. (**a**) SiRNA knockdown of BiP/GRP78 induction by MSA. Upper panel: real-time RT–PCR; lower panel: Western blot analysis. (**b**) Effect of BiP/GRP78 knockdown on MSA-induced signal transduction of the PERK–eIF2α pathway and activation of ATF6. (**c**) Effect of BiP/GRP78 knockdown on MSA-induced XBP1 splicing. XBP1 cDNA fragments were amplified by RT–PCR using XBP1-specific primers. After digestion with the *Pst*I restriction enzyme at 37°C for 3 h, the cDNA fragments were separated on a 2% agarose gel. (**d**) Enhanced MSA induction of CHOP/GADD153 by BiP/GRP78 knockdown. Upper panel: real-time RT–PCR; lower panel: Western blot analysis.

splicing between the control and BiP/GRP78 knockdown samples.

The expression of CHOP/GADD153 in cells transfected with scramble siRNA or BiP/GRP78 siRNA was examined at the mRNA level by quantitative real-time RT–PCR (Figure 2d, upper panel) and at the protein level by Western blot analysis (Figure 2d, lower panel). At the 6 h time point, the mRNA level was elevated by MSA treatment, and this increase was sustained at 12 h. More importantly, the effect was significantly magnified in the BiP/GRP78 knockdown samples. The boost in MSA induction of CHOP/GADD153 by BiP/GRP78 knockdown could be accounted for in part by the prolonged activation of ATF6, as shown in Figure 2b.

Enhanced MSA effect on growth arrest by BiP/GRP78 knockdown

Next, we used two different end points to examine the biological consequence of BiP/GRP78 knockdown in cells treated with MSA. Cell proliferation was measured by the 5-bromo-2′-deoxyuridine (BrdU) incorporation assay (Figure 3a). After exposure to 10 μM MSA for 12 h, DNA synthesis was suppressed by $\sim$38% in cells transfected with scramble siRNA. The inhibition was significantly greater ($\sim$52%, $P<0.05$) in cells with reduced BiP/GRP78 expression.

The results of the cell cycle distribution analysis are shown in Figure 3b. Without MSA treatment, no difference was observed in cell cycle distribution between transfection with scramble siRNA or BiP/GRP78 siRNA. After cells were treated with 10 μM MSA for 12 h, the percentage of S-phase cells was significantly decreased, while the percentages of both G_0/G_1- and G_2/M-phase cells were increased (Figure 3b, upper panel). The comparative changes in cell cycle distribution profile between the scramble siRNA and BiP/GRP78 siRNA-transfection groups are highlighted in the lower panel of Figure 3b. The effect of MSA on cell cycle arrest was notably enhanced by BiP/GRP78 knockdown.

Enhanced MSA effect on expression of cell cycle regulatory molecules by BiP/GRP78 knockdown

In order to gain further insight into the mechanism of UPR-induced cell cycle arrest, we examined the expression of several key cell cycle regulatory molecules by Western blot analysis. These molecules were selected based on our previous MSA data in PC-3 cells. As shown in Figure 3c, MSA treatment downregulated cyclin-dependent kinase (CDK)1 and CDK2, but upregulated their inhibitor wild-type p53-activated fragment p21 ($p21^{WAF}$). The effect of MSA on the expression of these molecules was significantly enhanced

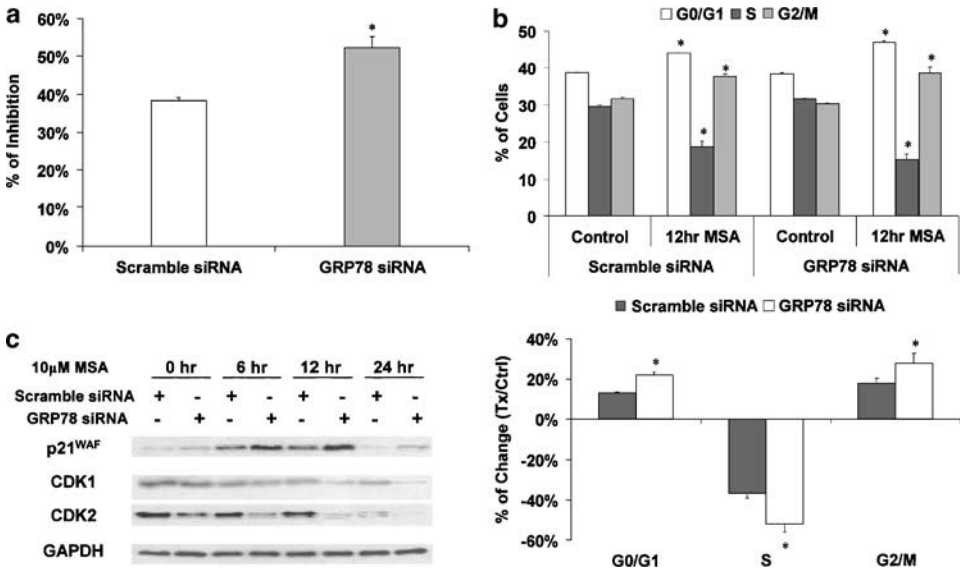

Figure 3 Enhanced MSA effect on growth arrest by BiP/GRP78 knockdown. The Western blot data are representative of the results from three independent experiments. (**a**) Enhanced MSA effect on DNA synthesis suppression by BiP/GRP78 knockdown. Percentage of inhibition was calculated based on the percentages of BrdU-positive cells in MSA-treated samples and untreated control. The results are presented as mean ± standard error ($n=3$). *BiP/GRP78 knockdown results are statistically different ($P<0.05$) compared to the scramble control. (**b**) Enhanced MSA effect on cell cycle arrest by BiP/GRP78 knockdown. The upper panel shows the cell cycle distribution data in cells transfected with scramble or BiP/GRP78 siRNA, with or without 10 μM MSA treatment. The results are presented as mean ± standard error ($n=3$). *MSA-treated results are statistically different ($P<0.05$) compared to the untreated control. The lower panel shows the difference between the scramble control and BiP/GRP78 knockdown samples. *BiP/GRP78 knockdown results are statistically different ($P<0.05$) compared to the scramble control. (**c**) Enhanced MSA effect on expression of cell cycle regulatory molecules by BiP/GRP78 knockdown. The protein levels of $p21^{WAF}$, CDK1, and CDK2 were examined by Western blot analysis.

by knocking down BiP/GRP78, that is, more pronounced decreases with CDK1 and CDK2, and greater increase with $p21^{WAF}$.

Reduced MSA induction of $p21^{WAF}$ expression by CHOP/GADD153 knockdown

As shown in Figures 2d and 3c, the expression of CHOP/GADD153 and $p21^{WAF}$ was induced by MSA in a parallel manner as a function of time. The protein levels of these two molecules were further elevated by knocking down BiP/GRP78. In order to investigate the role of CHOP/GADD153 in upregulating the expression of $p21^{WAF}$, we used the siRNA technique to knockdown the induction of CHOP/GADD153. A concentration of 100 nM siRNA was used since it was the highest nontoxic dose based on preliminary titration experiments. As shown in Figure 4a, the induction of CHOP/GADD153 by MSA was knocked down by more than 50% at both the mRNA (upper panel) and protein levels (lower panel) over a course of 12 h. The expression of $p21^{WAF}$ was then examined in this CHOP/GADD153 knockdown model (Figure 4b). At the 6 h time point, the induction of $p21^{WAF}$ mRNA (upper panel) and protein (lower panel) by MSA was reduced markedly in cells transfected with siRNA against CHOP/GADD153. At the 12 h time point, the difference in $p21^{WAF}$ mRNA levels between the CHOP/GADD153 knockdown and scramble control cells became marginal, while the difference in $p21^{WAF}$ protein levels still remained significant. Based on the above data, we conclude that CHOP/GADD153 may play a positive role in upregulating the expression of $p21^{WAF}$ in a p53-independent manner (PC-3 cells are p53 null).

Discussion

In this study, we systematically investigated the induction of UPR by MSA in an effort to link ER stress to the anticancer action of selenium. All three UPR transducer pathways, PERK–eIF2α, ATF6, and IRE1–XBP1, are activated very rapidly, leading to increased expression of UPR target genes. Activation of PERK–eIF2α signaling is meant to block general protein synthesis in order to reduce the burden of more unfolded proteins. Knocking down BiP/GRP78 by siRNA elicits a differential response of the three stress transducer pathways; the net outcome is an enhanced selenium effect on cell growth arrest. The above findings suggest that UPR may be an important done in mediating the anticancer activities of selenium.

As a negative regulator of UPR, BiP/GRP78 sequesters PERK, ATF6, and IRE1 on the ER membrane by binding to their luminal domains. There is also free BiP/GRP78 in the ER lumen, cycling between a monomeric and an oligomeric state (Freiden *et al*., 1992; Blond-Elguindi *et al*., 1993). Only the monomeric BiP/GRP78 associates with newly synthesized proteins to facilitate their folding. The oligomeric BiP/GRP78 represents a storage pool, from which monomeric BiP/GRP78 is recruited in the presence of unfolded protein accumulation. Depleting this reservoir during ER stress causes

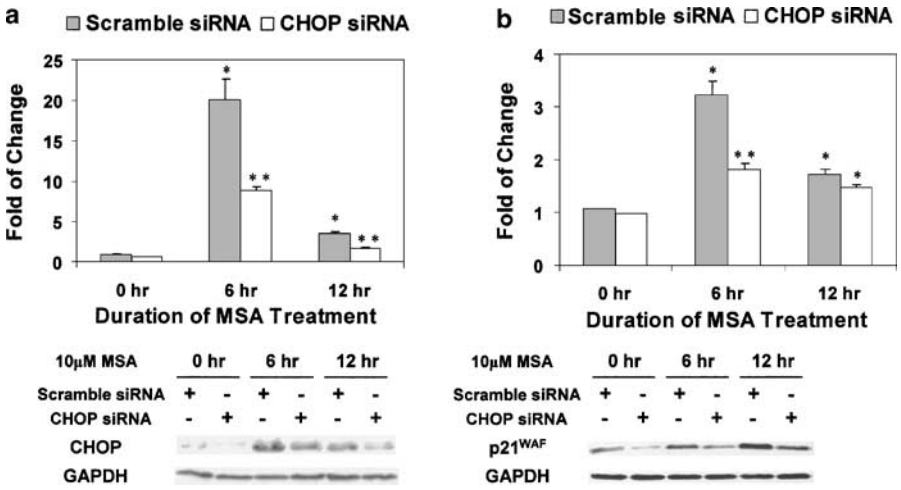

Figure 4 Reduced MSA induction of $p21^{WAF}$ by CHOP/GADD153 knockdown. The Western blot data are representative of the results from three independent experiments. The real-time RT–PCR results are presented as mean ± standard error ($n = 3$). *statistically different ($P < 0.05$) compared to the untreated control. **CHOP/GADD153 knockdown results are statistically different ($P < 0.05$) compared to the scramble control. (**a**) SiRNA knockdown of CHOP/GADD153 induction by MSA. Upper panel: real-time RT–PCR; lower panel: Western blot analysis. (**b**) Reduced MSA induction of $p21^{WAF}$ by CHOP/GADD153 knockdown. Upper panel: real-time RT–PCR; lower panel: Western blot analysis.

BiP/GRP78 to dissociate from PERK, ATF6, and IRE1, and leads to downstream UPR signaling. As a target gene, BiP/GRP78 is then upregulated to replenish the oligomeric pool.

Since the increased expression of BiP/GRP78 is designed to help cells cope with ER stress, our strategy was to suppress the induction of BiP/GRP78 by RNA interference in order to intensify the stress signal in the ER. Interestingly, the three transducer pathways respond differently to BiP/GRP78 knockdown, suggesting that there might be distinctive mechanisms regulating their activation. PERK and IRE1 are both type I transmembrane protein kinases. Their ER luminal domains are homologous and interchangeable (Bertolotti *et al*., 2000). However, the oligomerization and BiP/GRP78 binding domains of IRE1 overlap partially (Liu *et al*., 2003), whereas those of PERK are distinctive (Ma *et al*., 2002). When excessive unfolded proteins are present in the ER, BiP/GRP78 is titrated competitively from the luminal domains of PERK and IRE1 to effect their oligomerization and activation (Schroder and Kaufman, 2005). On the other hand, ATF6 is a type II transmembrane protein. There are two independent and redundant Golgi localization sequences (GLSs), GLS1 and GLS2, in the ER luminal domain of ATF6 (Shen *et al*., 2002). BiP/GRP78 only binds to GLS1 and keeps ATF6 in an inactive state. After the release of BiP/GRP78 from GLS1, GLS2 becomes dominant and regulates the translocation of ATF6 to the Golgi, where ATF6 is activated through proteolysis. Thus, the three signaling arms of the UPR may have distinctive sensitivities to fluctuations of the free BiP/GRP78 pool. Crosstalks also exist among the three transducer pathways. For example, $p58^{IPK}$, a downstream target of ATF6, has been reported to inhibit the activity of PERK (Yan *et al*., 2002; van Huizen *et al*., 2003). Our results showed that a modest knockdown of BiP/GRP78 induction is sufficient to cause a prolonged activation of ATF6, which may account for the decrease in PERK activity (potentially mediated by $p58^{IPK}$) at the later time points. During ER stress, the PERK-mediated translational block is short-lived, since the primary adaptive mechanism is to upregulate the transcription of UPR target genes. It is possible that differences in the binding affinity of BiP/GRP78 to each of the three transducers, as well as the interactions between downstream signaling pathways, are critical factors in fine-tuning UPR signalings.

CHOP/GADD153 is a member of the CCAAT/enhancer binding protein (C/EBP) family and is present normally at a very low expression level. It is induced rapidly when the functions of the ER are perturbed. The induction of CHOP/GADD153 is regulated primarily at the transcriptional level. All three transducer pathways of ER stress are involved in this process (Harding *et al*., 2000; Wang *et al*., 2000; Gotoh *et al*., 2002). The overexpression of CHOP/GADD153 has been shown to be involved in ER stress-induced cell cycle arrest and/or apoptosis (Barone *et al*., 1994; Friedman, 1996). However, very little information is available on the signaling events or the downstream targets of CHOP/GADD153. Based on our experience, CHOP/GADD153 is one of the most highly inducible genes in a number of cancer cell lines treated with MSA. Previously, we investigated the gene expression profile in MSA-treated PC-3 cells by oligonucleotide array analysis (Dong *et al*., 2003). Hundreds of genes are affected by MSA, among which is a large set of cell cycle regulatory genes. They are mostly modulated in a manner consistent with cell cycle arrest. In this study, we examined the expression of CHOP/GADD153, $p21^{WAF}$, CDK1, and CDK2 in the context of UPR. Our data showed that in the presence of MSA, the mRNA and protein levels of CHOP/GADD153 are

raised even higher by knocking down BiP/GRP78. The effect of MSA on $p21^{WAF}$, CDK1, and CDK2 is also magnified by a muted induction of BiP/GRP78, suggesting that the modulation of these genes by MSA is associated with ER stress response. In particular, $p21^{WAF}$ is upregulated in a pattern that similar to that of CHOP/GADD153. The upregulation in $p21^{WAF}$ is severely dampened by CHOP/GADD153 knockdown. PC-3 cells are p53 null. Therefore, the increase of $p21^{WAF}$ gene expression in PC-3 cells during ER stress is likely to be mediated by CHOP/GADD153 in a p53-independent manner. Future studies will investigate the possible transcriptional control of $p21^{WAF}$ by CHOP/GADD153.

ER stress has been studied mostly in neuropathology, such as Parkinson's disease and Alzheimer's disease (Lehotsky *et al*., 2003). Scanty information is available regarding UPR in cancer research. Since the key selenium metabolite, methylselenol, is generated endogenously, the induction of UPR by selenium is likely to be a universal phenomenon and is not cell type specific. That is to say, proteins in normal cells are vulnerable to redox modification by selenium as well. However, different cells may have different abilities to manage and cope with stress. The selectivity of selenium as a primary chemopreventive agent has been well documented (Ip *et al*., 2002). A recent study reported that preadministration of selenium increases the therapeutic efficacy of irinotecan in the nude mice tumor xenograft model (Cao *et al*., 2004). More importantly, selenium is highly protective of normal cells, and is able to overcome the dose-limiting toxicity of the drug. The above finding implies that selenium may favor survival response in normal cells, but facilitates apoptotic response in cancer cells. Indeed, the protective role of pre-conditioned ER stress response against cytotoxicity has been reported in normal cells (Hung *et al*., 2003; Bednard *et al*., 2004). Many factors may impact on ER stress response to selenium. For example, the microenvironment may determine whether the outcome of UPR is survival or death. Hypoxia is a known inducer of ER stress (Koumenis *et al*., 2002; Tajiri *et al*., 2004). The hypoxic condition of a solid tumor could sensitize cancer cells to selenium. Our laboratory has preliminary data (unpublished) showing that hypoxia significantly enhances selenium induction of apoptosis. The genetic background of a particular cell may be another factor in tipping the balance toward either survival or death in responses to the same stress signal. The growth arrest induced by ER stress can be viewed not only as the primary effect of selenium in cancer prevention, but also as a priming mechanism in potentiating the therapeutic selectivity of therapeutic drugs.

Materials and methods

Cell culture and treatments

PC-3 human prostate cancer cells were obtained from ATCC (Manassas, VA, USA). These cells were cultured in RPMI 1640 medium supplemented with 10% fetal bovine serum, 100 U/ml penicillin, 100 μg/ml streptomycin, and 2 mM glutamine, and were maintained in an atmosphere of 5% CO_2 in a 37°C humidified incubator. Cells were exposed to 10 μM MSA for different periods of time, either at 48 h after seeding or 12 h after transfection.

Transient siRNA-transfection

The annealed siRNAs were synthesized by Ambion Inc. (Austin, TX, USA). The BiP/GRP78-specific siRNA (sense sequence, 5′-GGACAUCAAGUUCUUGCCGtt-3′; antisense sequence, 5′-CGGCAAGAACUUGAUGUCCtg-3′) was used to knock down the induction of BiP/GRP78 by MSA. The CHOP/GADD153-specific siRNA (sense sequence, 5′-CCAG GAAACGGAAACAGAGtt-3′; antisense sequence, 5′-CUC UGUUUCCGUUUCCUGGtt-3′) was used to knock down the induction of CHOP/GADD153 by MSA. The scramble nonsense siRNA (sense sequence, 5′-AGUACUGCUUAC GAUACGGtt-3′; antisense sequence, 5′-CCGUAUCGUAA GCAGUACUtt-3′) that has no homology to any known genes was used as control. In the flow cytometry experiments, carboxyfluorescein (FAM)-labeled siRNAs (synthesized by Ambion Inc.) were used in combination with unlabeled siRNAs at a ratio of 1:5 to target the transfected population.

PC-3 cells were placed in six-well cell culture plates at a density of 6×10^4 cells/cm^2. At 48 h after seeding, the cells were transfected with GRP78 siRNA or scramble siRNA by using Oligofectamine Reagent (Invitrogen) according to the manufacturer's protocol. Briefly, for each well in a six-well plate, 4 μl of oligofectamine was diluted in 11 μl of Opti-MEM I medium (Invitrogen). This mixture was carefully added to a solution containing 75 or 100 nmol of siRNA in 185 μl of Opti-MEM I medium. The solution was incubated for 30 min at room temperature, and then gently overlaid onto 80% confluent PC-3 cells in 800 μl of Opti-MEM I medium. After 6 h of transfection, cells were refed with regular growth medium for 12 h before exposure to different treatments.

Cell lysis and Western blot analysis

Whole cell lysate was prepared by using 1 × cell lysis buffer (Cell Signaling Technology, Beverly, MA, USA), and protein concentration was determined by using the BCA Protein Assay Kit (Pierce Biotechnology, Rockford, IL, USA). Whole cell lysates were then resolved over 8–15% SDS–PAGE and transferred to a PVDF membrane. The blot was blocked in blocking buffer (5% nonfat dry milk, 10 mM Tris, pH 7.5, 10 mM NaCl, and 0.1% Tween 20) at 37°C for 1 h, incubated with the primary antibody overnight at 4°C, followed by incubation with a horseradish peroxidase-conjugated secondary antibody (Bio-Rad, Hercules, CA, USA) at room temperature for 30 min. Individual proteins were visualized by an enhanced chemiluminescence kit obtained from Amersham Pharmacia Biotech (Piscataway, NJ, USA).

The antibodies (source) to the following proteins were used in this study: phospho-PERK (Thr980), eIF2α, phospho-eIF2α (Ser51), and cleaved PARP (Cell Signaling Technology, Beverly, MA, USA), BiP/GRP78, CHOP/GADD153, and $p21^{WAF}$ (Santa Cruz Biotechnology Inc., Santa Cruz, CA, USA), CDK1 and CDK2 (BD Transduction Laboratories, San Jose, CA, USA), and GAPDH (Chemicon, Temecula, CA, USA). The rabbit antiserum raised against human ATF6 p50 (activated form) was purified as described previously (Haze *et al*., 1999).

XBP1 splicing analysis

Total RNA was isolated with the TRIzol reagent (Life Technologies Inc.). First-strand cDNA was synthesized from 100 ng of total RNA by SuperScript II reverse transcriptase

(Invitrogen) following the manufacturer's protocol. The XBP1-specific primers were synthesized by Integrated DNA Technologies Inc. (Coralville, IA, USA). PCR with the sense primer (5′-AAACAGAGTAGCAGCTCAGACTGC-3′) and the antisense primer (5′-TCCTTCTGGGTAGACCTCTGGG AG-3′) amplified a 473-bp cDNA product encompassing the IRE1-mediated splicing site. This fragment was further digested by *Pst*I to reveal a restriction site that is lost after IRE1-mediated splicing of the XBP1 mRNA. The cDNA fragments were resolved on a 2% agarose gel containing ethidium bromide and then visualized with an AlphaImager 1220 Documentation and Analysis system (Alpha Innotech, San Leandro, CA, USA).

Quantitative real-time RT–PCR

First-strand cDNA was synthesized as described previously. The PCR primers and TaqMan probes for β-actin, BiP/GRP78, and CHOP/GADD153 were Assays-on-Demand products from Applied Biosystems (Foster City, CA, USA). An aliquot of 2 μl of first-strand cDNA was mixed with 25 μl of 2 $\times$ Taqman Universal PCR Master Mix (Applied Biosystems) and 2.5 μl of 20 $\times$ primers/probe mixture in a 50 μl final volume. Temperature cycling and real-time fluorescence measurements were performed using an ABI prism 7700 Sequence Detection System (Applied Biosystems). The PCR conditions were as follows: initial incubation at 50°C for 2 min, then denaturation at 95°C for 10 min, followed by 40 cycles of 95°C for 15 s and 60°C for 1 min.

The relative quantitation of gene expression was performed by using the comparative C_T ($\Delta\Delta C_T$) method. Briefly, the threshold cycle number (C_T) was obtained as the first cycle at which a statistically significant increase in fluorescence signal was detected. Data normalization was carried out by subtracting the C_T value of β-actin from that of the target gene. The $\Delta\Delta C_T$ was calculated as the difference of the normalized C_T values (ΔC_T) of the treatment and the control samples: $\Delta\Delta C_T = \Delta C_{T\ \text{treatment}} - \Delta C_{T\ \text{control}}$. Finally, $\Delta\Delta C_T$ was converted to fold of change by the following formula: fold of change $= 2^{-\Delta\Delta C_T}$.

BrdU incorporation and cell cycle distribution analysis

After transfection with scramble siRNA or BiP/GRP78 siRNA (combined with FAM-labeled siRNAs at a ratio of 5:1), cells were exposed to regular growth medium with or without 10 μM of MSA for 12 h. The BrdU incorporation and cell cycle distribution analysis was then performed by using the BrdU Flow Kit from BD Pharmigen (San Diego, CA, USA) according to the manufacturer's protocol. Briefly, cells were labeled with 10 μM BrdU during the last hour of treatment. They were then trypsinized, fixed, treated with DNase I, and stained with phycoerythrin (PE)-conjugated anti-BrdU antibody and 7-amino-actinomycin D (7AAD). Stained cells were then subjected to flow cytometric analysis, and the data were analysed with the WinList software (Variety Software House, Topsham, ME, USA).

Statistical analysis

The Student's *t*-test was used to determine statistical differences between treatments and controls, and $P<0.05$ was considered significant.

Abbreviations

ATF6, activating transcription factor 6; BiP/GRP78, immunoglobulin heavy chain-binding protein/glucose-regulated protein, 78 kDa; BrdU, 5-bromo-2′-deoxyuridine; CDK, cyclin-dependent kinase; CHOP/GADD153, CCAAT/enhancer binding protein-homologous protein/growth arrest- and DNA damage-inducible gene; EDEM, endoplasmic reticulum degradation-enhancing alpha-mannosidase-like protein; eIF2α, eucaryotic initiation factor 2α; ER, endoplasmic reticulum; ERSE, ER stress response element; ESI, electrospray ionization; GLS, Golgi localization sequences; IRE1, inositol requiring 1; MSA, methylseleninic acid; MALDI-TOF, matrix-assisted laser desorption ionization-time-of-flight; $p21^{WAF}$, wild-type p53-activated fragment p21; $p58^{IPK}$, protein kinase inhibitor p58; PERK, double-stranded RNA-activated protein kinase-like ER kinase; RNase, ribonuclease; RT–PCR, reverse transcription–polymerase chain reaction; siRNA, small interference RNA; UPR, unfolded protein response; XBP1, x-box-binding protein 1.

Acknowledgements

This work was supported by Grant CA 09796 from the National Cancer Institute and Grant 62-2198 from the Roswell Park Alliance Foundation, and was partially supported by core resources of the Roswell Park Cancer Institute Cancer Center Support Grant P30 CA 16056 from the National Cancer Institute.

References

Barone MV, Crozat A, Tabaee A, Philipson L, Ron D. (1994). *Genes Dev* **8**: 453–464.
Bednard K, MacDonald N, Collins J, Cribb A. (2004). *Basic Clin Pharmacol Toxicol* **94**: 124–131.
Bertolotti A, Zhang Y, Hendershot LM, Harding HP, Ron D. (2000). *Nat Cell Biol* **2**: 326–332.
Blond-Elguindi S, Fourie AM, Sambrook JF, Gething MJ. (1993). *J Biol Chem* **268**: 12730–12735.
Calfon M, Zeng H, Urano F, Till JH, Hubbard SR, Harding HP *et al*. (2002). *Nature* **415**: 92–96.
Cao S, Durrani FA, Rustum YM. (2004). *Clin Cancer Res* **10**: 2561–2569.
Chen X, Shen J, Prywes R. (2002). *J Biol Chem* **277**: 13045–13052.
Dong Y, Zhang H, Hawthorn L, Ganther HE, Ip C. (2003). *Cancer Res* **63**: 52–59.
El Bayoumy K, Sinha R. (2004). *Mutat Res* **551**: 181–197.
Ellgaard L, Helenius A. (2003). *Nat Rev Mol Cell Biol* **4**: 181–191.
Freiden PJ, Gaut JR, Hendershot LM. (1992). *EMBO J* **11**: 63–70.
Friedman AD. (1996). *Cancer Res* **56**: 3250–3256.
Gotoh T, Oyadomari S, Mori K, Mori M. (2002). *J Biol Chem* **277**: 12343–12350.
Harding HP, Novoa I, Zhang Y, Zeng H, Wek R, Schapira M *et al*. (2000). *Mol Cell* **6**: 1099–1108.
Harding HP, Zhang Y, Ron D. (1999). *Nature* **397**: 271–274.
Haze K, Yoshida H, Yanagi H, Yura T, Mori K. (1999). *Mol Biol Cell* **10**: 3787–3799.
Hung CC, Ichimura T, Stevens JL, Bonventre JV. (2003). *J Biol Chem* **278**: 29317–29326.
Ip C. (1998). *J Nutr* **128**: 1845–1854.

Ip C, Dong Y, Ganther HE. (2002). *Cancer Metast Rev* **21**: 281–289.
Ip C, Ganther HE. (1990). *Cancer Res* **50**: 1206–1211.
Ip C, Hayes C, Budnick RM, Ganther HE. (1991). *Cancer Res* **51**: 595–600.
Ip C, Thompson HJ, Zhu Z, Ganther HE. (2000). *Cancer Res* **60**: 2882–2886.
Jessop CE, Chakravarthi S, Watkins RH, Bulleid NJ. (2004). *Biochem Soc Trans* **32**: 655–658.
Kadowaki H, Nishitoh H, Ichijo H. (2004). *J Chem Neuroanat* **28**: 93–100.
Koumenis C, Naczki C, Koritzinsky M, Rastani S, Diehl A, Sonenberg N *et al*. (2002). *Mol Biol Cell* **22**: 7405–7416.
Kuznetsov G, Chen LB, Nigam SK. (1994). *J Biol Chem* **269**: 22990–22995.
Lee K, Tirasophon W, Shen X, Michalak M, Prywes R, Okada T *et al*. (2002). *Genes Dev* **16**: 452–466.
Lehotsky J, Kaplan P, Babusikova E, Strapkova A, Murin R. (2003). *Physiol Res* **52**: 269–274.
Liu CY, Schroder M, Kaufman RJ. (2000). *J Biol Chem* **275**: 24881–24885.
Liu CY, Wong HN, Schauerte JA, Kaufman RJ. (2002). *J Biol Chem* **277**: 18346–18356.
Liu CY, Xu Z, Kaufman RJ. (2003). *J Biol Chem* **278**: 17680–17687.
Ma K, Vattem KM, Wek RC. (2002). *J Biol Chem* **277**: 18728–18735.
Ma Y, Hendershot LM. (2004). *J Chem Neuroanat* **28**: 51–65.
Okada T, Haze K, Nadanaka S, Yoshida H, Seidah NG, Hirano Y *et al*. (2003). *J Biol Chem* **278**: 31024–31032.
Park EM, Choi KS, Park SY, Zu K, Wu Y, Zhang H *et al*. (2005). *Cancer Genom Proteom* **2**: 25–36.
Satoh M, Nakai A, Sokawa Y, Hirayoshi K, Nagata K. (1993). *Exp Cell Res* **205**: 76–83.
Schroder M, Kaufman RJ. (2005). *Mutat Res* **569**: 29–63.
Shen J, Chen X, Hendershot L, Prywes R. (2002). *Dev Cell* **3**: 99–111.
Shen X, Zhang K, Kaufman RJ. (2004). *J Chem Neuroanat* **28**: 79–92.
Tajiri S, Oyadomari S, Yano S, Morioka M, Gotoh T, Hamada JI *et al*. (2004). *Cell Death Differ* **11**: 403–415.
Tirasophon W, Lee K, Callaghan B, Welihinda A, Kaufman RJ. (2000). *Genes Dev* **14**: 2725–2736.
Tirasophon W, Welihinda AA, Kaufman RJ. (1998). *Genes Dev* **12**: 1812–1824.
Tu BP, Weissman JS. (2004). *J Cell Biol* **164**: 341–346.
van Huizen R, Martindale JL, Gorospe M, Holbrook NJ. (2003). *J Biol Chem* **278**: 15558–15564.
Wang Y, Shen J, Arenzana N, Tirasophon W, Kaufman RJ, Prywes R. (2000). *J Biol Chem* **275**: 27013–27020.
Yan W, Frank CL, Korth MJ, Sopher BL, Novoa I, Ron D *et al*. (2002). *Proc Natl Acad Sci USA* **99**: 15920–15925.
Yoshida H, Haze K, Yanagi H, Yura T, Mori K. (1998). *J Biol Chem* **273**: 33741–33749.
Yoshida H, Matsui T, Hosokawa N, Kaufman RJ, Nagata K, Mori K. (2003). *Dev Cell* **4**: 265–271.
Yoshida H, Matsui T, Yamamoto A, Okada T, Mori K. (2001). *Cell* **107**: 881–891.
Yoshida H, Okada T, Haze K, Yanagi H, Yura T, Negishi M *et al*. (2000). *Mol Cell Biol* **20**: 6755–6767.
Zu K, Ip C. (2003). *Cancer Res* **63**: 6988–6995.